1-1-1968

Theoretical and experimental investigation of biaxially loaded rectangular tubular columns.

Zia Razzaq
University of Windsor

THEORETICAL AND EXPERIMENTAL INVESTIGATION OF BIAXIALLY LOADED RECTANGULAR TUBULAR COLUMNS

A Thesis
Submitted to the Faculty of Graduate Studies through the
Department of Civil Engineering in Partial Fulfilment
of the Requirements for the Degree of
Master of Applied Science at the
University of Windsor

by

Zia Razzaq

B.E.(Hons.), University of Peshawar, 1966

Windsor, Ontario
1968

ABK0404

Approved By: W North

Gronfalw

J S Kennedy

219881

ABSTRACT

This investigation is a theoretical and experimental study of biaxially loaded beam-columns. The columns considered are simply supported at each end and loaded with a constant axial load with a constantly increasing moment applied at one end. Rectangular, tubular cross-sections are considered. The analysis presented includes the effect of strain-hardening.

Five tests were performed and moment-deflection curves obtained. The tests were on medium length columns acted upon by light to medium loads. Comparison of the theoretical curves with the experimental curves shows good agreement with the maximum error in predicted ultimate moment being about two percent. Because of residual stresses, the predicted deflections are generally less than those observed. Measurements of twisting of the cross-section indicate that it is negligible as expected since the section used has a large torsional stiffness.

Limited theoretical results indicate that for some columns, at least, strain-hardening can substantially increase their strength.

ACKNOWLEDGEMENTS

The author is deeply indebted to Dr. William McVinnie, under whose direction this thesis was prepared, for his criticism, advice, and constant encouragement.

All the computational work was carried out at the Computer Center of the University of Windsor. Financial assistance for this project was provided by the National Research Council of Canada.

TABLE OF CONTENTS

	Page
ABSTRACT	iii
ACKNOWLEDGEMENTS	iv
TABLE OF CONTENTS	v
LIST OF FIGURES	vii
LIST OF TABLES	ix
I INTRODUCTION	1
1.1 Preliminary Statement	1
1.2 Object and Scope of Investigation	6
II THEORETICAL SOLUTION	7
2.1 Description of the Problem	7
2.2 Theoretical Behavior of the Column	7
2.3 Load-Moment-Curvature Relationship	11
2.3.1 Establishing the M-Ø Curves	11
III EXPERIMENTAL SET-UP AND TEST PROCEDURE	16
3.1 General Considerations	16
3.2 Overall Description	16
3.3 End Fixtures	17
3.4 Application and Measurement of the Loads	18
3.4.1 Direct Axial Load	18
3.4.2 Biaxial Bending Moment	19
3.5 Specimen Preparation	21
3.6 Test Procedure	21
IV DISCUSSION OF RESULTS	25
4.1 Specimens Tested	25
4.2 Experimental Results	28

		Page
	4.3 Theoretical Study	31
	4.3.1 Study of Variables	31
	4.3.2 Column Integration Using Single Pass	33
V	CONCLUSIONS AND FUTURE RESEARCH	37
	5.1 Conclusions	37
	5.2 Future Research	38
APPENDIX - THRUST-MOMENT-CURVATURE RELATIONS		81
BIBLIOGRAPHY		99
NOMENCLATURE		102
VITA		104

LIST OF FIGURES

Figure		Page
2.1	A Typical Biaxially Loaded Beam-Column	39
2.2	Beam-Column Cross-Section	39
2.3	Moment-Deflection Curve	40
2.4	Column Deflection Curve	40
2.5	Correction for θ_o^y	41
2.6	Stress-Strain Relationship for Material of the Beam-Column	41
2.7	Moment-Curvature curves	42
2.8	Possible Yield Configurations in a Biaxially Loaded Rectangular Tubular Beam-Column	43
2.9	Sequence for Checking Yield Patterns	44
2.10	Constant Moment, Curvature Curves	45
3.1	Elevation and End-View of the Apparatus shown Schematically	46-47
3.2	Test Set-up	48
3.3	Sectional Elevation, Plan, and Sectional End-View of the End Fixture	49-50
3.4	Schematic View of the End Fixture	52
3.5	End-Support for the Beam 4	53
3.6	Axial Load, Load Cell	54
3.7	Strain Measuring Apparatus	54
3.8	Load Cell for Measuring the Moment-Inducing Load W; and, Lever Arm and Its Connection with the Tie Rods	55
3.9	Measurement of End Rotation	56
4.1	Stress-Strain Curve for the Material of Specimen 1	57

Figure		Page

4.2	Stress-Strain Curve for the Material of Specimens 2 and 5	58
4.3	Stress-Strain Curve for the Material of Specimen 3	59
4.4	Moment vs. Lateral Displacement Components at Midheight, Rotation Components at End A, and Rotation Components at End B, respectively, for Specimen 1	60-62
4.5	Moment vs. Lateral Displacement Components at Midheight, Rotation Components at End A, and Rotation Components at End B, respectively, for Specimen 2	63-65
4.6	Moment vs. Lateral Displacement Components at Midheight, Rotation Components at End A, and Rotation Components at End B, respectively, for Specimen 3	66-68
4.7	Moment vs. Lateral Displacement Components at Midheight, Rotation Components at End A, and Rotation Components at End B, respectively, for Specimen 4	69-71
4.8	Moment vs. Lateral Displacement Components at Midheight, Rotation Components at End A, and Rotation Components at End B, respectively, for Specimen 5	72-74
4.9	Magnitude of the Variation in Axial Load $\overline{P}$ During the Tests	75
4.10	Comparison of the Strains for Column 5	76
4.11	Effect of Varying γ on the Peak Moments	77
4.12	Moment-Rotation Curves showing the Effect of Strain-Hardening	78
4.13	Effect of Varying the Number of Points for Column Integration, on the Peak Moments	79
4.14	Effect of Varying L_r on the Peak Moments	80

LIST OF TABLES

Table		Page
4.1	Summary of the Tests Performed	35
4.2	Comparison of Theoretical and Experimental Peak Moments about the x-axis	36

CHAPTER I - INTRODUCTION

1.1 Preliminary Statement

The analysis of members loaded inelastically is becoming more and more important because of the increased use of plastic analysis and design. By allowing inelastic strains to penetrate into a structural member, its load-carrying capacity is increased appreciably without resulting in excessive deformation.

The behavior of columns stressed inelastically is of prime concern in structural design. Determination of the strength of such a member becomes very complicated since the bending stiffness varies along its length due to the varying extent of yielding. A fairly large number of papers have appeared in the past on inelastic single axis bending. Most of the methods given in these papers such as those presented by Bleich (3) and Timoshenko and Gere (28) are numerical types and are based on an assumed shape for the column.

Closed solutions for the displacements of beam-columns loaded inelastically are not possible. One form of the solution is to replace the governing differential equation(s) by equivalent finite difference equation(s) and write a set of homogeneous, simultaneous equations by applying the difference equation(s) at panel points on the member. The determinant of the coefficients must be zero for a nontrivial solution to exist. Successive approximations may be used to find the lowest root of the polynomial resulting from the expansion of the determinant (the lowest root yields the critical load for the member). This method has been proposed by Salvadori (20).

Newmark (17) has presented an iterative numerical technique in which external moments are found from an assumed deflection curve and a new deflection curve calculated by numerical integration using the moment-curvature relation for the cross-section considered. This process is continued until the correct shape is obtained, that is, until the calculated deflection curve is the same as the assumed one. Ketter, Kaminisky, and Beedle (14) and Galambos and Ketter (9) have applied Newmark's procedure to determine load-deflection curves of wide-flange columns. The theoretical solutions given in these investigations are also compared to tests by Mason, Fisher, and Winter (15).

Ketter (13) has determined the combination of load and moment necessary to cause collapse of a member subjected to a constant load with increasing moment. Jordan (12) has considered the problem of an eccentrically loaded column subjected to loads which resulted in small amounts of inelastic action. He determined the load-deflection curve for the given column from two families of curves derived from simple equilibrium conditions and assumed stress distributions in the members. This method proves to be rational, but difficult to apply. Shanley (22) has proposed a semi-rational method in which he used approximate moment-load curves, the ultimate bending moment for the section, and the critical buckling load for the centrally loaded column.

Osgood (18) has proposed an approximate method which essentially consists of replacing the given beam-column by an eccentrically loaded column. Available methods are then applied to the resulting eccentrically loaded column. Theoretical solutions are presented for several cases but no test data is given.

The differential equations governing the elastic response of the biaxially loaded column have been formulated by Goodier (10), Timoshenko (27), Bleich (3), and Vlasov (29). Approximate solution to these equations are given by Thurlimann (26), Dabrowski (5), and Prawel and Lee (19). The exact solution of these equations has been given by Culver (4).

The study of the inelastic behavior of the biaxially loaded beam-column has only recently been attempted. This is because of the much more complex nature of this problem compared with that of single axis bending. Sharma (23) and Birnstiel and Michalos (2) have presented analytical solutions of biaxially loaded wide flange columns. Sharma has presented an approximate method for determining the ultimate load of columns having the same eccentricity of loading at each end. The basis of this procedure is the assumption that the lateral and twisting displacements vary sinusoidally along the column. At midheight, a value of the second derivative of one of the lateral displacements is specified, and equilibrium between internal and external forces and moments is established. Knowing the displacement at midheight thus determines the deflected shape of the column. By incrementing the specified second derivative, a load-deflection curve is obtained. Comparison of the theoretical results with a large number of test results showed good agreement. In the analysis presented by Birnstiel and Michalos, the column is first divided into a number of panels. Values of the second derivatives of the three displacements, that is, the lateral displacements in two directions and a rotation of the section about its center of twist, are assumed at each panel point. A trial equilibrium position is then determined by numerical integration. The values of the curvatures and the second derivatives of the angle of twist are adjusted until equilibrium between external and internal forces and moments is established at each panel point. Internal moments and forces are found by dividing the cross-section into a number of elements by a rectangular grid, determining the strain on each element, and summing the results over all the elements of the cross-section. By assuming increasing values of the second derivatives of the displacements, a curve of load versus deflection is obtained, which leads directly to the collapse load of the column.

Another solution has been presented by Ellis (7,8) who determines the ultimate carrying capacity of biaxially loaded columns using the overlapping shape failure criterion (6). Briefly, this criterion requires that two intersecting column curves be determined so that a column on the verge of collapse has been defined, since between the points of intersection, two column deflected shapes exist for the same axial load and end conditions. Column deflection curves are found only for a square tubular section. Since this type of section is torsionally stiff, twisting displacements are neglected and thus only two deflections at any point along the column need to be determined. These deflections are found by considering a short element which is systematically subjected to rotations about each principal axis and acted upon by a specified axial load. For each combination of end rotations, the axial strain and bending moments are determined. This information is then used to " build-up " a column deflection curve.

McVinnie (16) considered the analytical study of a biaxially loaded column as an integral part of an orthogonal space frame. Load-deflection curves were set up using a numerical integration procedure for rectangular tubular columns of an elastic-perfectly-plastic material. Scott (21) used this method for analyzing biaxially loaded solid rectangular beam-columns. The same method forms the basis for the analytical study in this thesis and is described in detail shortly.

Birnstiel and Michalos (2) and Sharma (23) have given a review of the literature on the experimental investigations of biaxially loaded columns. Most of these experimental results are for columns having equal eccentricities at each end with cross-section being either wide-flange, I, or channel. Baker (1) tested beam-columns having solid rectangular and wide-flange sections. No experimental results for biaxially loaded columns of rectangular tubular cross-section have been published to the author's knowledge.

1.2 Object and Scope of Investigation

The object of this investigation is to study analytically and experimentally, simply-supported columns loaded with a constant axial load and a biaxial moment at one end. The moment increases from zero to the ultimate capacity of the column. Previous theoretical solutions (16,21) are extended to include a material which exhibits strain-hardening. Only rectangular, tubular cross-sections are considered.

Five columns were tested and moment-deflection data obtained from each test. Theoretical results are determined and compared with each of the five tests. In addition, a theoretical study of some parameters which were not considered experimentally is presented. A thorough study of all the parameters involved is beyond the scope of the present investigation.

CHAPTER II - THEORETICAL SOLUTION

2.1 Description of the Problem

A biaxially loaded beam-column of the type studied is shown in Fig. 2.1. The column has a length h and is simply-supported at each end, that is, the displacements are zero, but rotations are permitted about the x and y axes. The loads on the column are such that the axial load $\overline{P}$ is applied and maintained constant and then end moments about the x and y axes, M_h^x and M_h^y respectively, are applied at one end of the column and increased simultaneously to collapse. To further define the loading, the ratio M_h^y/M_h^x is maintained constant at a value γ.

Rectangular tubular cross-sections are assumed in this investigation (Fig. 2.2). The half depth of the cross-section is taken as D, the half width as K_2D. The x and y axes are the principal axes of the cross-section.

2.2 Theoretical Behavior of the Column

The behavior of the column is fully defined by a moment-deflection curve of the type shown in Fig. 2.3. The deflection plotted may be any of a number of deflections associated with the column deflected shape, deflections taken to include rotations.

The analysis used has been previously given by Scott (21) in a study of solid rectangular cross-sections and is briefly summarized.

The assumptions involved in this analysis are:

1) Deflections and rotations are small in accordance with the small deflection theory.

2) Deflections occur in the x and y directions only, no twisting of the column is allowed.

3) Plane sections before bending remain plane after bending.

4) The material is mild structural steel which is assumed to have strain-hardening in the inelastic range, the stress-strain curve for which is of the type shown in Fig. 2.6. It is further assumed that the tension and compression stress-strain curves are identical.

5) No unloading occurs in yielded portions of the column.

6) Residual stresses are neglected.

7) The column is originally straight and prismatic.

8) Axial shortening of the column is neglected.

9) The effect of shear on the bending resistance of the cross-section is neglected.

A typical point on the moment-displacement curve is found from a column deflection curve (Fig. 2.4) which is defined by the shape a column will take if the load and deflection at any point are specified. In this problem, the x and y displacements, u and v respectively, are zero at the origin whereas the rotations at this point about the x and y axes, θ_o^x and θ_o^y, are specified. Integration for the column deflection curve is started at the origin and proceeds a panel length "a" at a time until the desired length, h, is reached. The equations used are given shortly. The column deflection curve is then rotated about the origin until the displacements at h are zero. This gives a deflected column acted upon by the moments

$$M_h^x = \bar{P}\, v_h ,$$

$$\text{and } M_h^y = \bar{P}\, u_h .$$

If $M_h^y/M_h^x = \gamma$ for the assumed values of θ_o^x and θ_o^y, then one point on the moment-deflection curve for the column has been determined. In this case, θ_o^x and θ_o^y are incremented and a second point found. This procedure is continued until the curve is completely defined.

If for any combination of θ_o^x and θ_o^y the moment ratio M_h^y/M_h^x is not equal to γ, adjustment to one of the initial rotation values must be made. This adjustment is best described using Fig. 2.5. A value of θ_o^x is assumed and a value of θ_o^y is calculated such that if the column were to remain elastic, M_h^y/M_h^x would be equal to the value of γ for the problem. This results in point a of the curve in Fig. 2.5. A new value of θ_o^y is found by approximating the curve (which is unknown) by the secant O-a which results in point b on the curve. If the calculated ratio M_h^y/M_h^x at b is not close enough to γ, the curve is then approximated by the secant a-b. This procedure is repeated until an acceptable value of M_h^y/M_h^x is attained.

The dimensionless extrapolation equations similar to those used by Scott for determining the column deflection curve are given as:

$$\frac{v_{i+1}}{D} = \frac{v_i}{D} + \frac{a}{D}\,\frac{\pi}{3}\,\frac{r_c^x}{D}\sqrt{\epsilon_y}\,\frac{\theta_i^x}{\theta_y^x} - \frac{\epsilon_y}{2}\left(\frac{a}{D}\right)^2 \frac{\phi_i^x}{\phi_y^x} \qquad (2.1)$$

$$\frac{u_{i+1}}{D} = \frac{u_i}{D} + \frac{a}{D}\,\frac{\pi}{3}\,\frac{r_c^x}{D}\sqrt{\epsilon_y}\,\frac{\theta_i^y}{\theta_y^x} - \frac{\epsilon_y}{2}\left(\frac{a}{D}\right)^2 \frac{\phi_i^y}{\phi_y^x} \tag{2.2}$$

$$\frac{\theta_{i+1}^x}{\theta_y^x} = \frac{\theta_i^x}{\theta_y^x} - \frac{3D}{\pi r_c^x}\sqrt{\epsilon_y}\left(\frac{a}{D}\right)\frac{\phi_i^x}{\phi_y^x} \tag{2.3}$$

$$\frac{\theta_{i+1}^y}{\theta_y^x} = \frac{\theta_i^y}{\theta_y^x} - \frac{3D}{\pi r_c^x}\sqrt{\epsilon_y}\left(\frac{a}{D}\right)\frac{\phi_i^y}{\phi_y^x} \tag{2.4}$$

where u_i and v_i are the x and y displacements at a panel point i, and u_{i+1} and v_{i+1} are the displacements at i+1. Likewise, θ_i^x and θ_i^y are the slopes at i of the projections of column deflection curve onto the y-z and x-z planes, respectively; and θ_{i+1}^x and θ_{i+1}^y are the slopes at i+1. ϵ_y is the yield strain of the material.

These equations are based upon the assumption that over a panel length "a" of the column, the deflected shape is a segment of a circle, the curvature of which is the curvature at start of the segment. As evident from Equations 2.1 to 2.4 the displacements at point i+1 on the column deflection curve are determined from the displacements at i and the curvature at i. The moments at i are given by:

$$M_i^x = \overline{P}\, v_i \tag{2.5}$$

$$M_i^y = \overline{P}\, u_i \tag{2.6}$$

Once the moments are known, the curvatures are found using the procedure outlined in Section 2.3.

The accuracy of Equations 2.1 to 2.4 is increased by first obtaining the deflections at point i+1 assuming the curvature of the segment between i and i+1 to be equal to the values at i. Using the values of the deflections at i+1 thus obtained, curvatures at this point are found and a second set of deflections at i+1 calculated assuming the segment curvatures to be the average of those at i and i+1.

2.3 Load-Moment-Curvature Relationship

The load-moment curvature relationship described has been partially given elsewhere (16). This procedure is summarized herein and extended to include the effect of strain-hardening in the material of the column. Detailed derivation of equations used is given in the Appendix.

The relationship between load, moment, and curvature is conveniently represented by the two sets of curves shown in Fig. 2.7. For both sets of curves, the load is constant at $\overline{P}$. Each curve in Fig. 2.5(a) gives the relationship between M^x/M_y^x and ϕ^x/ϕ_y^x for constant values of ϕ^y/ϕ_y^x. In Fig. 2.5(b) the curves show the relationship between M^y/M_y^x vs. ϕ^y/ϕ_y^x for constant values of ϕ^x/ϕ_y^x.

2.3.1 Establishing the M-ϕ Curves

Neglecting the variation in strain through the wall thickness, there are ten possible yield configurations for the biaxially loaded cross-section. These configurations are shown in Fig. 2.8 where the shaded portions represent the yielded material. A particular configuration for a given set of moments and load is determined by the strain distribution while, on the other hand, any strain distribution determines a load and a moment about each axis of the cross-section.

Assuming that plane sections remain plane (which is consistant with neglecting twist) the normal strain ϵ at any point (x,y) on the cross-section may be written as

$$\epsilon = \phi^x y + \phi^y x + \epsilon_o \tag{2.7}$$

where ϵ_o is the uniform normal strain due to the thrust and ϕ^x and ϕ^y are, respectively, the curvatures about the x y axes of the section. In this equation, tensile strains are considered as positive. Referring to the bilinear stress-strain curve of Fig. 2.6, the stress distribution corresponding to Equation 2.7 can be expressed in the following form:

$$\sigma = E\epsilon - E\,(1 - \alpha)\ \ [\epsilon \pm \epsilon_y] \tag{2.8}$$

where α is the strain-hardening factor given by E_t/E, that is, ratio of the tangent modulus to Young's modulus for the material and ϵ is given by Equation 2.7. The brackets [] have the special significance that when $|\epsilon| < \epsilon_y$, the term in the brackets is zero. When ϵ is negative and $|\epsilon| > \epsilon_y$, the plus sign is used for the term inside the brackets and the brackets are replaced by parentheses, that is, normal multiplication. When ϵ is positive and greater than ϵ_y, the negative sign is used for the term inside the brackets and the brackets are replaced by parentheses. A typical stress-strain curve for strain-hardening material is shown dashed in Fig. 2.6. The bilinear approximation to this curve has been shown to yield fairly good results for many materials with the error involved in a load-deflection relation being on the order of 1 or 2 percent (24).

The axial thrust $\bar{P}$ acting on the section is expressed in terms of the stresses on the cross-section by the equation

$$\bar{P} = \int_A \sigma \, dA \tag{2.9}$$

Substituting σ from Equation 2.8 into 2.9:

$$\bar{P} = E \int_A \epsilon dA - E (1 - \alpha) \int_A [\epsilon \pm \epsilon_y] \, dA \tag{2.10}$$

In this equation the first integral represents the value of $\bar{P}$ if the section were everywhere elastic. The second integral accounts for yielding of the cross-section. Moments M^x and M^y about the x and y axes of the section are given by the following two equations.

$$M^x = E \int_A y \, \epsilon \, dA - E (1 - \alpha) \int_A y[\epsilon \pm \epsilon_y] \, dA \tag{2.11}$$

$$M^y = E \int_A x \, \epsilon \, dA - E (1 - \alpha) \int_A x[\epsilon \pm \epsilon_y] \, dA \tag{2.12}$$

Equations 2.7, 2.10, 2.11, and 2.12 relate the thrust and moments acting on a cross-section to the three factors defining the strain distribution on the cross-section, ϕ^x, ϕ^y, and ϵ_o. The analysis is complicated because each of Equations 2.10, 2.11, and 2.12 has a different form for each of the ten possible yield configurations. These are given in the Appendix.

The procedure used to determine the moment-curvature curves of Fig. 2.7 is summarized as follows:

1) For a given value of $\bar{P}$, ϕ^x and ϕ^y are assigned specific values, leaving ϵ_o as the only unknown in Equation 2.7.

2) Using Equation 2.10, a value for ϵ_o is determined that corresponds to the specified ϕ^x, ϕ^y, $\bar{P}$, and an assumed yield configuration. (An assumed configuration is required since there are ten possible forms for Equation 2.10, one for each possible yield pattern). The yield pattern corresponding to the calculated ϵ_o can be readily found (by checking the magnitude of total strains at corners of the cross-section) and compared with the assumed pattern. If these are the same, then ϵ_o has been determined. If the yield patterns are not the same, a new pattern must be assumed and a new value of ϵ_o calculated. The process is continued until a yield pattern compatible with the starting assumption is determined. The sequence used in considering the yield configurations is shown in Fig. 2.9. In this figure the $\bar{\epsilon}_i$ (i = 1, 2, 3, 4) is the strain caused by the curvatures only, that is, $\epsilon_o = 0$ in Equation 2.7. These "bending" strains control the path used in assuming the configurations.

3) Once ϵ_o has been determined, Equations 2.11 and 2.12 are used to find M^x and M^y.

4) By varying ϕ^x and ϕ^y systematically over the range of curvatures desired, the required curves are determined.

The above procedure is performed for each value of the axial thrust prior to making the numerical integrations necessary to determine the deflected shape of the column. The assumed range of curvatures ϕ^x and ϕ^y should be large enough to produce inelastic strains of at least ten times the yield strain.

For a given pair of moments (Equations 2.5 and 2.6) the curvatures are found in the following manner:

1) For any value of $M^x = M_o^x$, the curvatures resulting in this moment are found at the intersections of M_o^x with the constant ϕ^y curves of Fig. 2.7(a). A plot of these curves is shown as curve A of Fig. 2.10.

2) For any value of $M^y = M_o^y$ the curvatures resulting in this moment are found at the intersections of M_o^y with the constant ϕ^x curves of Fig. 2.7(b). A plot of these intersections is shown as curve B of Fig. 2.10.

3) The resulting curvatures for M_o^x and M_o^y acting together are determined by the intersection of curve A with curve B. The co-ordinates of the intersection point are designated as (ϕ_o^x, ϕ_o^y) in Fig. 2.10.

CHAPTER III - EXPERIMENTAL SET-UP AND TEST PROCEDURE

3.1 General Considerations

The experimental investigation described herein presented the author with the major problem of designing and constructing the test set-up and required a considerable amount of time and effort. The requirements for the design were to simulate in the laboratory the column support and load conditions described in Section 2.1. This necesitated end fixtures to permit free rotation about any horizontal axis and a means of applying and measuring the direct axial load and the biaxial bending moment. This chapter describes the test set-up and the test procedure.

3.2 Overall Description

The apparatus used for the column tests is shown in Figs. 3.1 and 3.2. Referring to Fig. 3.1, the test specimen [1]* is welded to base plates which in turn are bolted to end fixtures at the top and bottom [2] and [3]. The top end fixture is attached to a cross-beam [4] which is free to move in the vertical direction and which can be adjusted in the horizontal direction. The bottom end fixture is attached to a fixed support.

Axial load is applied to the specimen using two, 10-ton capacity jacks [6]. Biaxial moment is applied to the specimen at the bottom end fixture by means of a load (W) acting on a lever arm [5]. The overall assembly is mounted between

*Brackets refer to numbers in Fig. 3.1.

a pair of columns [9] which are bolted to a test bed at their base and braced at their tops.

3.3 End Fixtures

To provide the simply supported end-conditions referred to in Section 2.1, gimbals are used. Details of the end fixtures are shown in Fig. 3.3 and a schematic representation is given in Fig. 3.4. The inner part of the end fixture rotates on a shaft along center-line 1 which is supported by self-aligning spherical roller bearings housed in the walls of the outer part. Each end of the test specimen is welded to a 3/4 inch base plate and then bolted to the inner part of the end fixture. This provides nearly frictionless rotation at the end of the specimen about center-line 1.

The outer part of the end fixtures rotates on two stub shafts along center-line 2. These shafts are firmly attached to the walls of the outer part and supported by bearings in pillow-blocks. This arrangement provides nearly frictionless rotation of the entire end fixture about center-line 2. The net effect of the arrangement described is that rotation of the specimen end is permitted about any horizontal axis.

Using this arrangement, the column tested is not simply the specimen, but consists of the specimen plus the inner part of the end fixture above the point of rotation (the intersection of the center-line 1 with center-line 2). This distance is $3\frac{7}{8}$ inches at each end of the specimen and must be considered in the theoretical analysis of any specimen tested.

The seperate plates making up the inner and outer parts of the end fixtures were bolted together using high strength cap screws. Before being used, they were proof-loaded to 28,000 pounds in a hydraulic testing machine to check the strength and assure that bearings would rotate freely under this load.

3.4 Application and Measurement of the Loads

3.4.1 Direct Axial Load

The external support for the top end fixture is provided by the moveable cross-beam [4] (Fig. 3.1). The detail of the end support for the cross-beam is shown in Fig. 3.5. A channel shaped guide is attached to the support columns [9] (Fig. 3.1). Plates with spherical recesses machined in them are attached to the cross-beam using threaded rod. Ball-bearings are placed in the recesses with a total of eight balls used at each end. These ends then fit into the guide and ride on smooth, vertical inner surfaces to give free vertical movement. Horizontal adjustment of the cross-beam is provided by the threaded rods and is used for vertical alignment of the specimen.

The pillow-blocks supporting the top end fixture are mounted on the bottom of the cross-beam and direct axial load applied to the specimen using the two, 10-ton jacks resting on the top of the beam and reacting against a fixed member [8] (Fig. 3.1). These jacks are connected to a 300,000 pound Riehle hydraulic testing machine by a single hose with a Y connection at its end [7] (Fig. 3.1). Hydraulic pressure from the pump of the testing machine is used to operate the jacks. A fairly good indication of the load is given by

$$\frac{\text{(Total Area of the Jacks)}}{\text{(Area of the Testing Machine Cyliner)}} \times \text{Dial Load} \qquad (3.1)$$

A better value for the load was obtained using a load cell mounted between the top end fixture and the specimen (Fig. 3.6). The position of the load cell added a further modification to the theoretical solution since it also is a part of the column being tested. The load cell was constructed from a six inch long piece of 2 inch tubing which was the same as the square specimens tested. 3/4 inch plates were welded to the tube at each end for attachment to the end fixture and the specimen end. Eight strain gages were symmetrically mounted at mid-height and the cell calibrated. Because of the symmetry of the strain gages, the effect of any bending stress on the cell is eliminated. The strains from the load cell were recorded using a Budd automatic strain indicator.

The above described load cell was used for the last three specimens tested (see Section 4.1). For the first two specimens, strain gages were symmetrically mounted on the specimen itself and the load determined by taking the average strain times Young's modulus for the material of the column. Care was taken to mount the gages at a location which remained elastic throughout the test.

3.4.2 Biaxial Bending Moment

Biaxial moment is applied at the bottom end of the specimen using a lever arm attached to the inner part of the end fixture ([5], Fig. 3.1 and Fig. 3.8(b)). A moment-producing load W is applied near the end of the lever arm giving

$$M^x = W e^y$$

$$M^y = W e^x$$

where e^x and e^y are the eccentricities along the x and y axes, respectively. The angle of attachment of the lever arm is such that $e^x/e^y = 0.5$. Thus all tests were for $\gamma = 0.5$.

The load W is applied through two threaded rods about 50 inches long. These rods are separated at the top and bottom by thick steel plates about 9 inches long (Fig. 3.8) forming a closed ring. The bottom plate is connected to the lever arm by means of a ball and socket arrangement (Fig. 3.8(b)) and the top plate is connected to a load cell using a similar arrangement (Fig. 3.8(a)). The load cell is supported on a tripod. The column is deflected by tightening the nuts at the top of the rods and the load measured by the load cell.

The above described procedure for applying the moment to the specimen was used for the last four specimens tested. The initial test was performed using a small hydraulic jack in place of the load cell. Pressure was applied by means of a hand operated pump, and a calibration curve of pressure vs. load used to determine the moment on the specimen.

During trial testing, it was found that the specimen end reactions caused by the applied moment induced excessive lateral deflections at the top of the specimen. To alleviate this situation, tie rods ([10], Fig. 3.1(b)) were attached to the two top pillow-blocks. These were made adjustable so that any lateral deflections could be controlled during the progress of a test.

3.5 Specimen Preparation

Specimens to be tested were prepared by first cutting them to length using an automatic hacksaw. The ends were then milled to assure that the cut edges were flat and perpendicular to the axis of the specimen. The centers of the four sides were carefully determined and marked at each end. These marks were then matched with center marks on the base plates and clamped in a jig. The specimen and base plate were then welded all around.

The center marks on the base plates were carefully determined to coincide with projections of center-lines 1 and 2 of the end fixtures (Figs. 3.3 and 3.4). This arrangement automatically positioned the centroid of the specimen on the line of action of the axial load to within the accuracy of the assembly.

3.6 Test Procedure

After the specimen was prepared, it was bolted in place for testing. The nuts at the end of the moveable cross-beam were then adjusted until the specimen was vertical. Vertical alignment was checked using a 30 inch spirit level placed on the sides of the specimen and rechecked using a transit.

Ames dial gages accurate to .001 inches were then placed to obtain the required deflections. Fig. 3.2 shows a typical placement of the dial gages. End rotations were measured by fixing a bar to each of the inner and outer parts of the end fixtures and measuring the deflection at a known distance from the center of rotation (Fig. 3.9). For rotation of the outer part of the end fixture the angle of rotation is given by

$$\theta^{x} = d^{x}/c^{x} \tag{3.2}$$

where θ^{x} = angle of rotation about the x axis (assumed to be small such that $\theta = \tan\theta$);

d^{x} = measured vertical displacement; and

c^{x} = horizontal distance from the x axis of rotation.

Rotation about the second axis is complicated by the fact that the bar used to measure the rotation was placed off center. Thus, displacements measured are functions of both rotations. A slightly more complicated expression for the rotation results and is given by

$$\theta^{y} = (d^{y} \pm \Delta^{y}\,\theta^{x})/c^{y} \tag{3.3}$$

where θ^{y} = angle of rotation about the y axis;

d^{y} = measured vertical displacement;

c^{y} = horizontal distance from the y axis of rotation; &

Δ^{y} = horizontal distance from the x axis of rotation.

The sign inside the parentheses (Equation 3.3) depends on the rotation θ^{x}.

Dial gages were also mounted at key spots on the apparatus to check movements external to the specimen. Typical locations were at the top and bottom pillow-blocks. Fig. 3.2 shows the gage locations for a typical test.

After obtaining zero readings for all dial gages and the load cells, a small bending moment was applied to the specimen in order to pretension the tie rods to the moveable cross-beam. The desired value of the axial load (to be maintained constant throughout the test) was then applied to the specimen assuming Equation 3.1 applies. The tie rods to the moveable cross-beam were then adjusted to remove any resulting lateral displacement of the top of the specimen. At this stage the load measured by the axial load load cell was determined from its calibration curve to see if the desired load was being applied to the specimen. It was generally found that due to frictional and other losses the load indicated on the Riehle testing machine dial had to be increased somewhat over that indicated by Equation 3.1.

Upon final adjustment of the axial load, load cell readings were automatically recorded, the dial gages read, and the load cell readings recorded again prior to the next increment in moment. In general it was found that both sets of column load cell readings were the same within the accuracy of the recorder. However, the load cell measuring the moment-producing load was found to drop very slightly, particularly in the latter stages of the test. This was probably due to "creep" or plastic flow. The magnitude of the moment was determined from the last set of load cell readings.

After all the readings were obtained, the moment was incremented and the procedure just described was repeated, that is,

1) The top tie rods were adjusted.

2) The axial load was adjusted if necessary. (It was found that with each moment increment, only a slight, if any, adjustment was required to the load indicated on the testing machine dial).

3) Load cell readings were recorded and the dial gages read.

4) The final load cell readings recorded.

In the early stages of the test, the moment was incremented by observing the load cell readings. In other words, an increment in moment-producing load was applied. In the latter stages of the test, an increment in one of the deflections was applied, that is, the column was strained rather than loaded.

CHAPTER IV - DISCUSSION OF RESULTS

4.1 Specimens Tested

In planning the experimental investigation, it was decided that only a few tests could be performed. Owing to the large number of possible variables (that is, slenderness ratio, axial load, cross-sectional shape, material properties, etc.), it was difficult to decide on which should be varied in the tests. Since the primary purpose of the ivestigation was to check the theoretical analysis, it was decided that at least two different cross-sectional should be investigated. Table 4.1 summarizes the specimens tested. As noted in this table a 2 inch square cross-section (specimens 1, 2, and 5) and a 1.5 inch by 2 inch cross-section (specimens 3 and 4) were selected. Specimens 1 to 4 inclusive had approximately the same minimum slenderness ratio ($\overset{*}{h}/r^{y}$) and can be considered as medium length columns. Medium length (as opposed to short or long) columns were selected so that column action is demonstrated, that is, stability failure. This length of column has the ability to carry fairly large bending moment along with medium size axial loads ($\overline{P}/P_y$ = 0.2 - 0.4, where P_y = yield load for the cross-section). Each type of cross-section was then tested under a medium load (specimens 2 and 3), comparison thus gives the effect of axial load on the moment carrying capacity of the column. A fifth specimen of square cross-section (specimen 5) but with a smaller slenderness ratio than the others was tested. The load for this specimen was about the same as for specimen 2 and direct comparison gives the effect of slenderness ratio on the strength of the column. Only two specimen lengths were tested because of the difficulty in changing the test set-up to accomodate different lengths.

Originally it was intended that the material should be the same for all specimens. However, a quick glance at Table 4.1 shows that this was not the case. All materials were hot-rolled, low-carbon steel. The tubes had a single weld along one side and cold formed. During initial stages of the investigation, 2 inch square tubing was purchased to provide one specimen and enough material for material properties tests. After completion of the tests, additional material was sought. Properties tests on the second, "similar" tubing indicated a much stronger material than the first. The rectangular tube was still a third type and was treated by heating to 1200° F for about 15 minutes and cooled in still air.

The properties of the material were determined by tests on stub columns having a slenderness ratio less than 10 and by tension tests. For the stub column tests, four electrical resistance strain gages were mounted symmetrically on the tube and the specimen tested in a Tinius-Olsen (small) hydraulic testing machine in accordance with the procedure given in Reference 11. The tension tests were performed in accordance with the ASTM specifications.

For specimen 1, only tension tests were performed. Test coupons were cut from all four sides and tested to determine the stress-strain curve. All the four curves were very similar in shape and showed a maximum variation in "yield stress" of about six percent. The average of the four sides is shown in Fig. 4.1 and was used to determine $\alpha(=E_t/E)$ and ϵ_y.

For the remaining specimens, stub column tests were used to determine the mechanical properties. In addition a tension test on material of specimen 2 was performed and found to be very similar to the stub column test. The main difference being that the knee of the curve from stub column test was not as sharp as from the tension tests owing to the effect of residual stresses in the cross-section. These stresses can be as high as 20 ksi (24).

Results of the stub column test from the material of the specimen 2 are given in Fig. 4.2 and those from specimen 3 are given in Fig. 4.3. The curve of Fig. 4.2 was assumed to represent the material of specimen 5 since it came from the same length as specimen 2. The specimen 3 and 4 were also the same material, but were received in two different pieces, thus it could not be determined if they were both from the same length. Tests on the material of specimen 4 indicated a yield of 38.3 ksi as compared with 34.8 ksi from specimen 3. In determining the yield stress for specimen 4 no strain gages were used, the yield load being determined by the stop of the dial and also local buckling of the walls of the specimen.

The approximation of the bilinear curve for specimen 2 and 5 needs some explanation. It was found from the theoretical results that due to the size of the axial load and slenderness of the columns, the maximum strains at failure were quite low (on the order of 4 times the yield strain). Strain measurements on specimen 5 (to be mentioned shortly) bore this out. Hence, if the stress-strain curve were approximated by neglecting the knee of the curve, the results would be erroneous. The bilinear curve used was found by approximating the curve up to about 5 times the yield strain. Although this is not a particularly good approximation, the theoretical results compared very favorably with the experimental results (Section 4.2).

4.2 Experimental Results

For the specimens described in Section 4.1 deflections in the principal directions of the cross-section were measured at the midpoint of the specimen excluding end fixtures. End rotations about each axis were also measured. Dimensionless plots of the experimental results are given in Figs. 4.4 to 4.8 inclusive along with theoretically obtained curves.

Since the moment arm was attached considerably ($11\frac{3}{8}$ in.) below the axes of rotation of the end fixture, a correction in the experimentally determined moments was made to account for the change in length of the moment arm due to the rotation of the end of the specimen. The maximum correction obtained was about three percent. Owing to the length of the rods applying the load to the lever arm (minimum of 50 in.), the load on the moment arm can be considered to be vertical.

In determining the theoretical curves, the theory was modified to include the end fixtures and the column load cell. For all practical purposes, the end fixtures used in this study can be considered as rigid; hence their curvatures are zero. The column load cell always remained elastic; thus its shape is easily determined from elastic theory.

Table 4.2 shows the theoretical and experimental values of the peak moment about the x-axis divided by M_y^x. As noted from this table the results compare very favorably with the maximum error being about two percent.

Of prime importance to the test results is the variation in axial load during the progress of a test, since comparison between theoretical and experimental deflections depends on the load being constant. The percent variation in load as determined by the strain gage readings is shown in Fig. 4.9 for each of the five tests. The maximum variation noted is three percent with the average variation being considerably less. As evident from these figures, a high degree of success was achieved in maintaining a constant axial load throughout the test. This can be credited to using fairly small increments in moment, adjusting the axial load at each increment, and a constant surveilence of the hydraulic testing machine load dial throughout the test.

Referring again to Figs. 4.4 to 4.8, it can be seen that the shapes of the experimental and theoretical curves are very similar. As expected, tests 2 and 5 show the most variation since the bilinear stress-strain curve is not too good an approximation to the true stress-strain curve. The effects of residual stresses is also quite evident in the results. Once inelastic action begins, the predicted deflections and rotations are less than those determined in the tests. As noted in previous research (23) the effect of residual stresses is to reduce the ultimate capacity by a small amount which depends on the dimension of the column. This is probably the main reason for the deviations noted in Table 4.2. The main effect of residual stresses is that yielding begins at a lesser moment which results in greater deflections. This can be seen clearly from Figs. 4.5 and 4.6 and partly from results of the remaining tests.

For all tests no twisting could be detected visually. Measurements on columns 4 and 5 were attempted by clamping a bar perpendicular to the column near midheight and measuring two displacements on the bar a distance 14 inches apart. The differences in the two gage readings for test 4 increased slightly (.02 inches) from zero to about two-thirds of the ultimate moment and then remained constant. For test 5 there was at most a difference in the two readings of .003 inches.

For column 5 a comparison was made of the maximum strains measured at a section 14 inches from the bottom end (excluding the end fixture) with those obtained theoretically as shown in Fig. 4.10. This also established the presence of residual stresses in the material used for specimens 2 and 5.

The effect of unloading and reloading was observed on specimens 2 and 5. Specimen 2 was reloaded after initial failure by first applying the moment given by peak of the curves in Fig. 4.5 and then applying the axial load. The column remained in equilibrium as long as the peak moment was there but became unstable on the application of a negligible amount of the axial load. Specimen 5 was reloaded by first applying the same constant axial load as given in Table 4.1 and then incrementing the moment till the column became unstable. The column could carry about 93 percent of the previous peak moment (that is, the peak moment in Fig. 4.8).

4.3 Theoretical Study

4.3.1 Study of Variables

The effect of varying the following factors is studied:

1) the moment ratio γ;

2) the strain-hardening factor α of the material;

3) the number of points to be used in a column integration; &

4) the length of the rigid end fixtures forming part of the beam-column in the apparatus used for the testing.

The column selected for the study of the above four factors has the same dimensions as for the first test specimen.

A plot of the peak moments versus γ is shown in Fig. 4.11. It is evident from the figure that an increase in the applied moment about one principal axis of the column cross-section reduces its carrying capacity about the other principal axis.

Fig. 4.12 shows effect of the strain-hardening on strength of the column. The variation of the peak moments with α follows approximately the relation

$$\left[M_A^x/M_y^x\right]_{max} = 0.9489 + 1.43\alpha$$

for this particular case and for α between 0.0 and 0.08. It is readily apparent that for $\alpha = 0.08$, the moment capacity of the column increases by about 12 percent. Larger values of α would undoubtedly show a much larger increase in moment capacity.

In effect, considering the strain-hardening would mean that the material in the column which is strained beyond the yield changes its modulus of elasticity to E_t which is less than E and is, therefore, still able to carry extra load, while neglecting it would mean that no load is carried by the yielded material in the column and the only load-resisting portion is the remaining elastic core. This can be clearly seen from the curves shown in Fig. 4.12. As long as the column remains elastic, strain-hardening does not come into play and the moment-deflection curve is common for all α values, however, thereafter, yielding begins and the column whose yielded material also offers resistance to the external load gives a higher peak moment than the one whose yielded material offers a little or no resistance.

The effect of the number of points selected for the column integration procedure (summarized in Section 2.2) on the prediction of the peak moment is shown in Fig. 4.13. The length of a panel (which in turn determines the number of points for column integration) directly affects the computational time required for convergence of the solution. Since the column integration is carried out on the basis of assuming each individual panel to be a segment of a circle, it implies that every section has the same moment. Speaking in the absolute terms, this is not true because the moment varies along the length. Nevertheless, it is reasonable to assume that the change in moment between two consecutive sections is fairly small if their mutual distance is small. Fig. 4.13 shows that, for the case considered, as low as seven points for column integration yield fairly good results.

Fig. 4.14 shows the variation of the peak moment with the length of the rigid end fixtures that form a part of the beam-column. For a small value of L_r/D, that is, the non-dimensional length of the rigid end fixture, the peak moment remains almost unaffected, however, it increases with bigger values of L_r/D. This is understandable because if a greater part of the column is rigid, the non-rigid portion will be more stocky and hence carry a higher load.

4.3.2 Column Integration Using Single Pass

For an increased accuracy, two passes through each panel point in the column integration procedure are made as described in Section 2.2. Since this involves extra computational time, the effect of making only a single pass through each panel point is studied by means of the following example:

Section : 2 in. by 2 in. by 0.1325 in.

Axial Load, $\bar{P}/P_y$ = - 0.2

Moment Ratio, γ = 0.75

Strain-hardening factor, α = 0.0322

Yield Strain, $\epsilon_y = 0.0011$ in. per in.

Slenderness Ratio, $h/r_c^y = 40.0$

It was observed that this resulted in a thirty percent saving in the total computational time as compared to that required by making two passes. A very slight variation in the collapse load and the deflections was noted even though a small slenderness ratio was chosen, and the results were found to be on the conservative side.

Table 4.1 Summary of the Tests Performed

Specimen Number	h_s (in.)	h^*/r^Y	Cross-Section (in.)	E (ksi)	$\alpha=(\frac{E_t}{E})$**	ϵ_Y in./in.	$\overline{P}/P_Y$
1	60.0	78.5	2 by 2 by .1325	29,600	.0322	.001311	-.209
2	60.0	78.5	2 by 2 by .1225	28,000	.1200	.001575	-.406
3	42.6	86.0	1.5 by 2 by .1238	26,400	.0000	.001320	-.326
4	42.9	86.0	1.5 by 2 by .1238	27,000	.0000	.001419	-.187
5	43.0	66.0	2 by 2 by .1225	28,000	.1200	.001575	-.406

**As determined from the bilinear approximation.

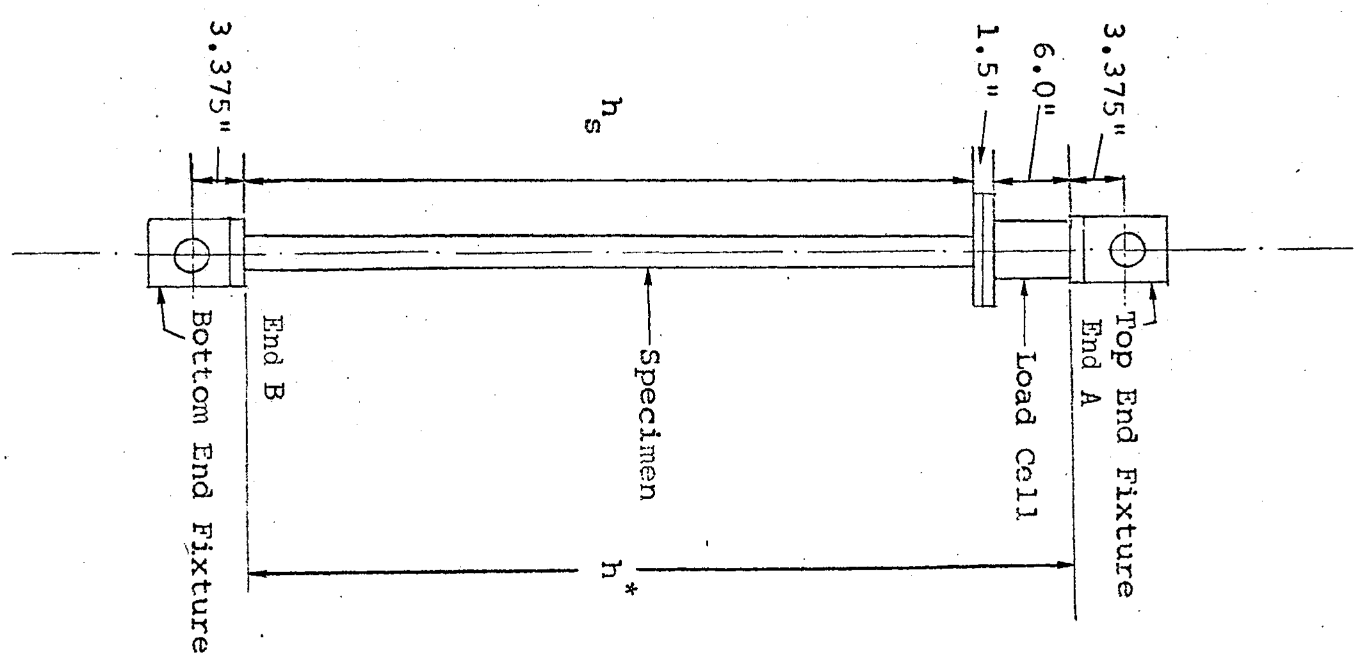

Table 4.2 Comparison of Theoretical and Experimental Peak Moments about the x-axis

Test (1)	M^x/M^x_y Experimental (2)	M^x/M^x_y Theoretical (3)	$\frac{(2)}{(3)}$
1	0.980	0.985	1.00
2	0.486	0.498	0.98
3	0.715	0.722	0.99
4	0.958	0.956	1.00
5	0.695	0.701	0.99

CHAPTER V - CONCLUSIONS AND FUTURE RESEARCH

5.1 Conclusions

The following conclusions are drawn from this study:

1) The experimental results agree very closely with those predicted by the theory. This shows that the theoretical solution can be used to predict the load-deflection curves and the collapse load with a high degree of accuracy, at least for the range of parameters considered.
2) Twisting may be neglected for columns of hollow tubular cross-section.
3) Residual stresses in the columns tested appear to have very little effect on their strengths.
4) Strain-hardening increases the carrying capacity of at least some columns. For design purposes, it will be conservative to neglect it. On the other hand, if considerable strain-hardening is present it should be considered in determining the strength of the column.
5) An increase in the bending moment about one principal axis of the column's section reduces its carrying capacity about the other principal axis assuming the same value of the axial load.
6) An increase in axial load or slenderness ratio results in a reduction of the moment carrying capacity of the column.

5.2 Future Research

A study of some of the remaining parameters not done in this thesis should be made such as the width-to-depth ratio of the section, wall thickness, effect of residual stresses, etc. A comparison of the carrying capacity of the beam-column with the section studied herein should be made with those having other cross-sectional shapes such as hollow circular, solid rectangular and wide flange to determine the most efficient section.

An attempt should be made to develop thrust-moment-curvature relationships for columns of nonlinear materials, since if this can be made possible, the same or a similar method of analysis can be applied to concrete and aluminum columns.

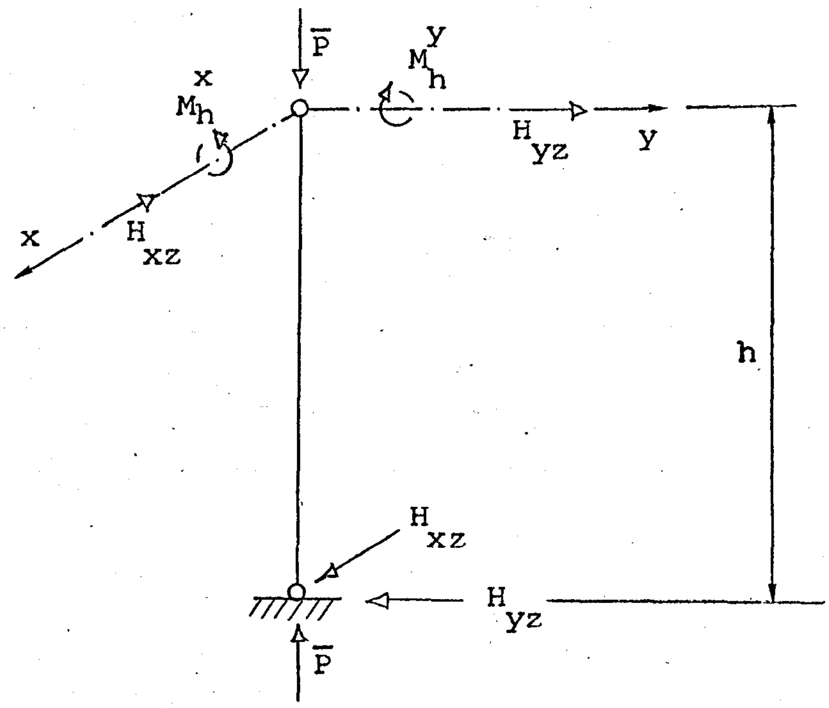

Fig. 2.1 A Typical Biaxially Loaded Beam-Column

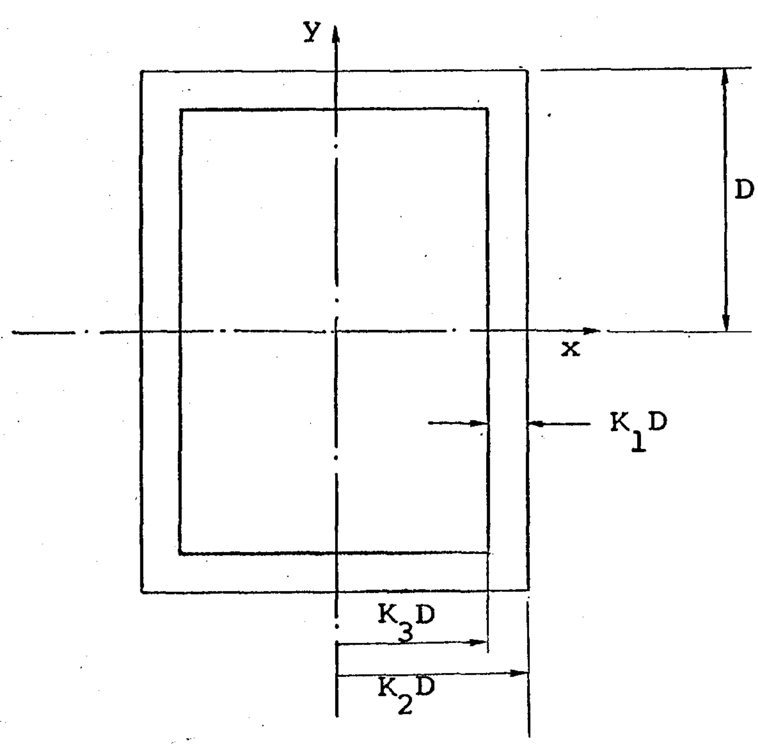

Fig. 2.2 Beam-Column Cross-Section

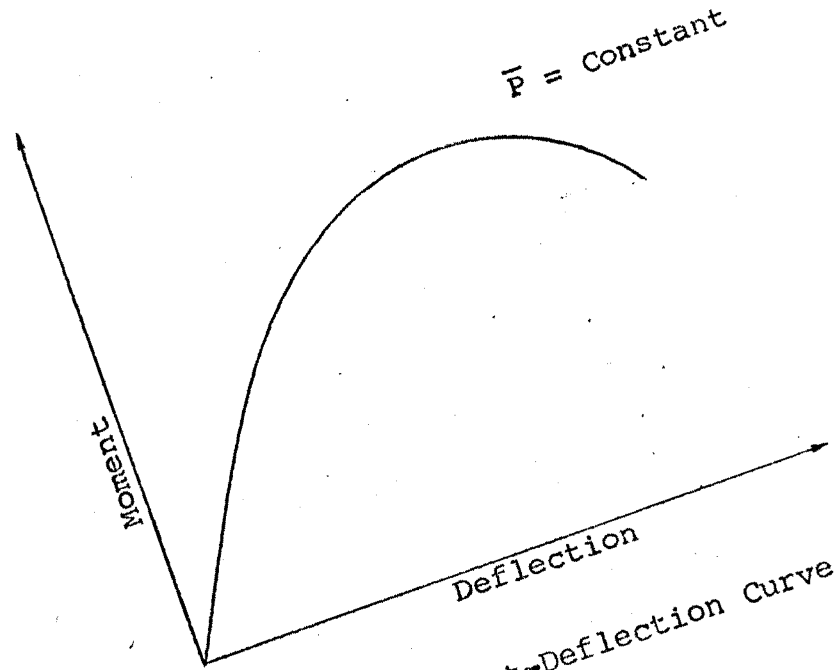

Fig. 2.3 Moment-Deflection Curve

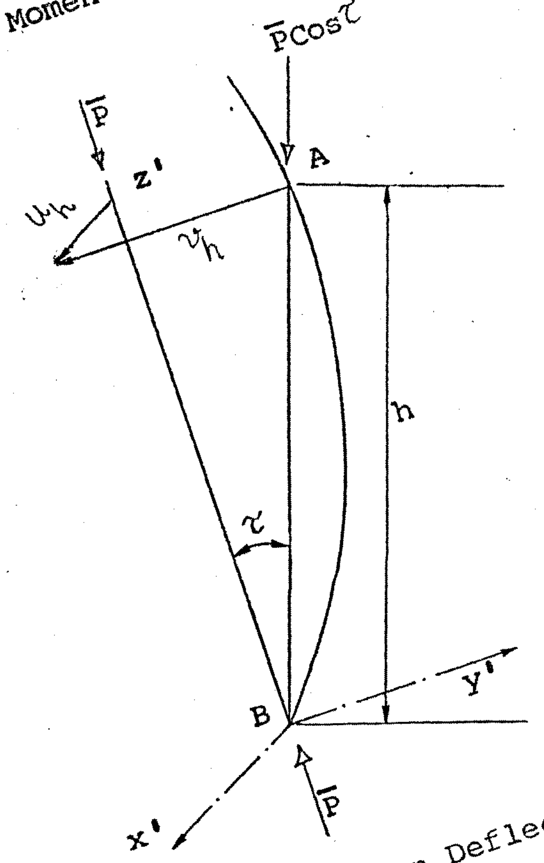

Fig. 2.4 Column Deflection Curve

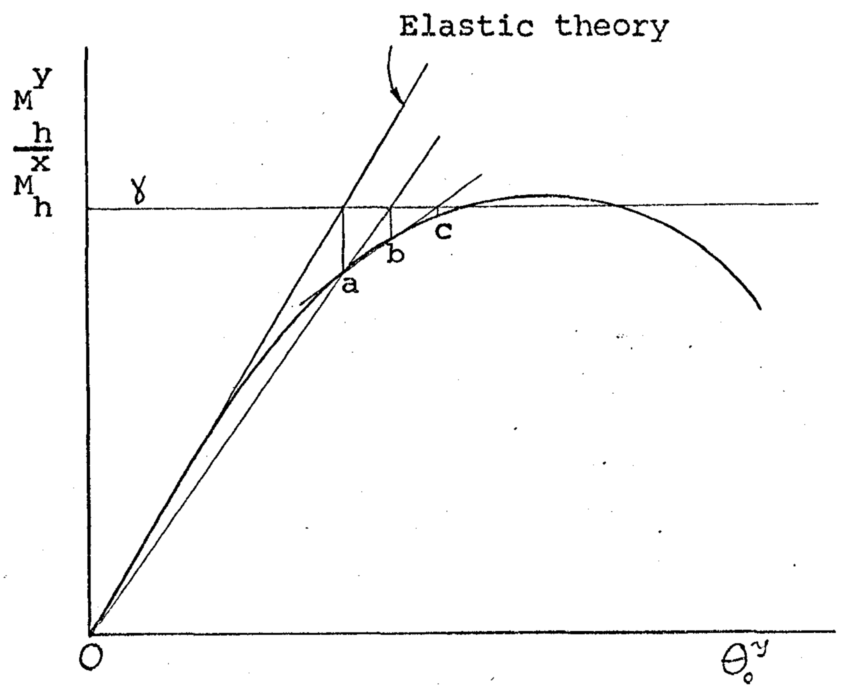

Fig. 2.5 Correction for θ_o^y

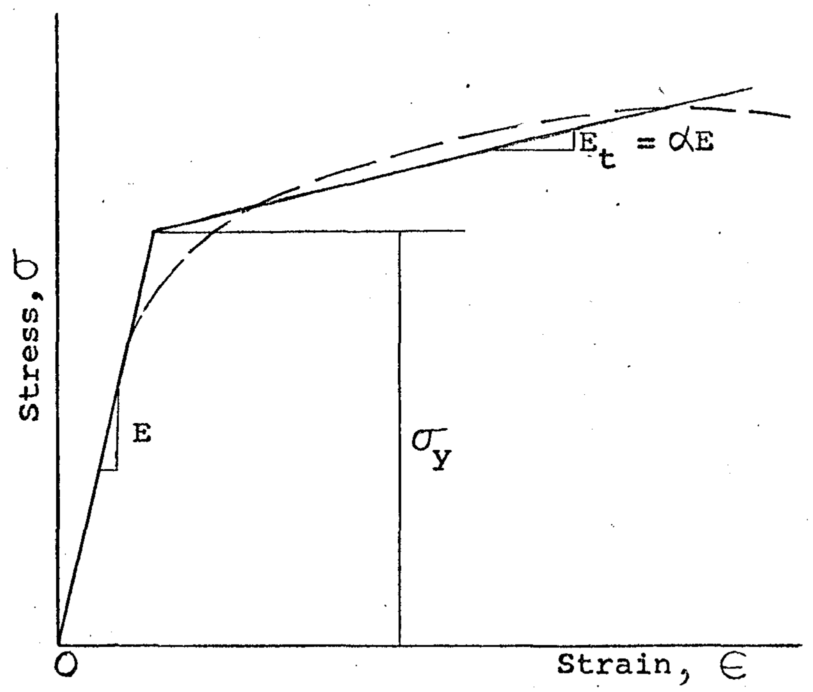

Fig. 2.6 Stress-Strain Relationship for Material of the Beam-Column

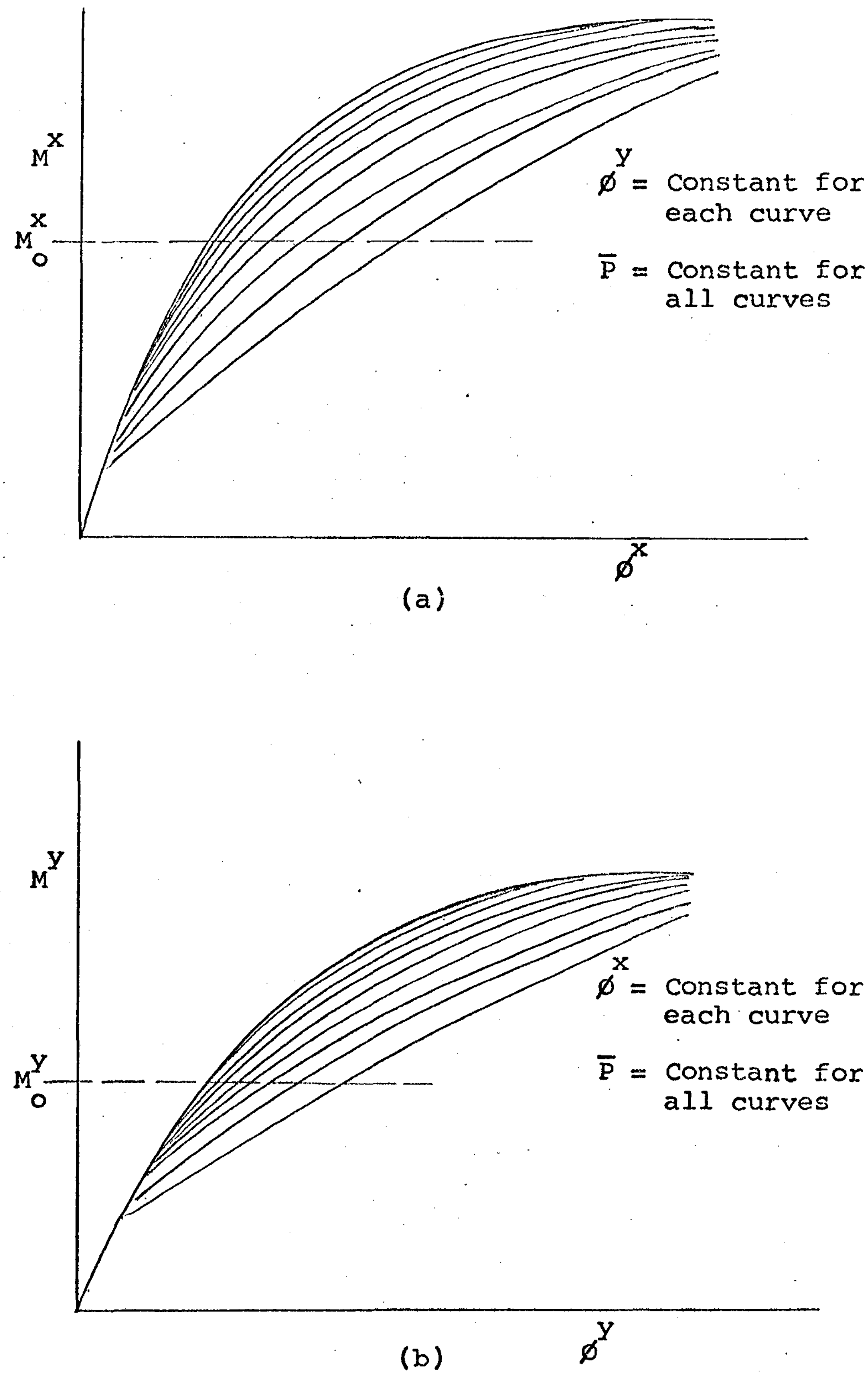

Fig. 2.7 Moment-Curvature Curves

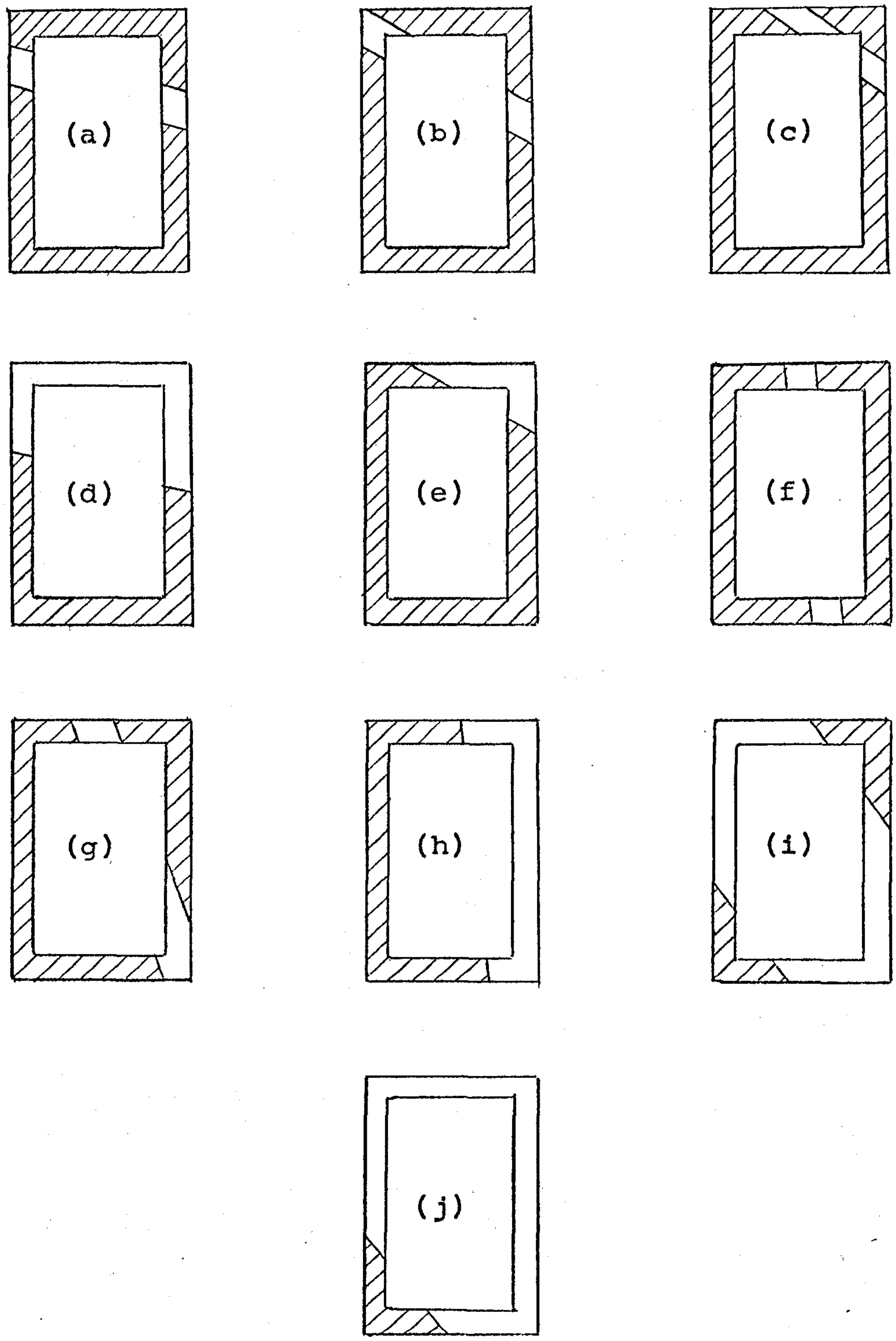

Fig. 2.8 Possible Yield Configurations in a Biaxially Loaded Rectangular Tubular Beam-Column

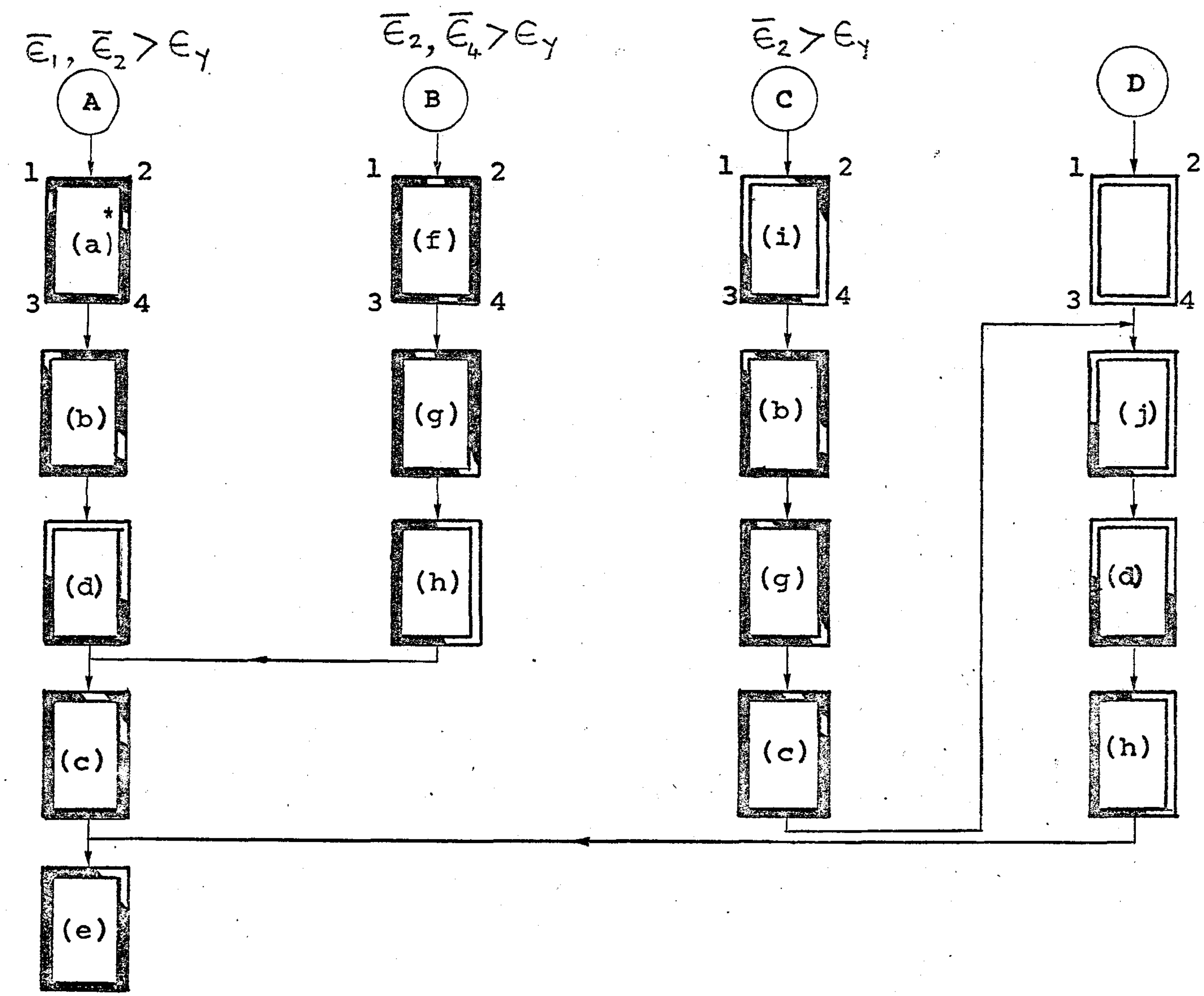

*Letters refer to Fig. 2.8

Fig. 2.9 Sequence for Checking Yield Patterns

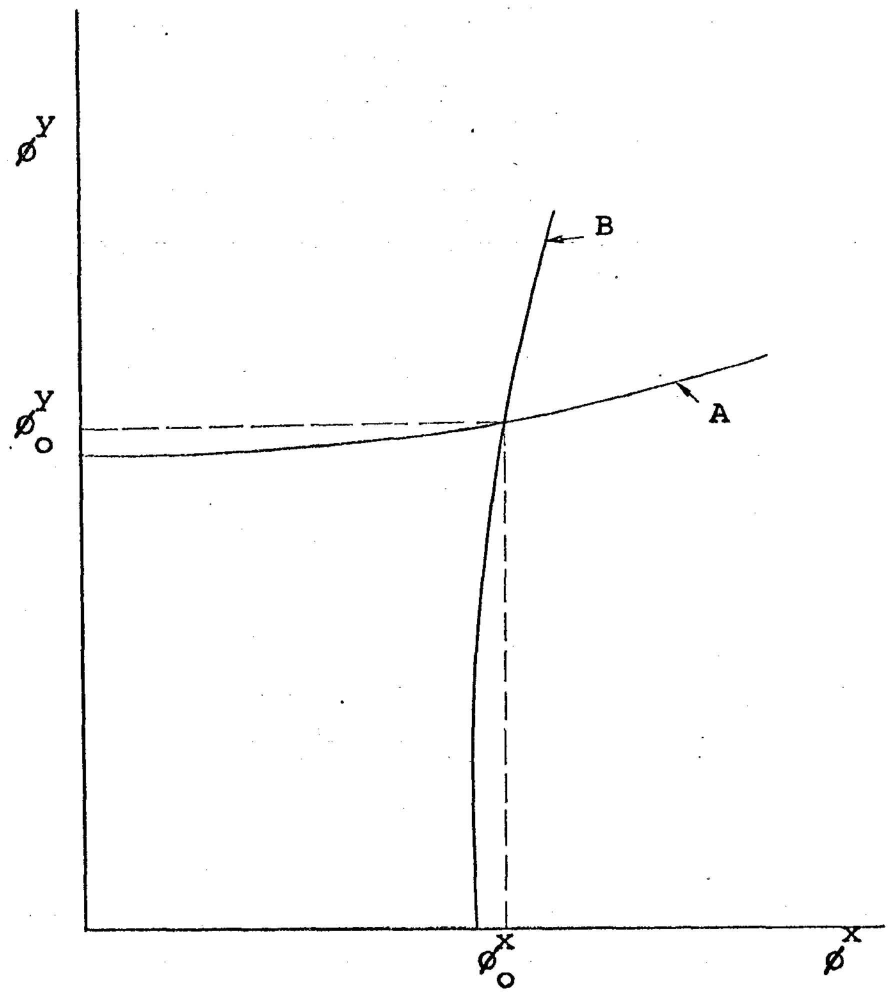

Fig. 2.10 Constant Moment, Curvature Curves

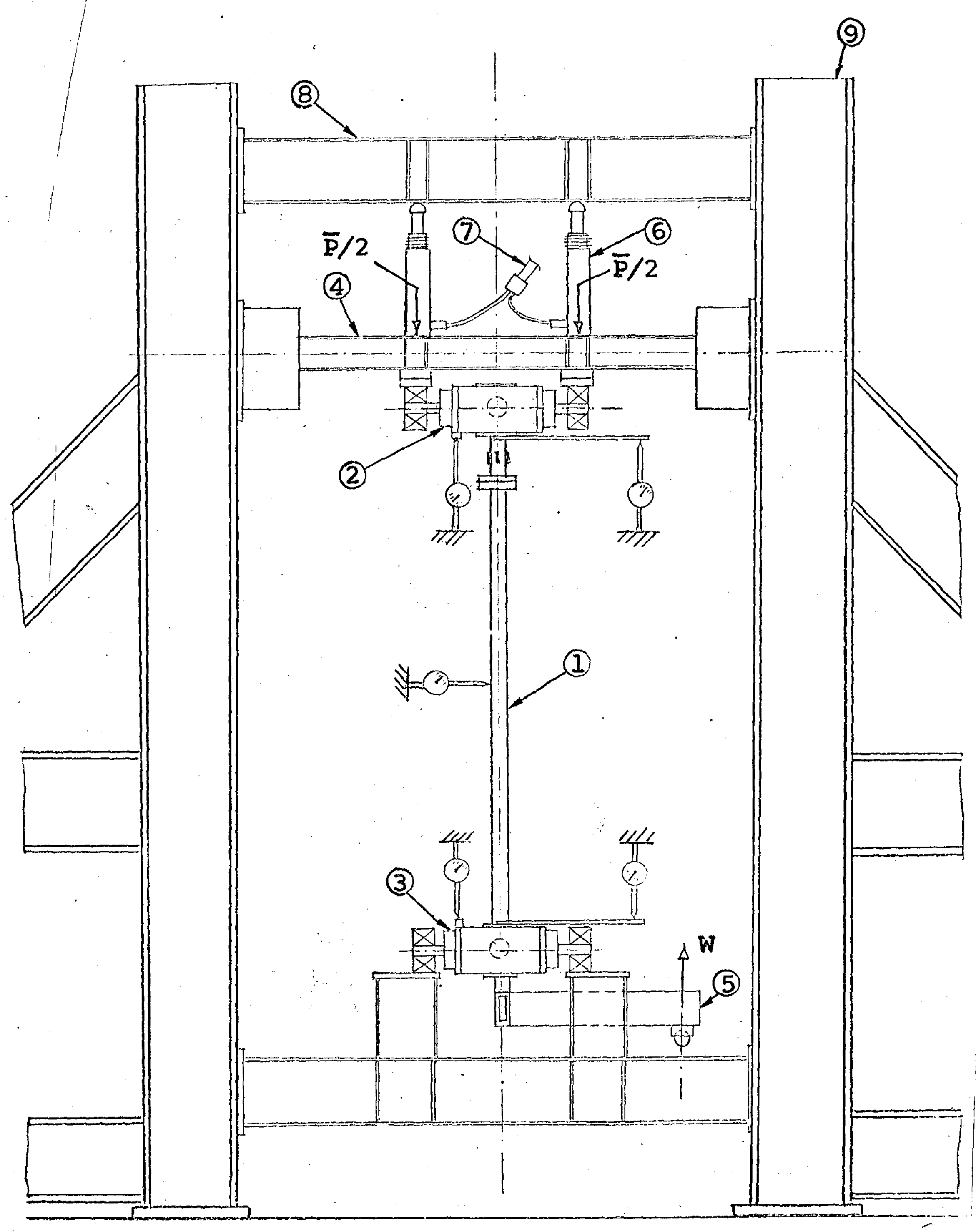

Fig. 3.1(a) Elevation of Main Skeleton of the Apparatus shown Schematically

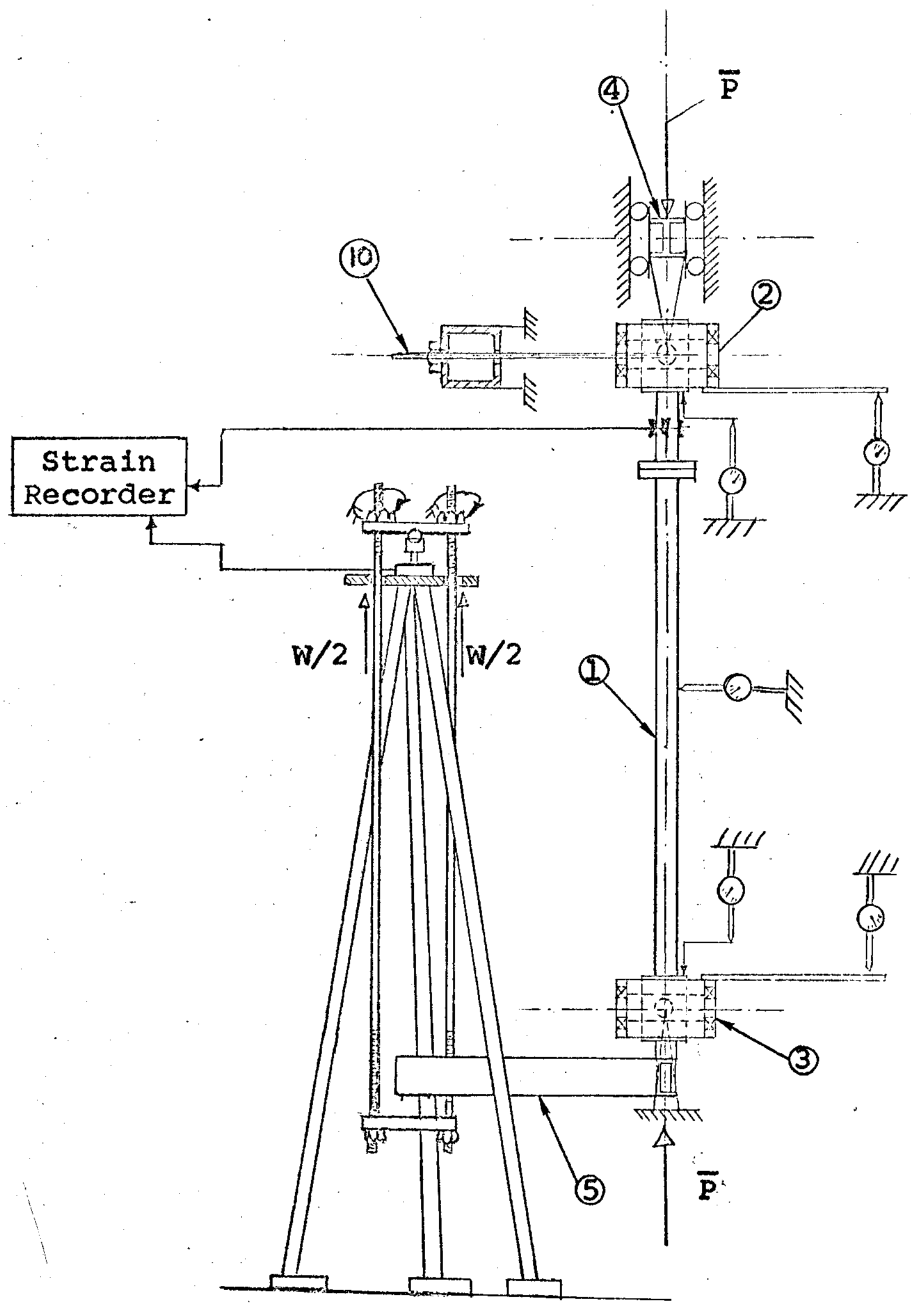

Fig. 3.1(b) Schematic End-View of the Apparatus

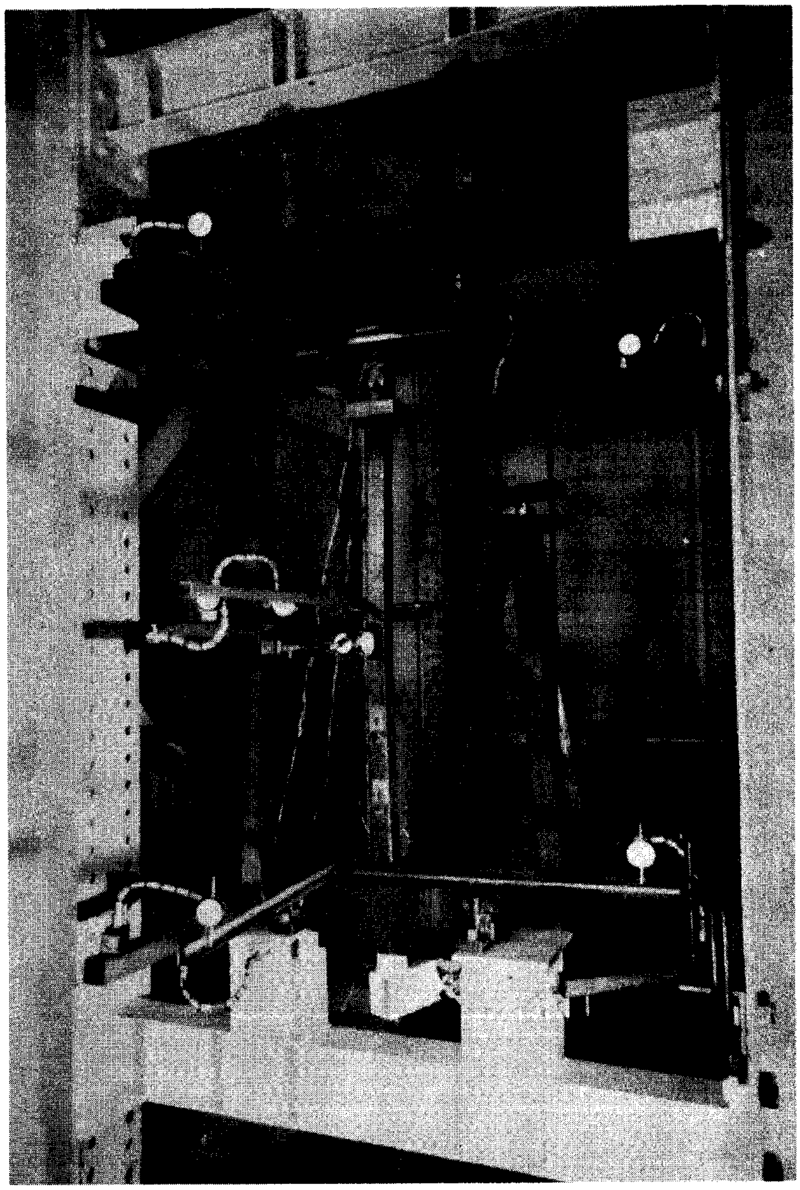

Fig. 3.2 Test Set-up

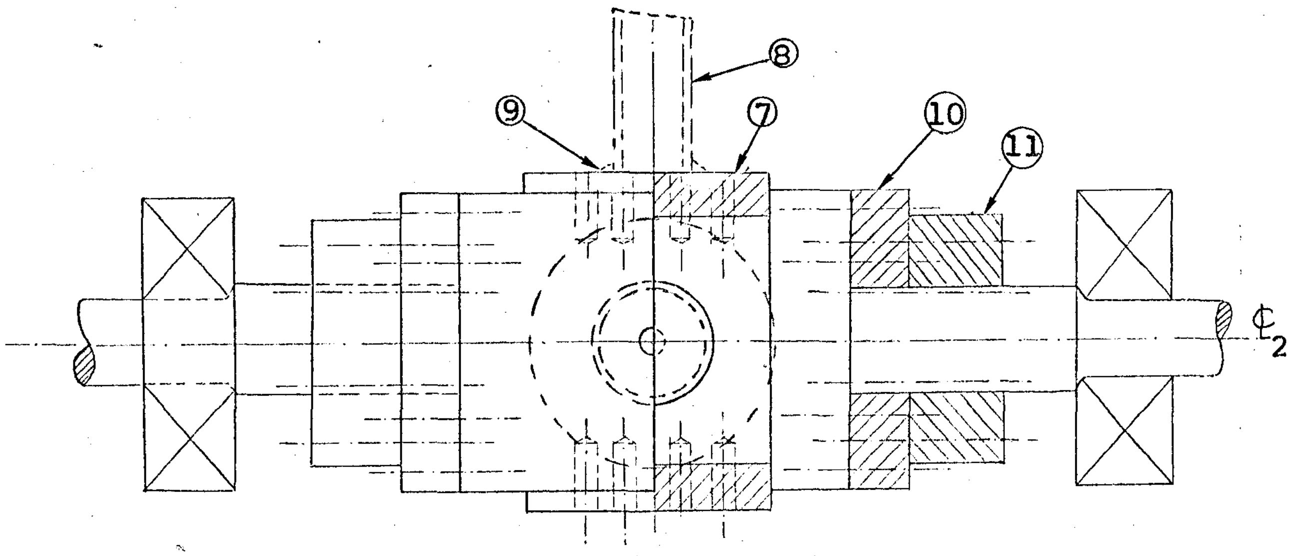

Fig. 3.3(a)* Sectional Elevation of the End Fixture

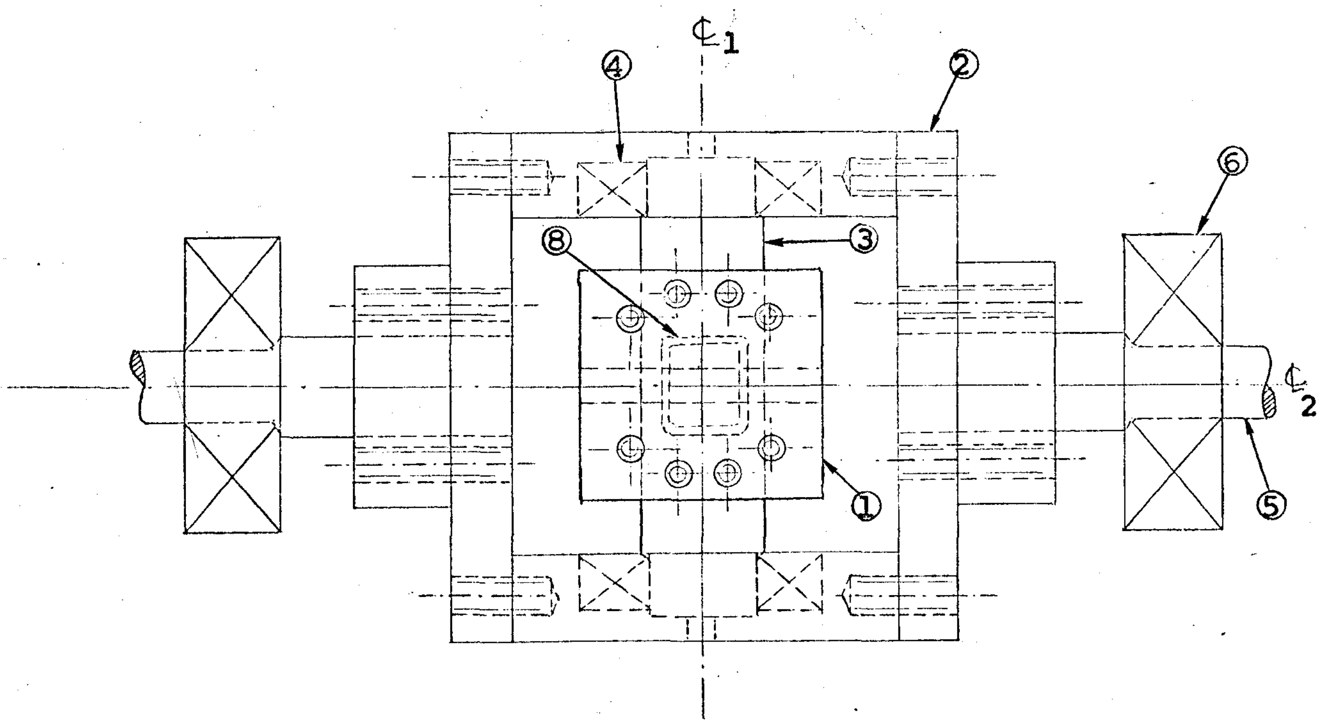

Fig. 3.3(b) Plan View of the End Fixture

*Refer to the Table on page 51.

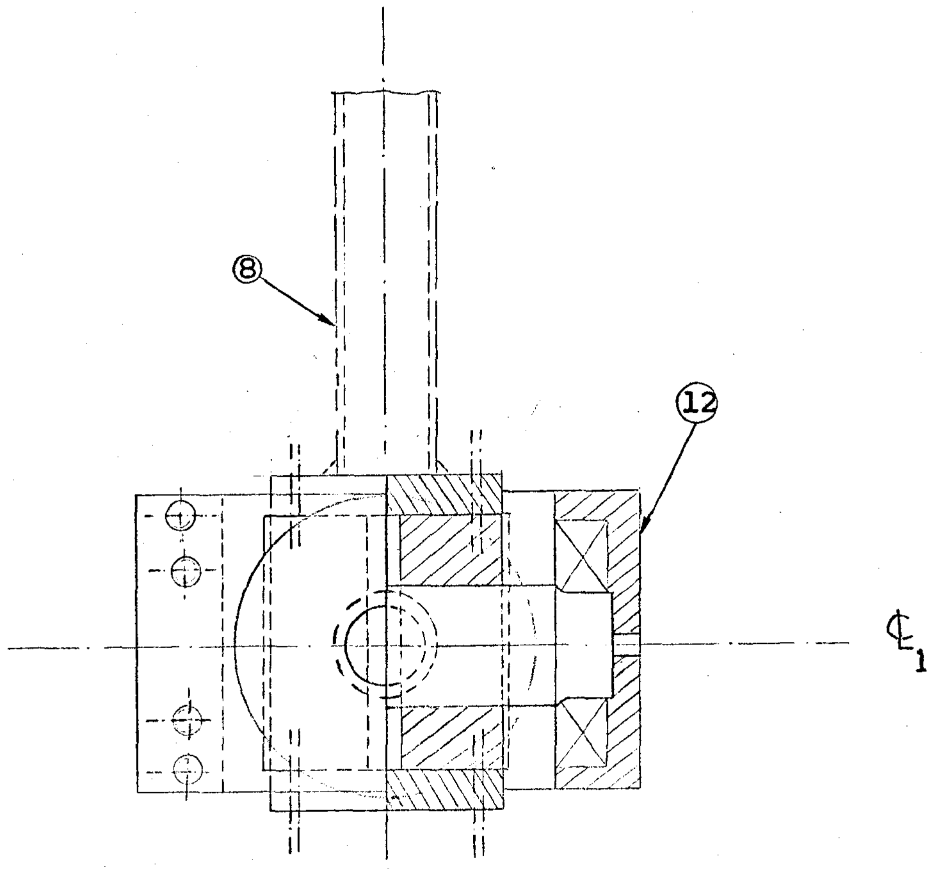

Fig. 3.3(c) Sectional End-View of the End Fixture

Table Corresponding to Fig. 3.3

1	Inner Part of the End Fixture
2	Outer Part of the End Fixture
3	Shaft with the center-line 1
4	Frictionless Spherical Roller-Bearing at end of the shaft
5	Shaft with the center-line 2
6	Frictionless Sperical Roller-Bearing in the Pillow-Block
7	Base-Plate for the Beam-Column End
8	Specimen Position
9	Weld
10	Wall of Outer Part of the End Fixture, housing shaft
11	Reinforcing Wall for 10
12	Wall of Outer Part of the End Fixture, housing 4

Notes: (1) The point of intersection of the center-line 1 with the center-line 2 is the real "end" of the beam-column.

(2) Bix dotted "X" mark represents a bearing.

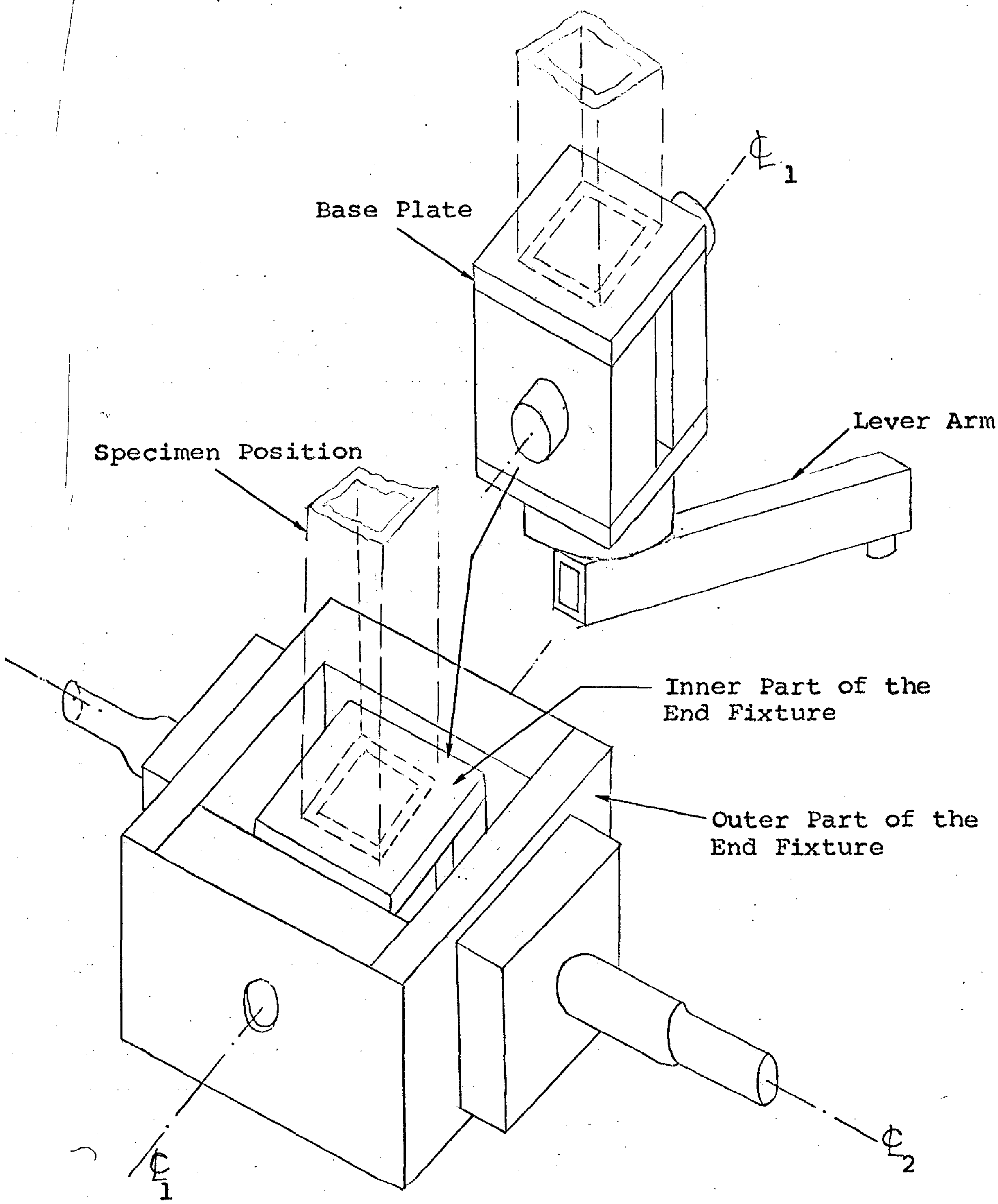

Fig. 3.4 Schematic View of the End Fixture

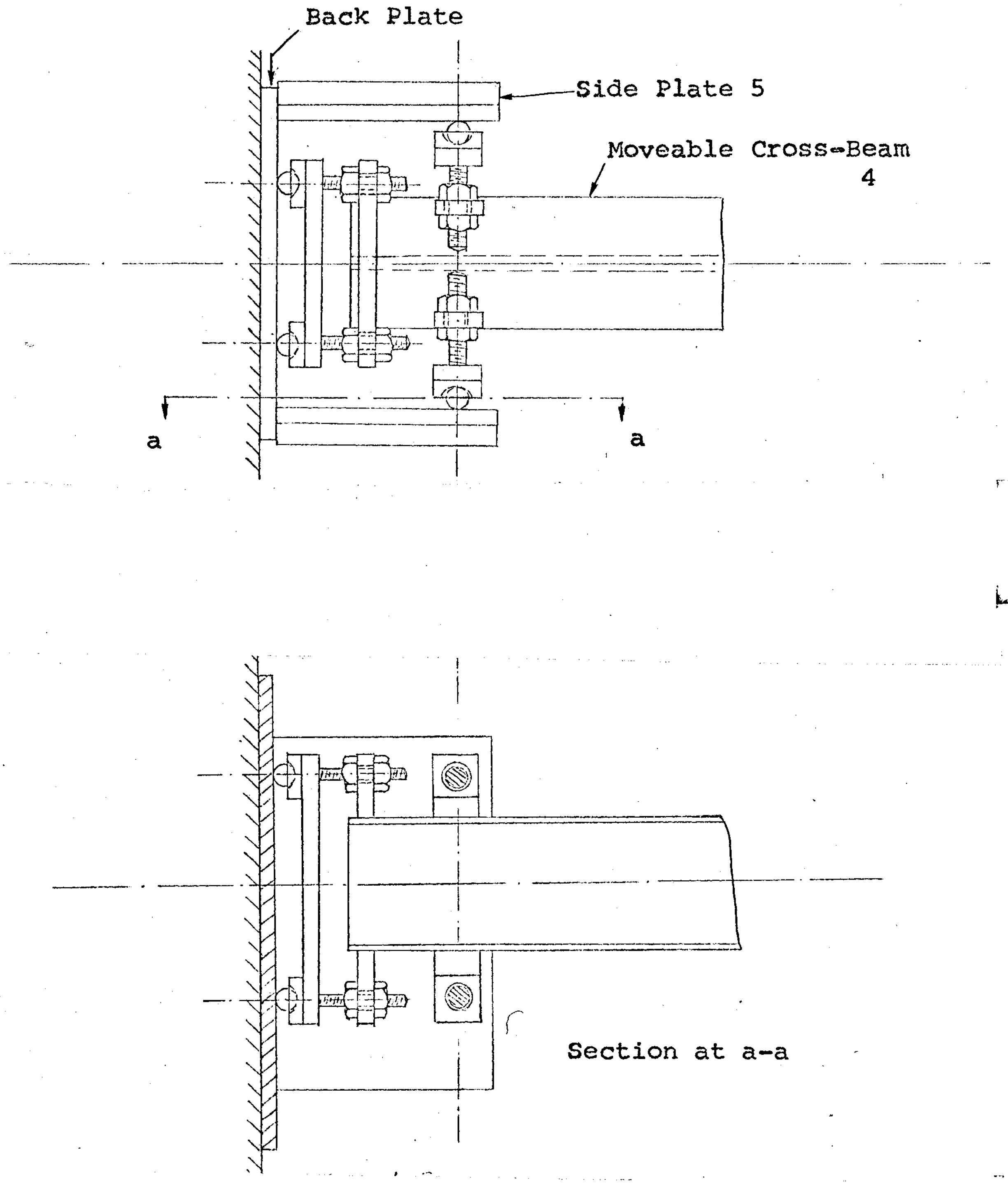

Fig. 3.5 End-Support for the Beam 4

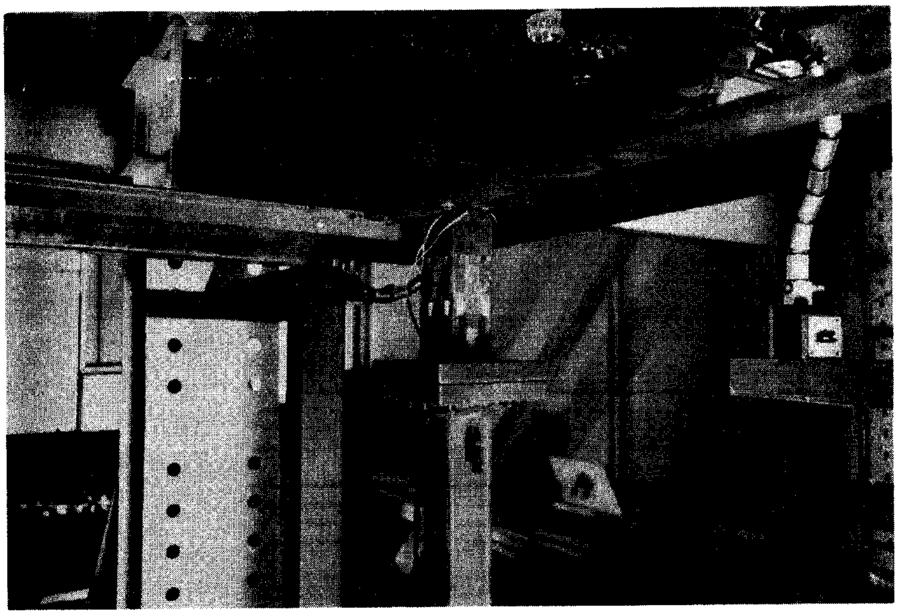

Fig. 3.6 Axial Load, Load Cell

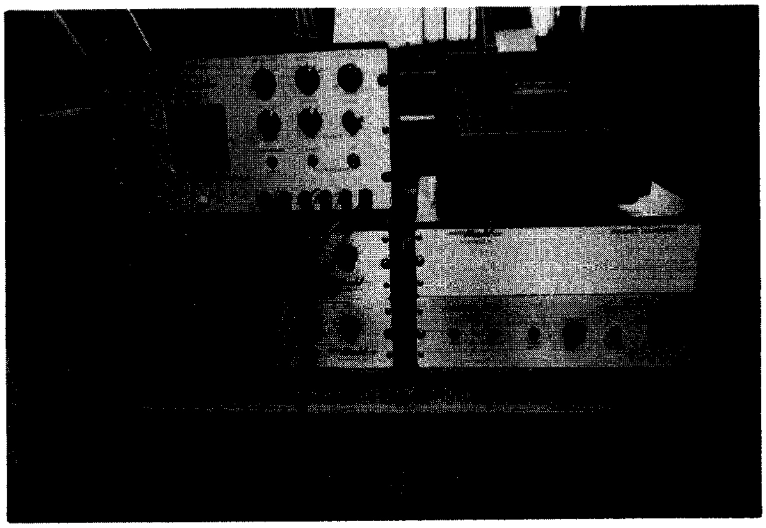

Fig. 3.7 Strain Measuring Apparatus

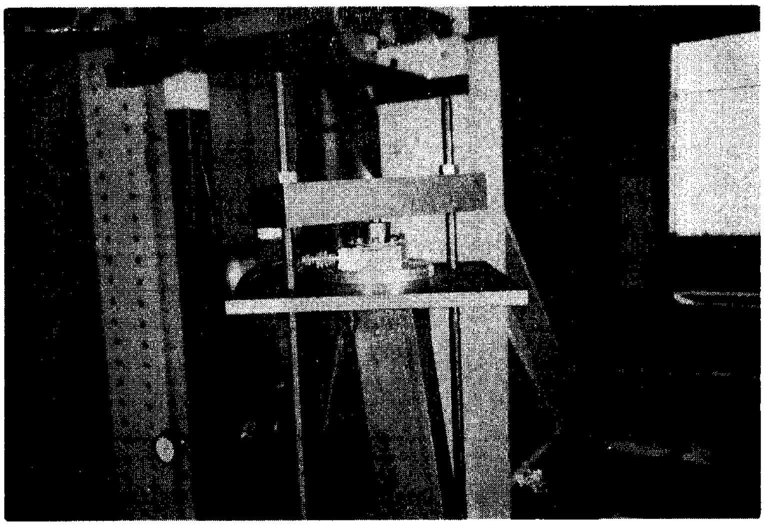

Fig. 3.8(a) Load Cell for Measuring the Moment-Inducing Load W, placed on the Tripod

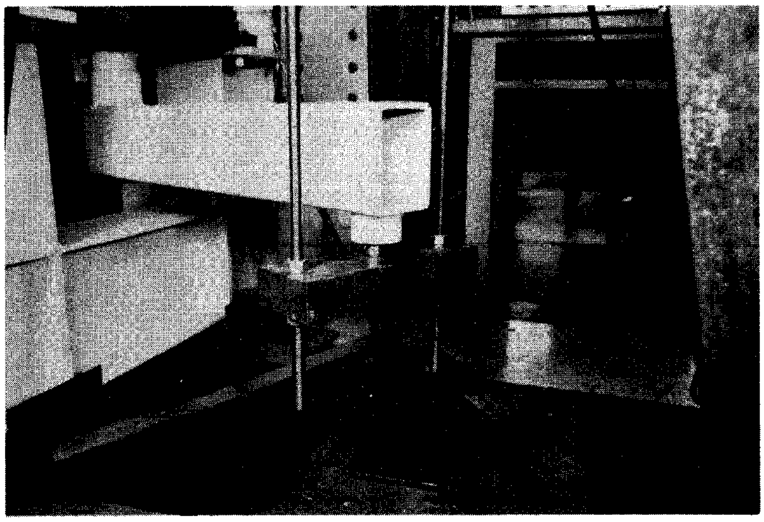

Fig. 3.8(b) Lever Arm and Its Connection with the Tie Rods

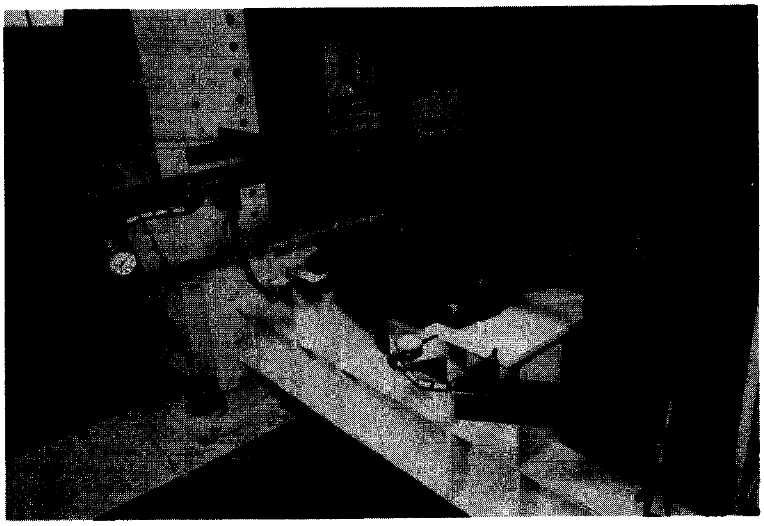

Fig. 3.9 Measurement of End Rotation

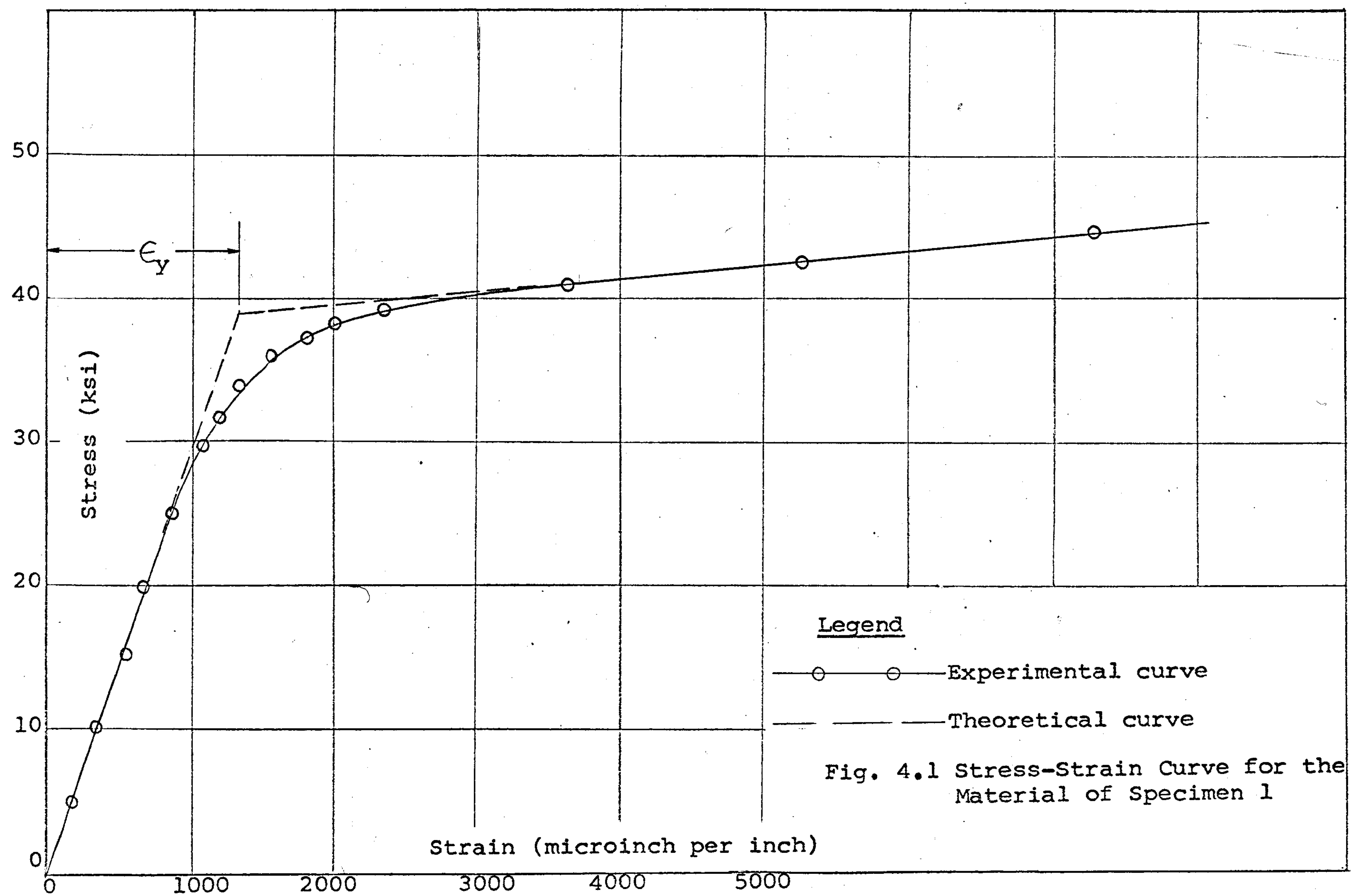

Fig. 4.1 Stress-Strain Curve for the Material of Specimen 1

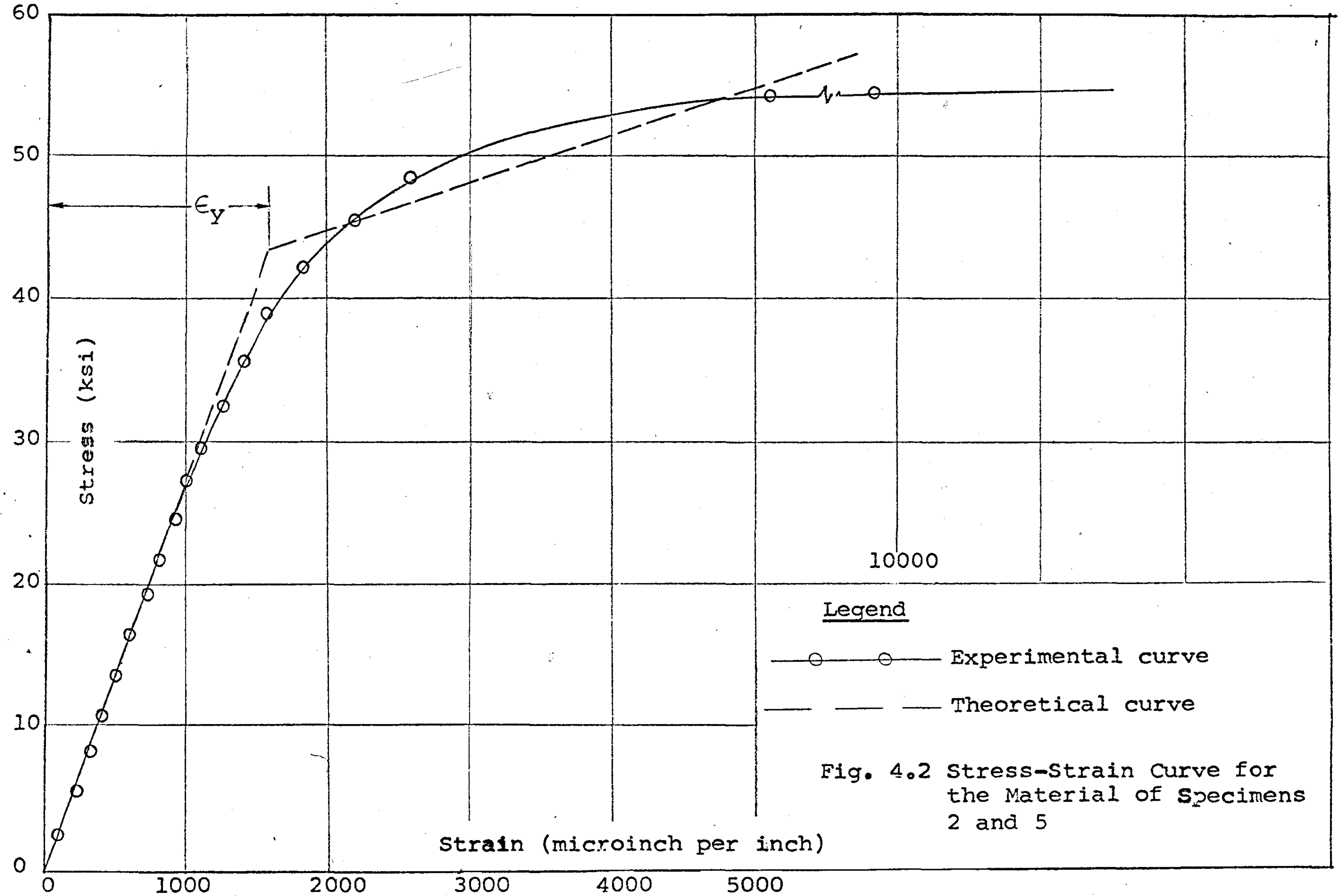

Fig. 4.2 Stress-Strain Curve for the Material of Specimens 2 and 5

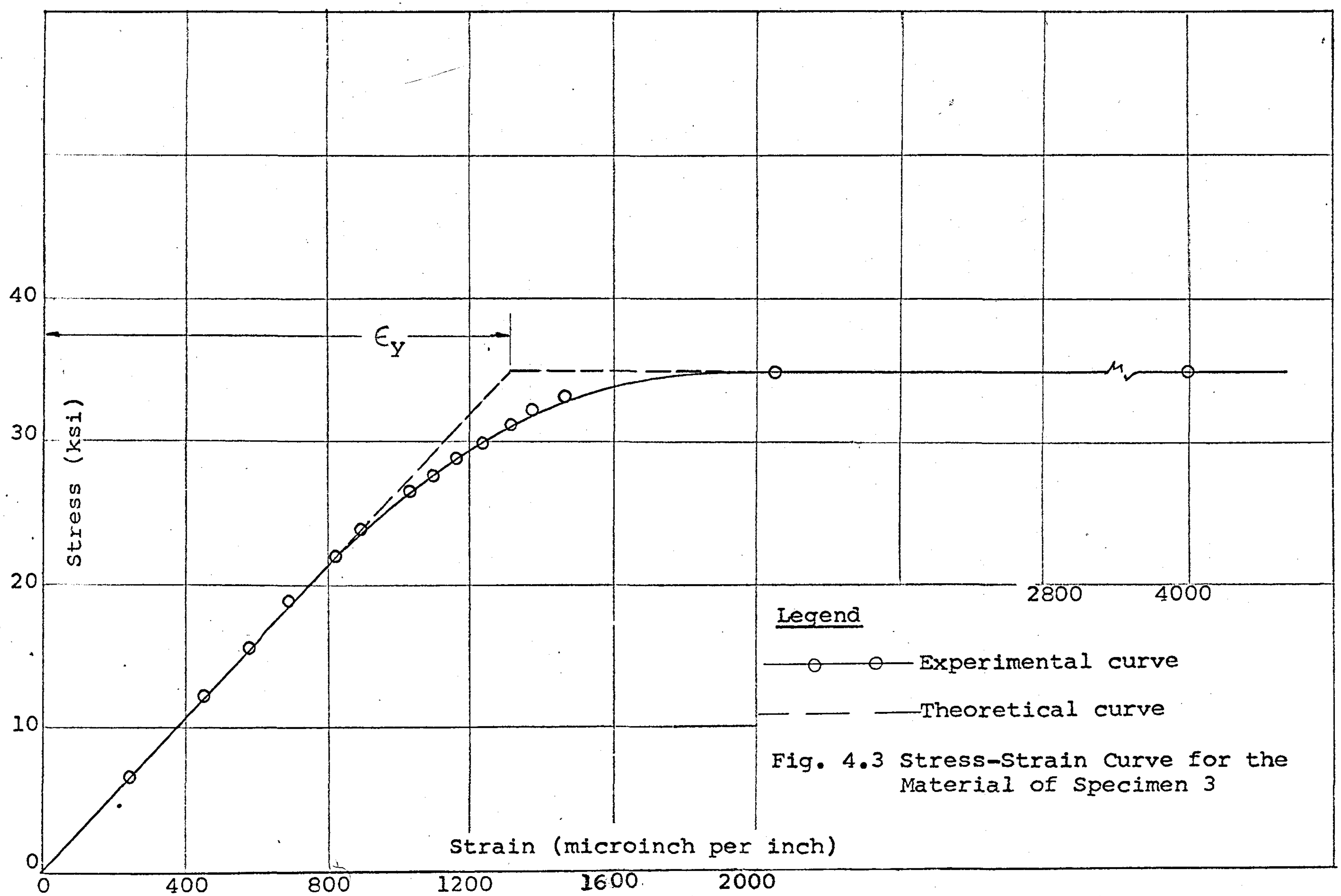

Fig. 4.3 Stress-Strain Curve for the Material of Specimen 3

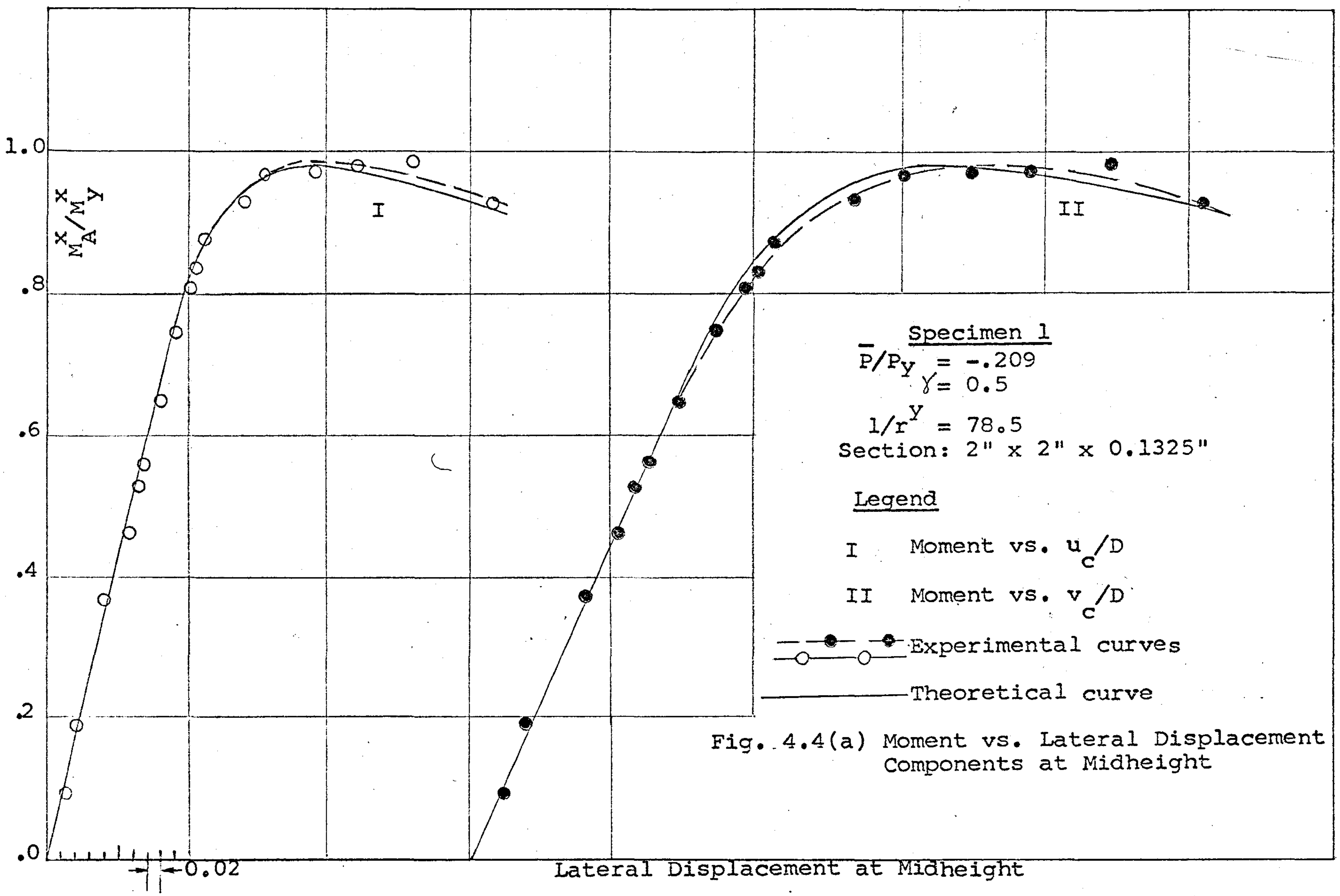

Fig. 4.4(a) Moment vs. Lateral Displacement Components at Midheight

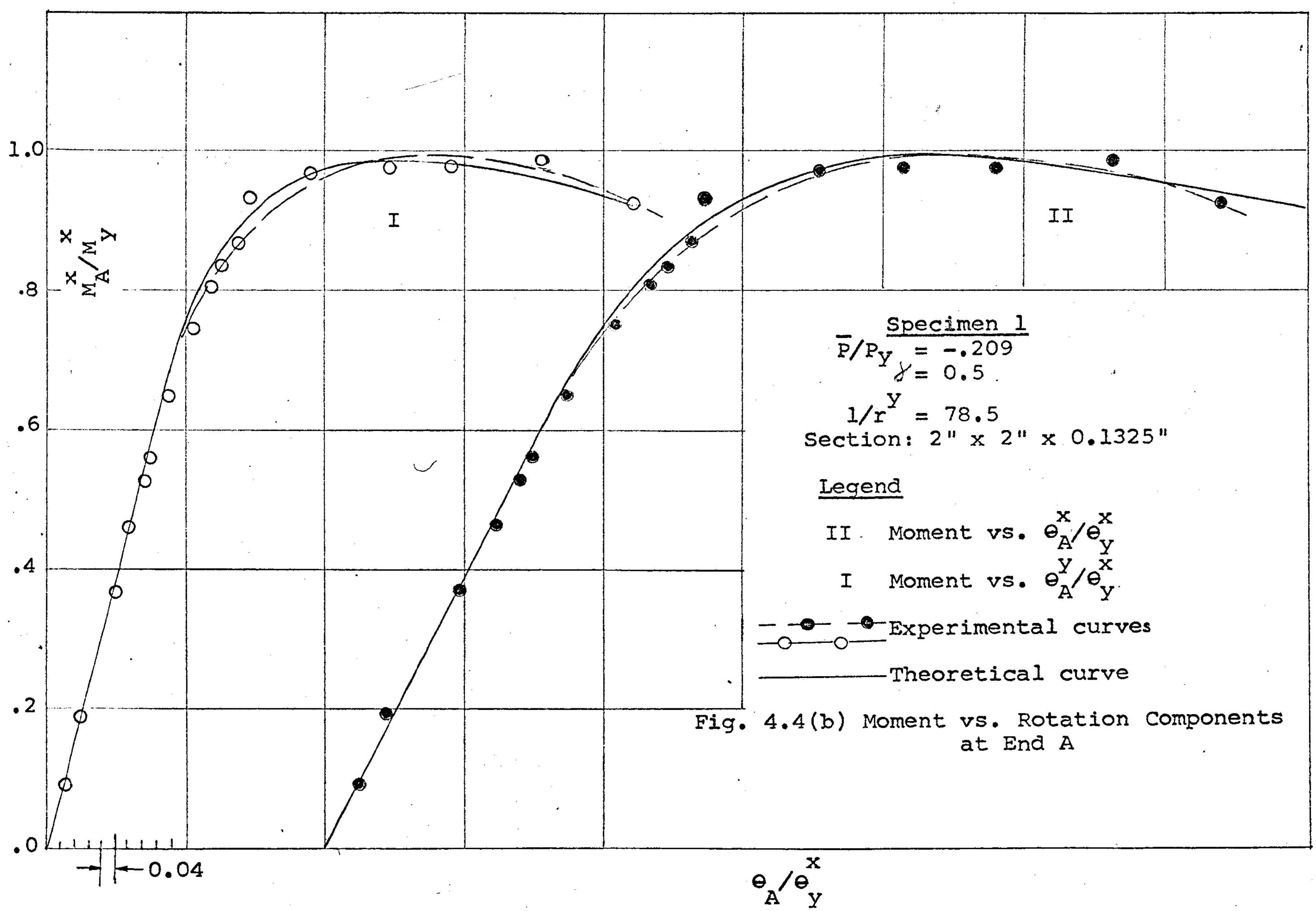

Fig. 4.4(b) Moment vs. Rotation Components at End A

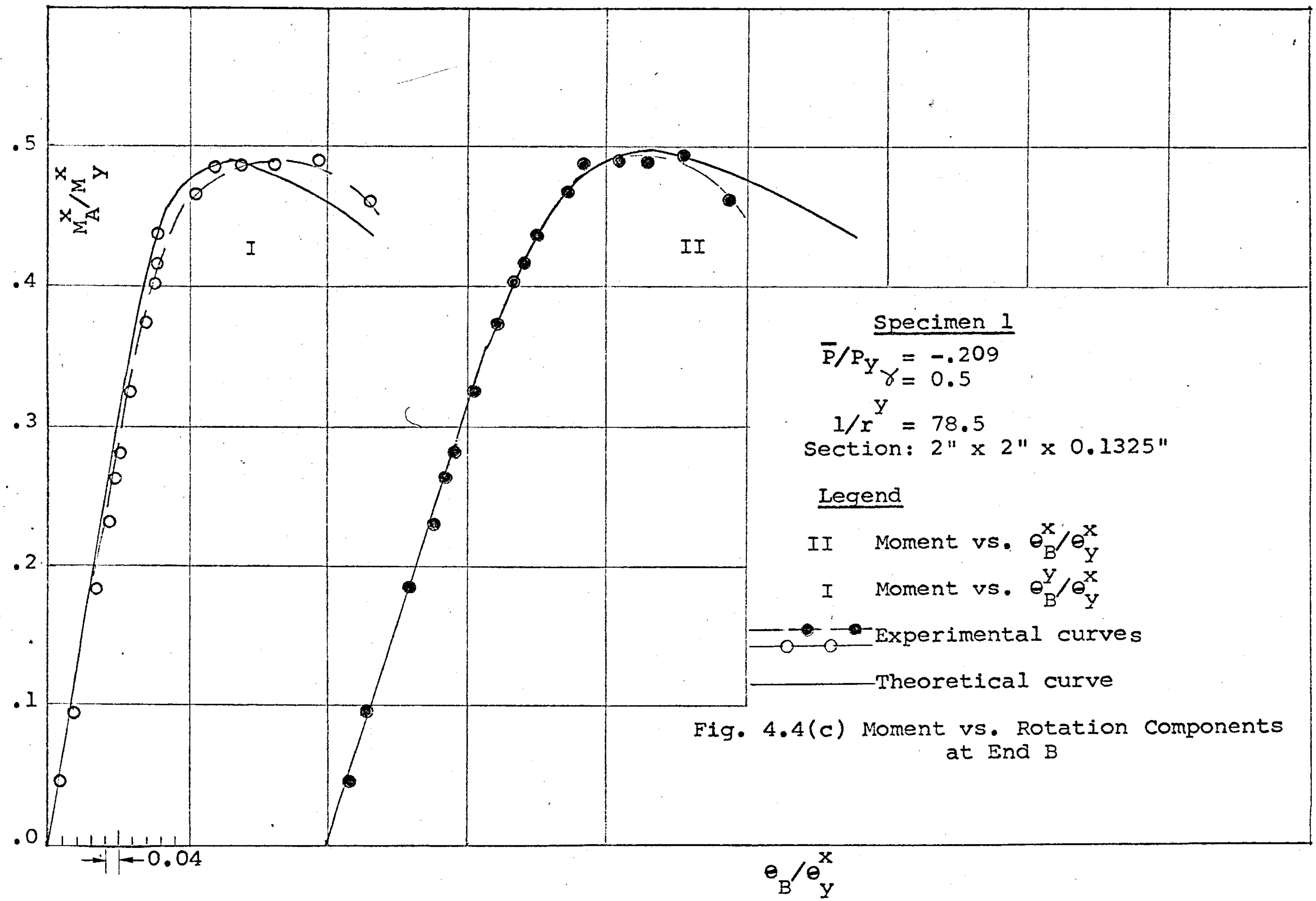

Fig. 4.4(c) Moment vs. Rotation Components at End B

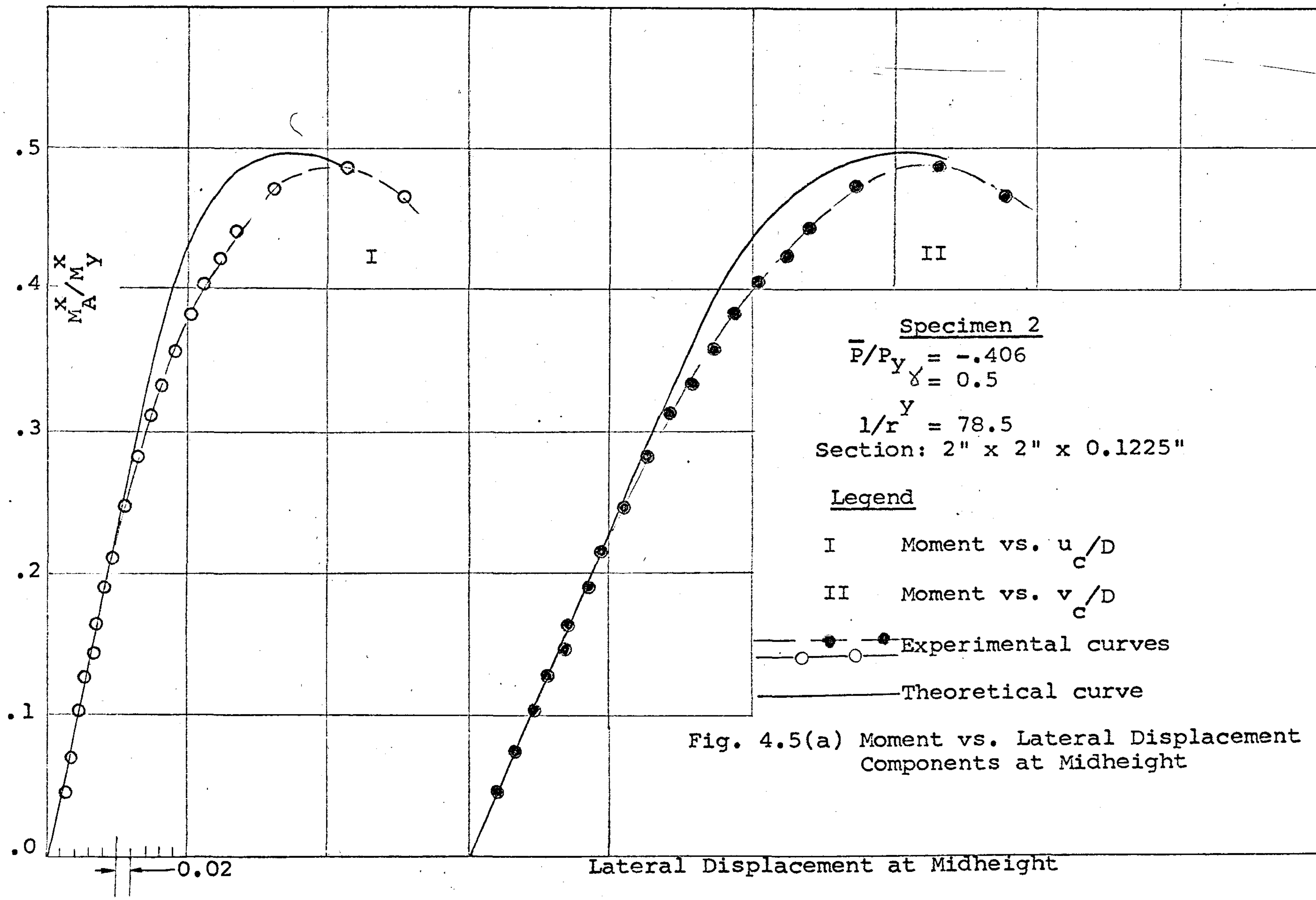

Fig. 4.5(a) Moment vs. Lateral Displacement Components at Midheight

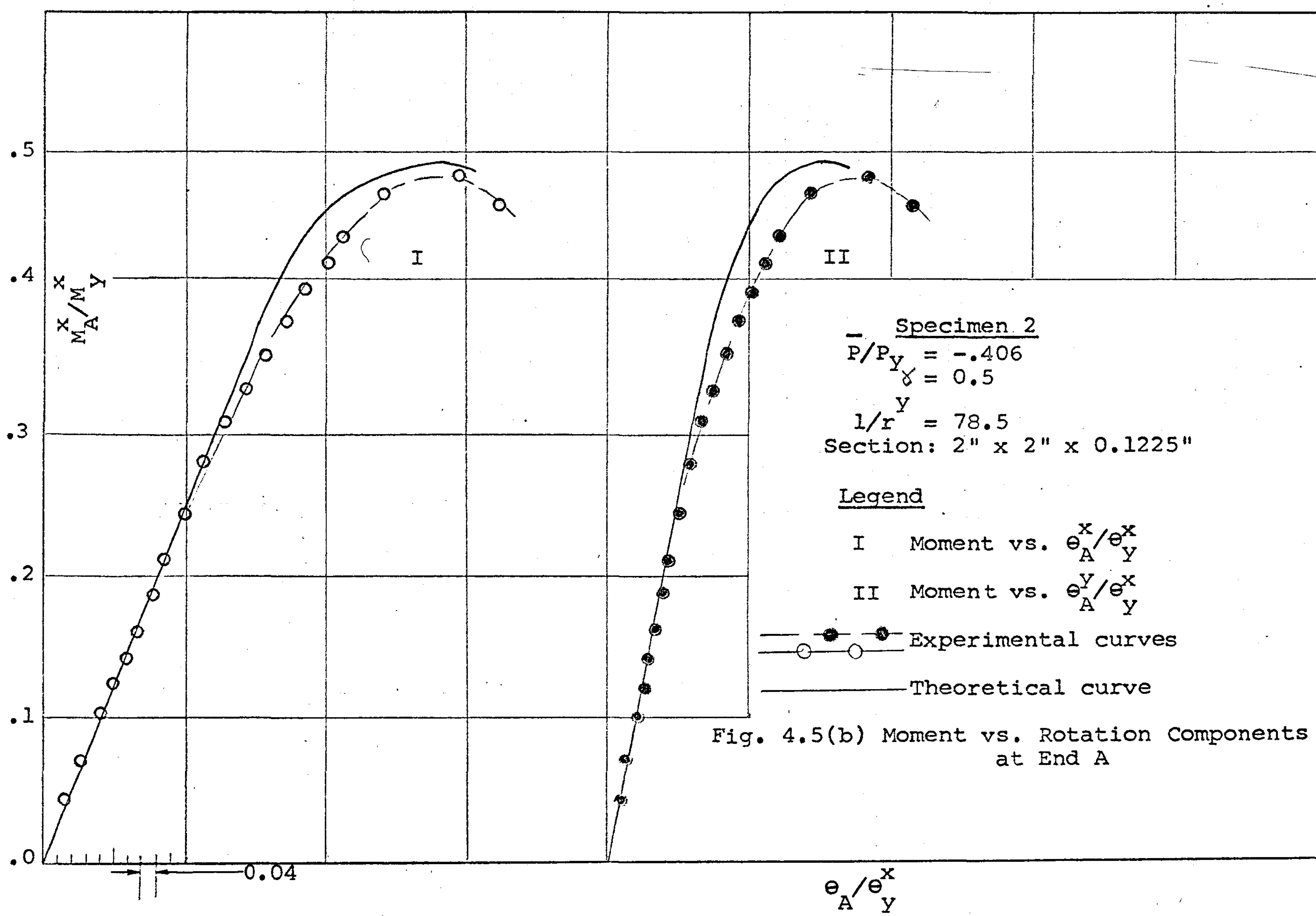

Fig. 4.5(b) Moment vs. Rotation Components at End A

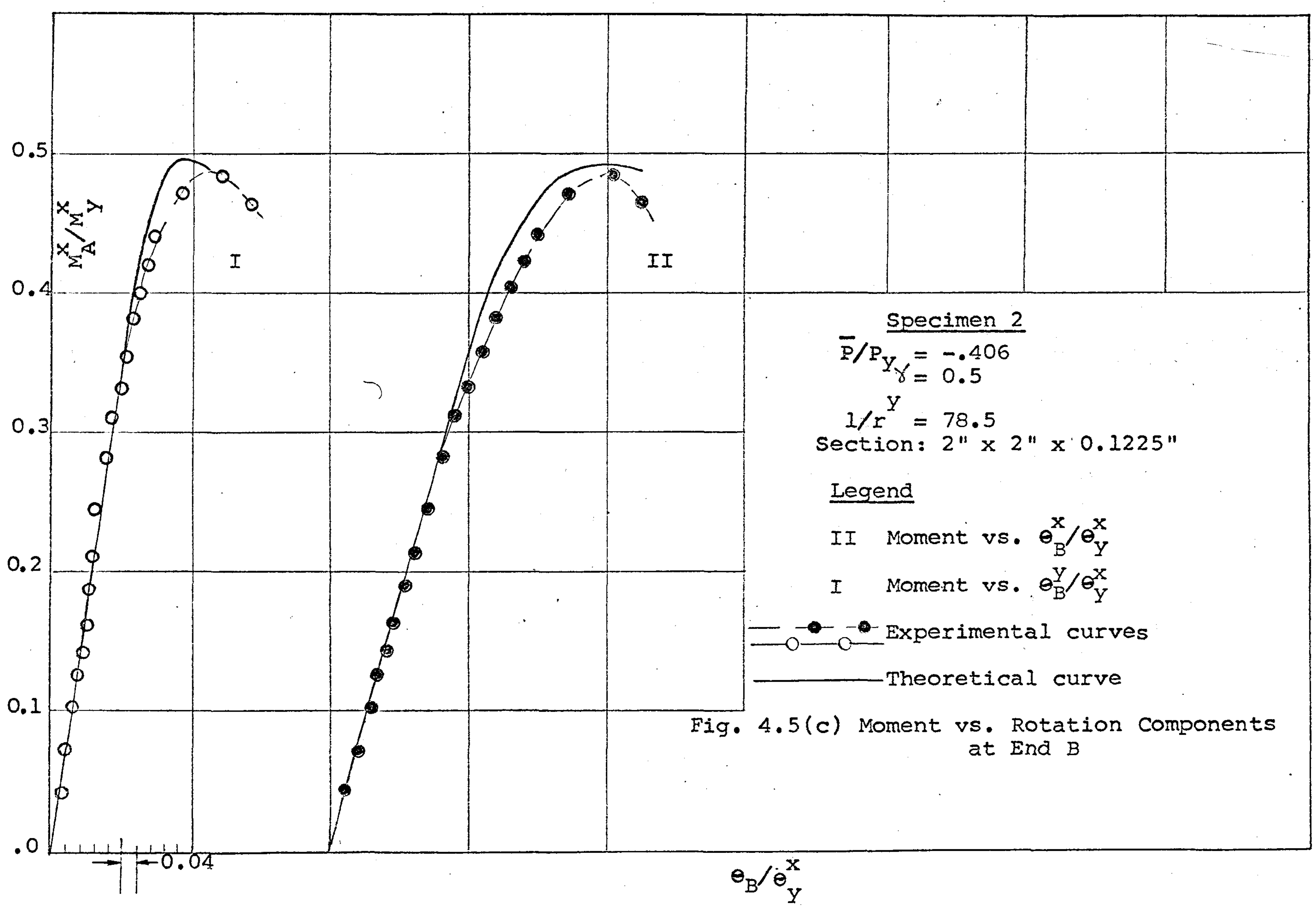

Fig. 4.5(c) Moment vs. Rotation Components at End B

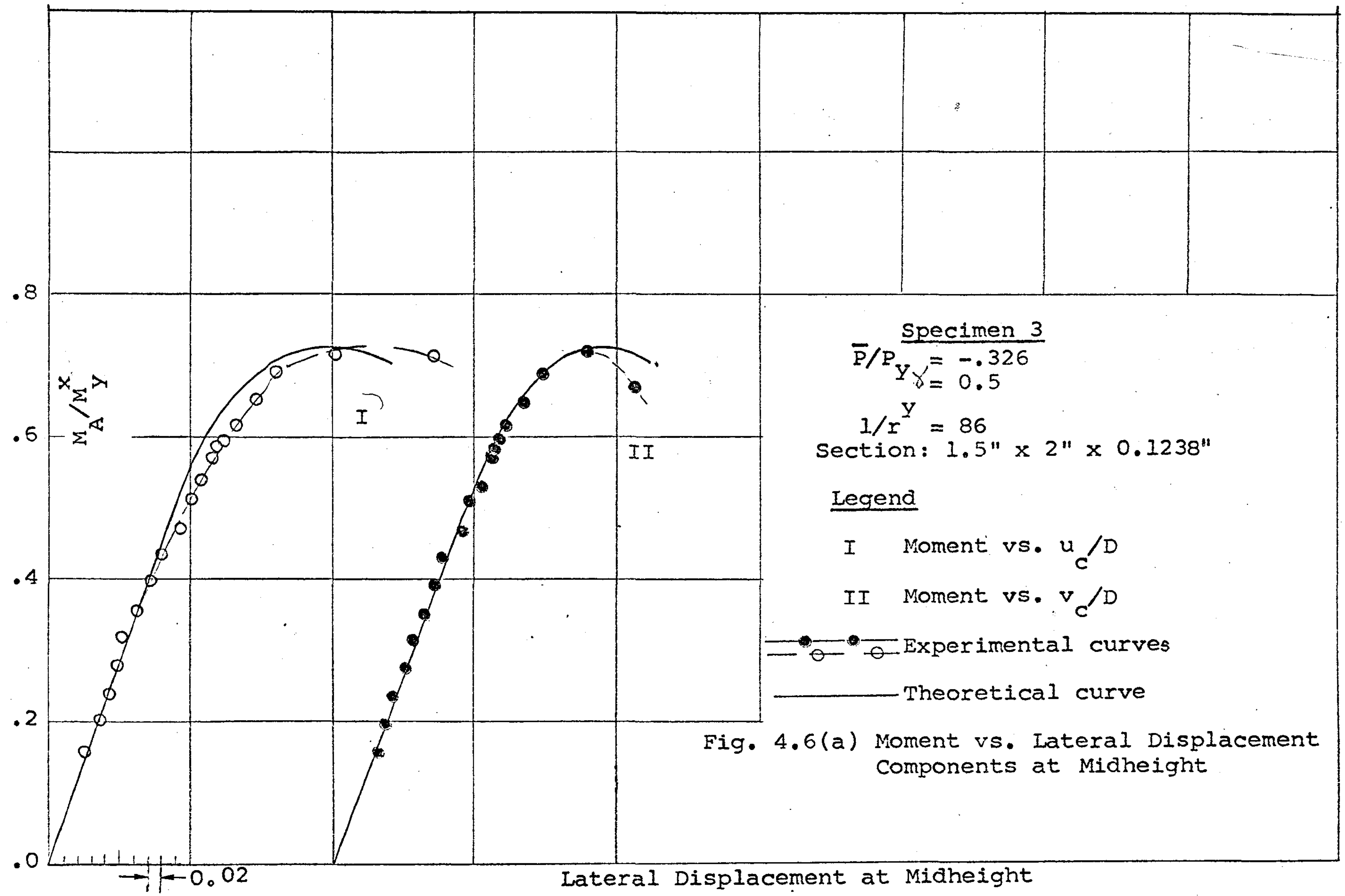

Fig. 4.6(a) Moment vs. Lateral Displacement Components at Midheight

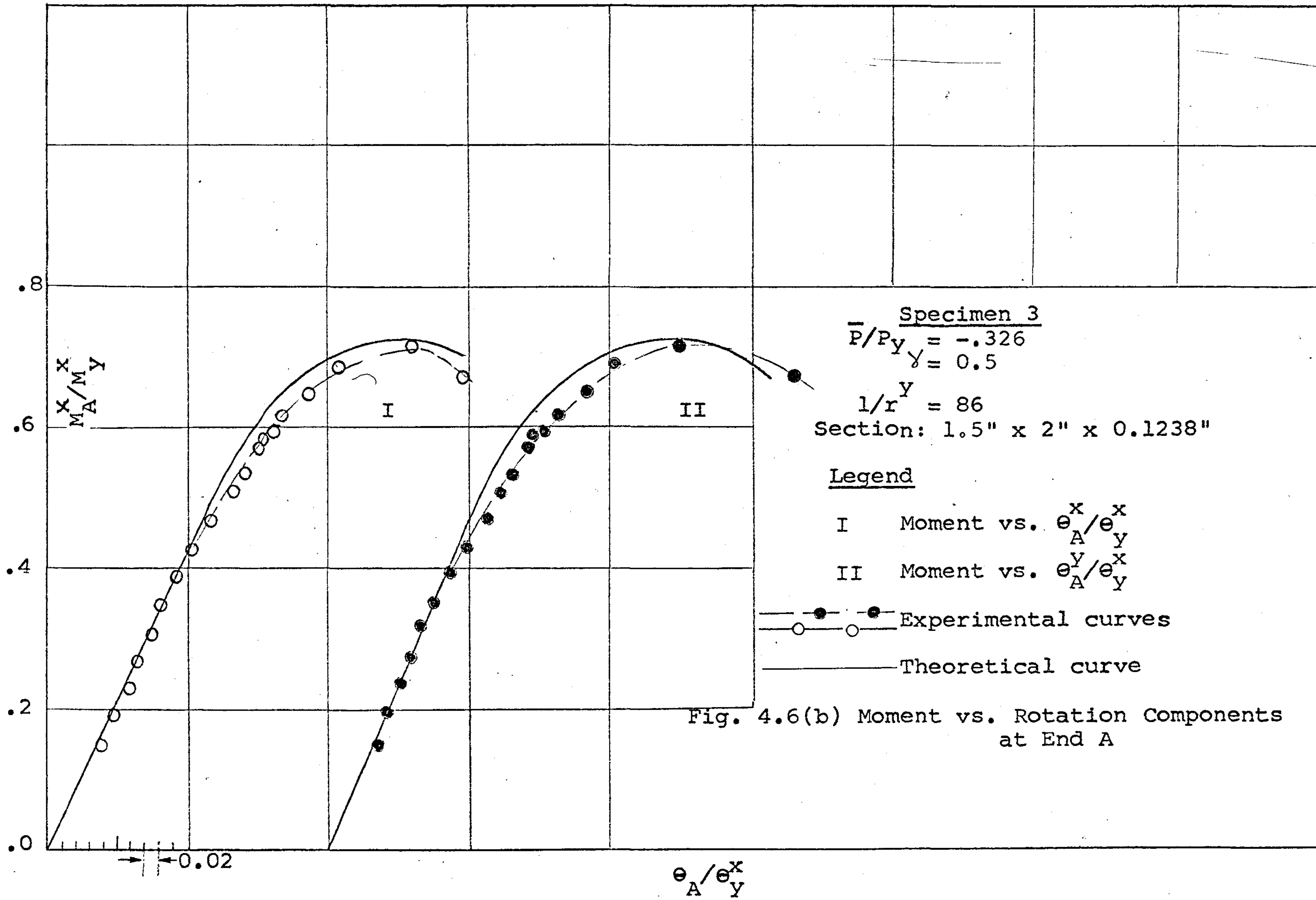

Fig. 4.6(b) Moment vs. Rotation Components at End A

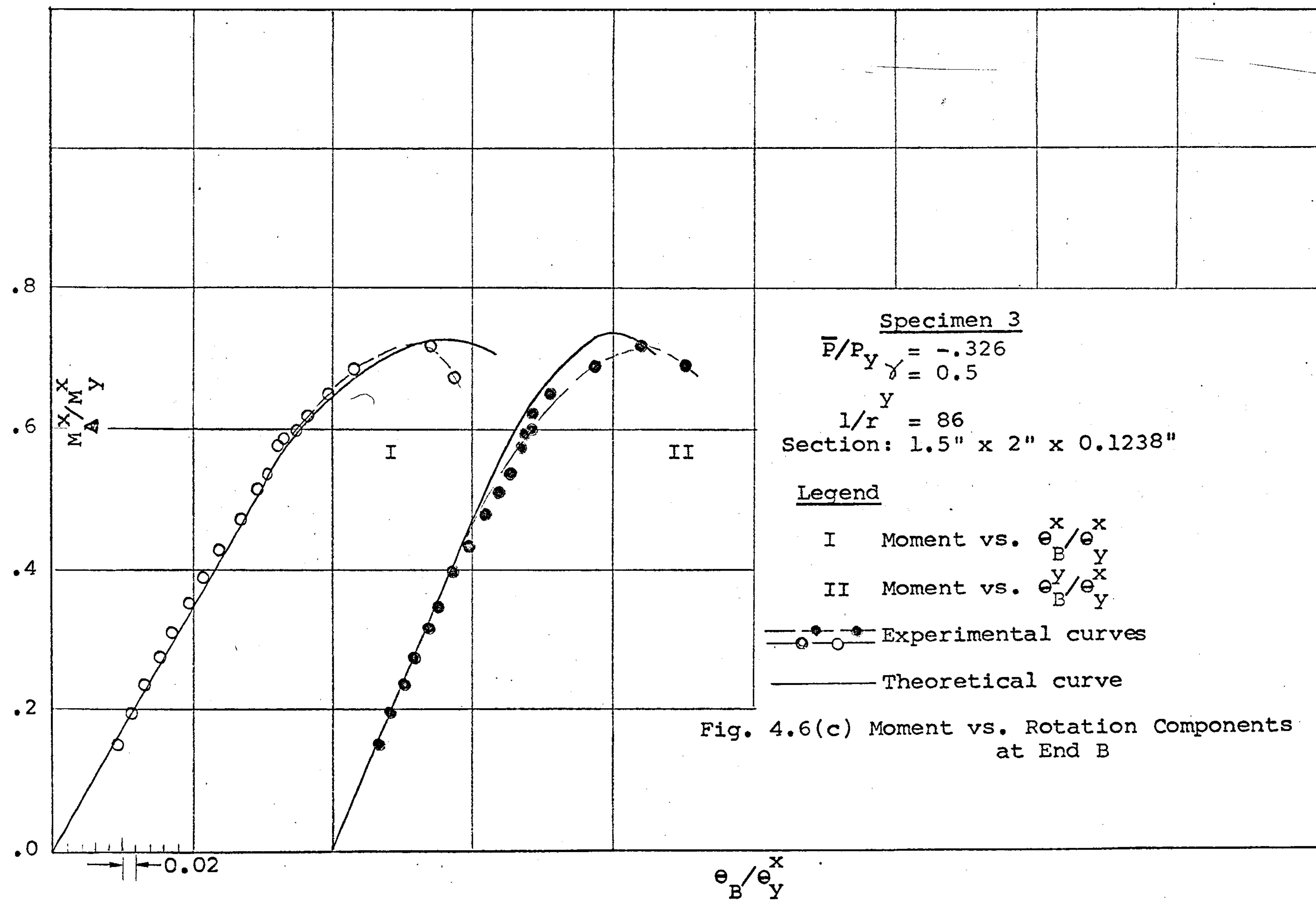

Fig. 4.6(c) Moment vs. Rotation Components at End B

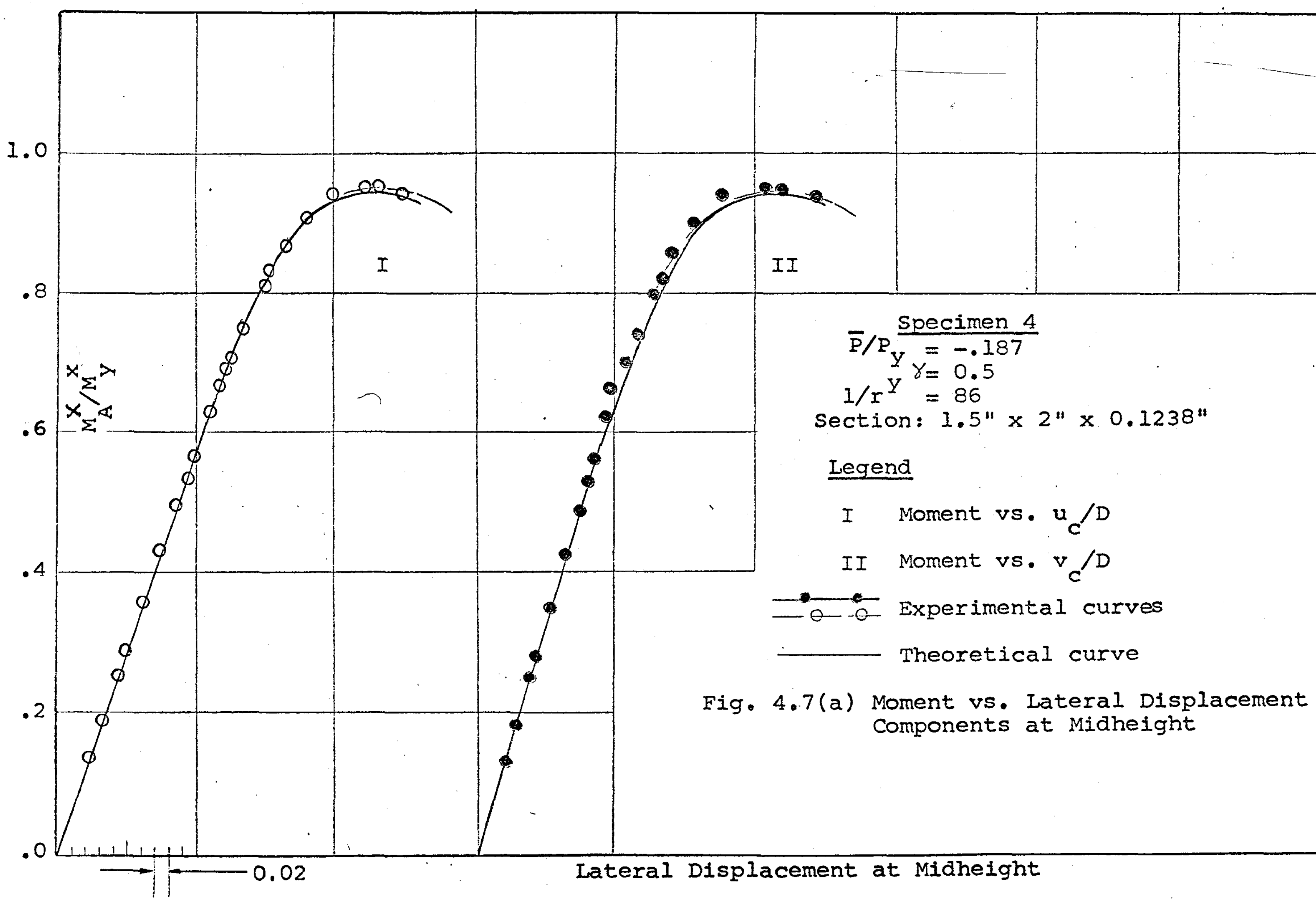

Fig. 4.7(a) Moment vs. Lateral Displacement Components at Midheight

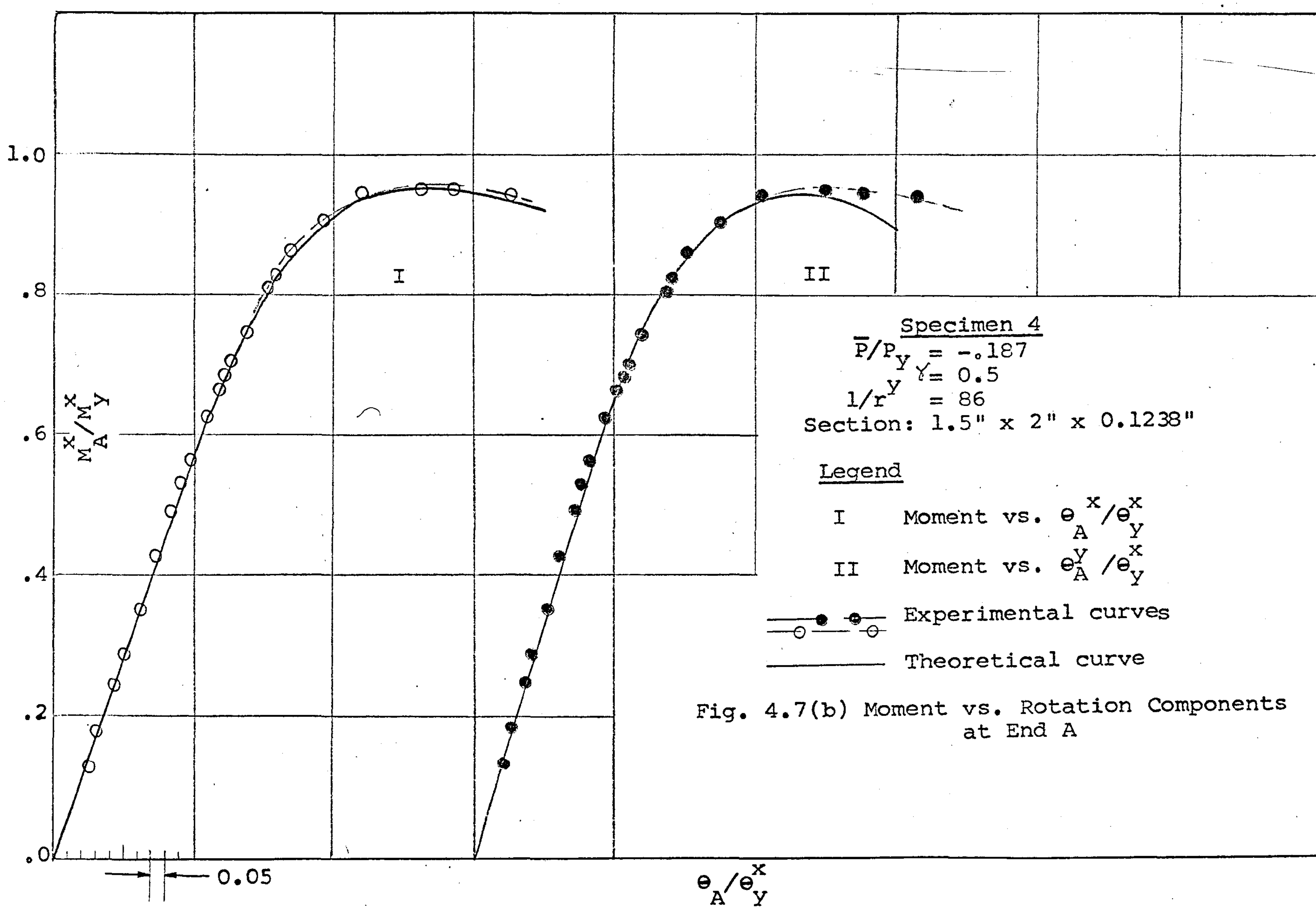

Fig. 4.7(b) Moment vs. Rotation Components at End A

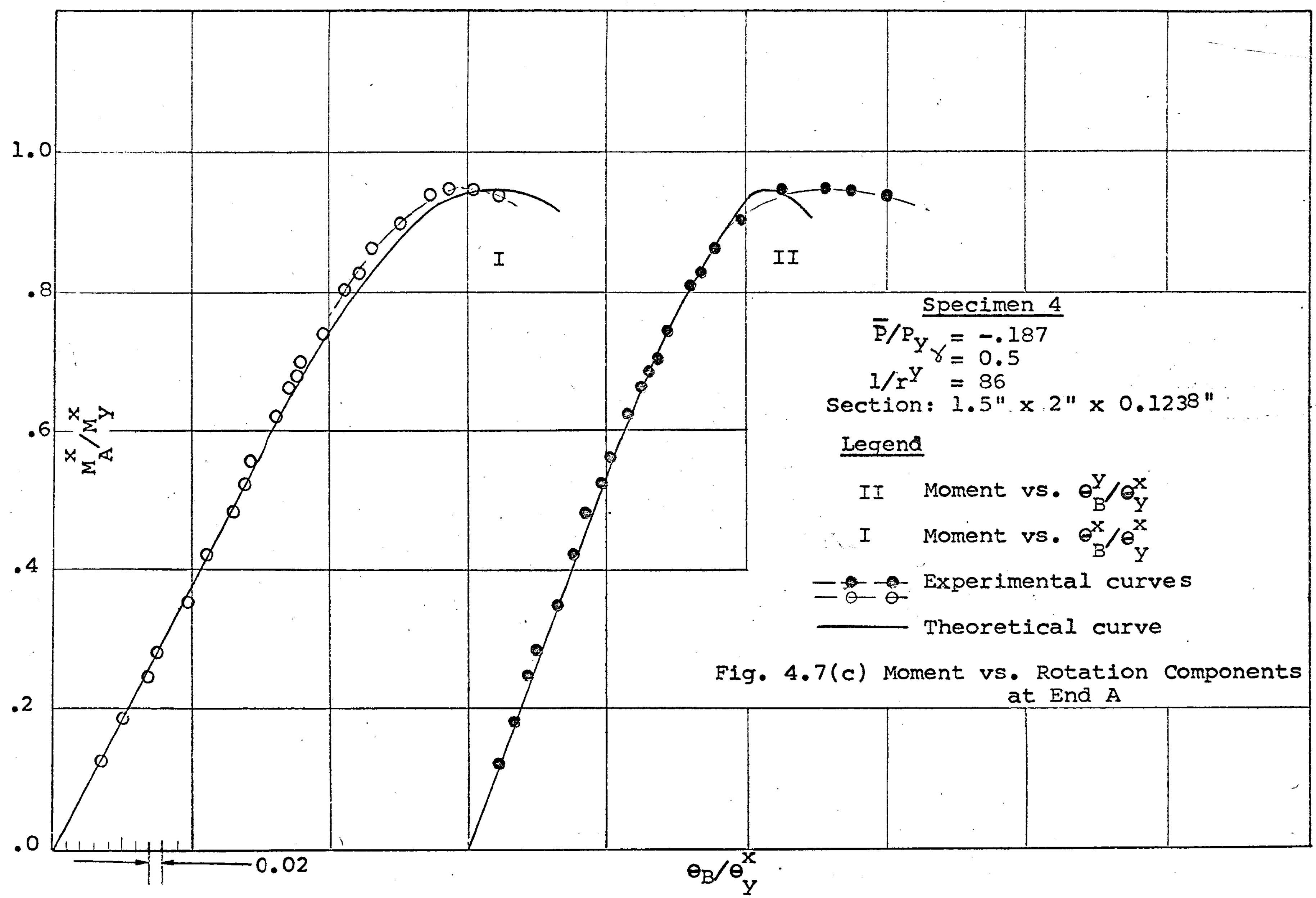

Fig. 4.7(c) Moment vs. Rotation Components at End A

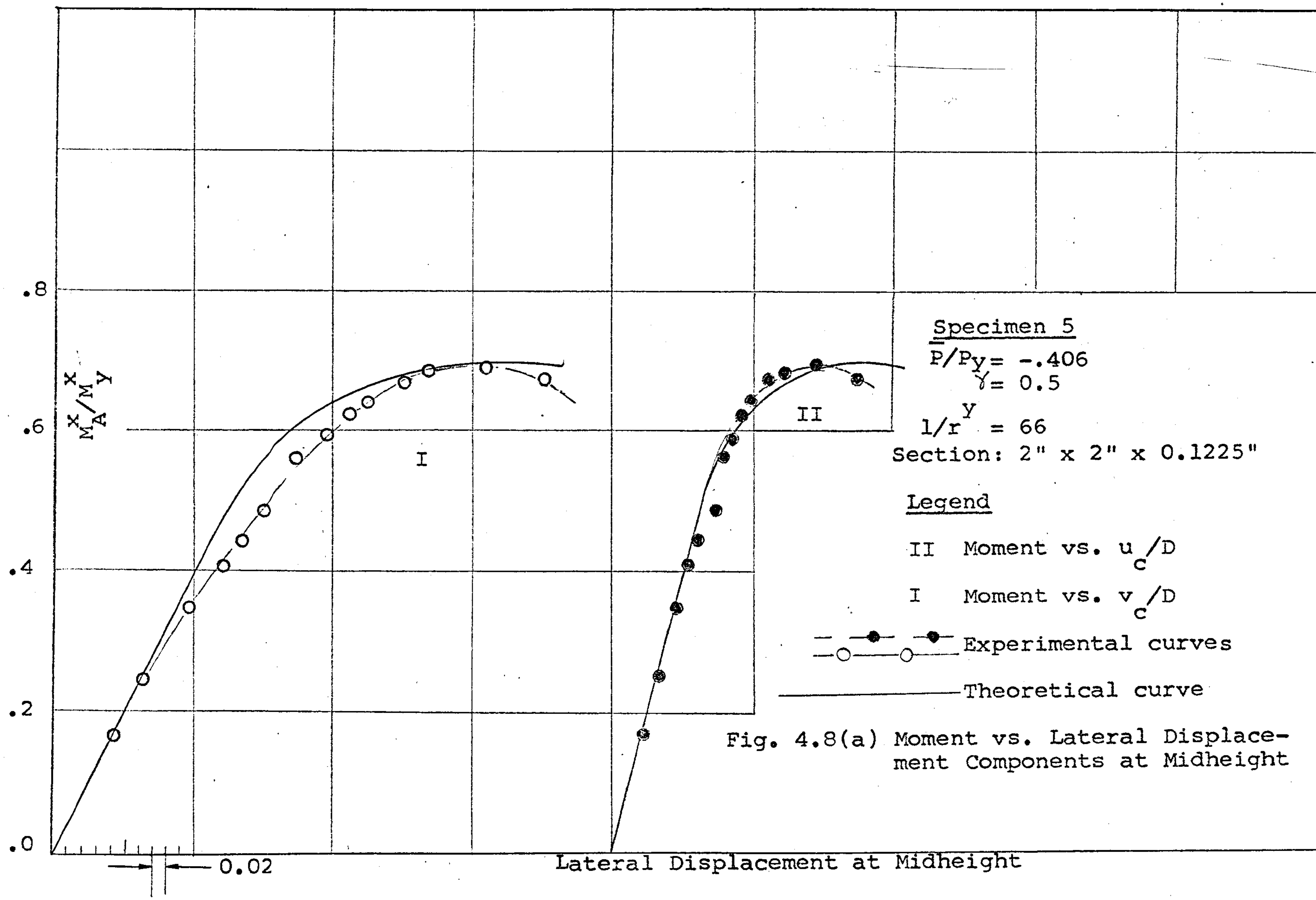

Fig. 4.8(a) Moment vs. Lateral Displacement Components at Midheight

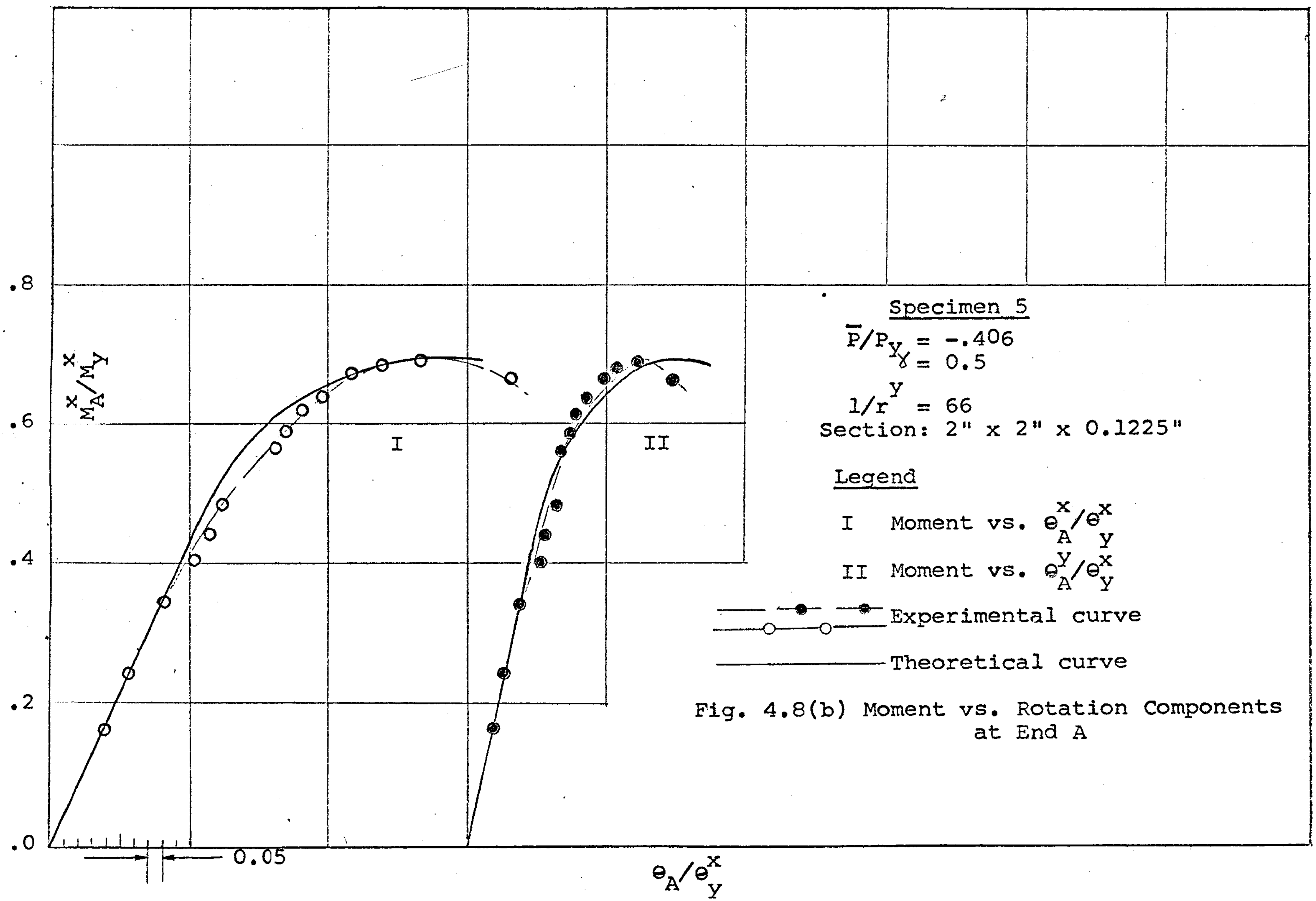

Fig. 4.8(b) Moment vs. Rotation Components at End A

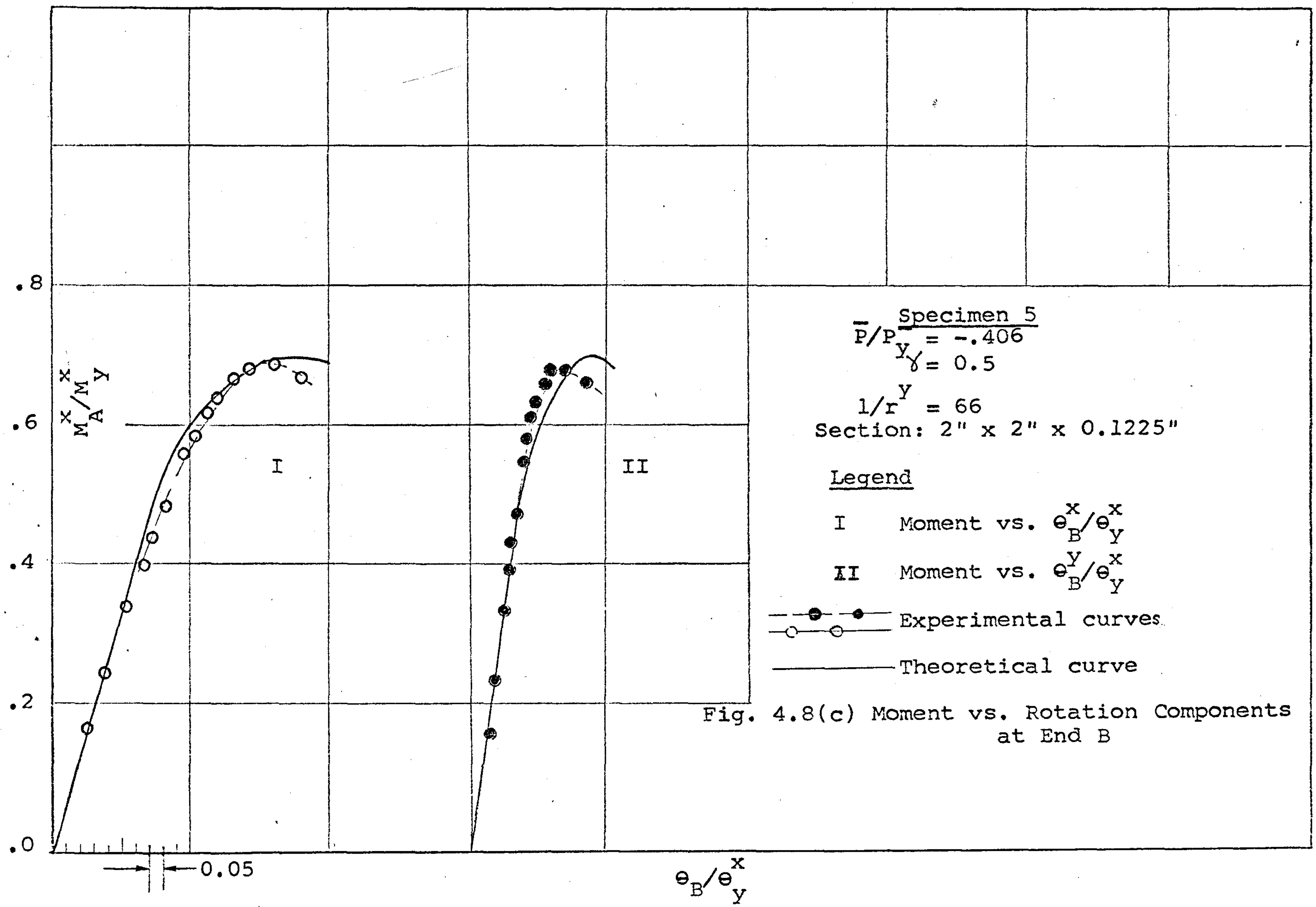

Fig. 4.8(c) Moment vs. Rotation Components at End B

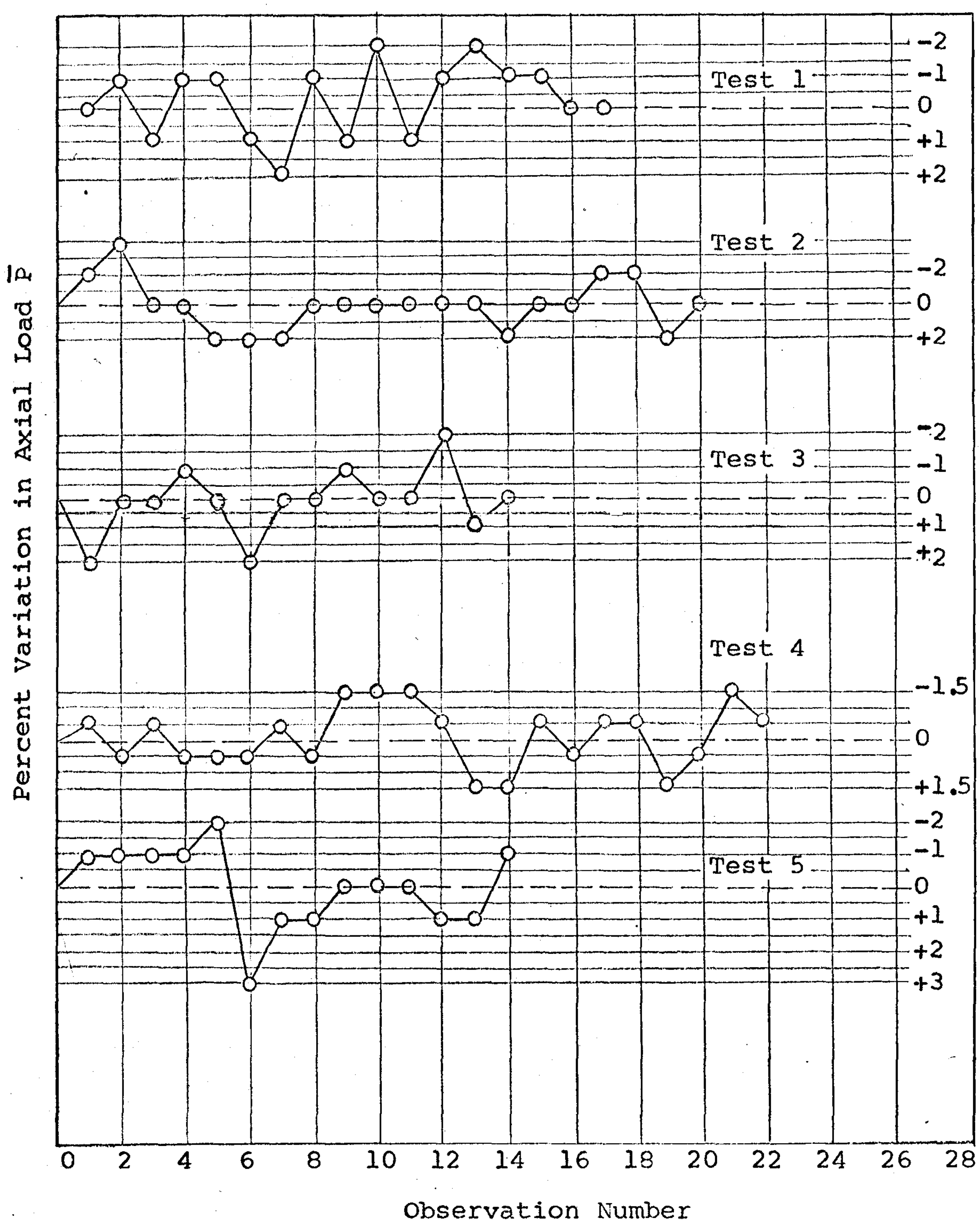

Fig. 4.9 Magnitude of the Variation in Axial Load $\bar{P}$ During the Tests

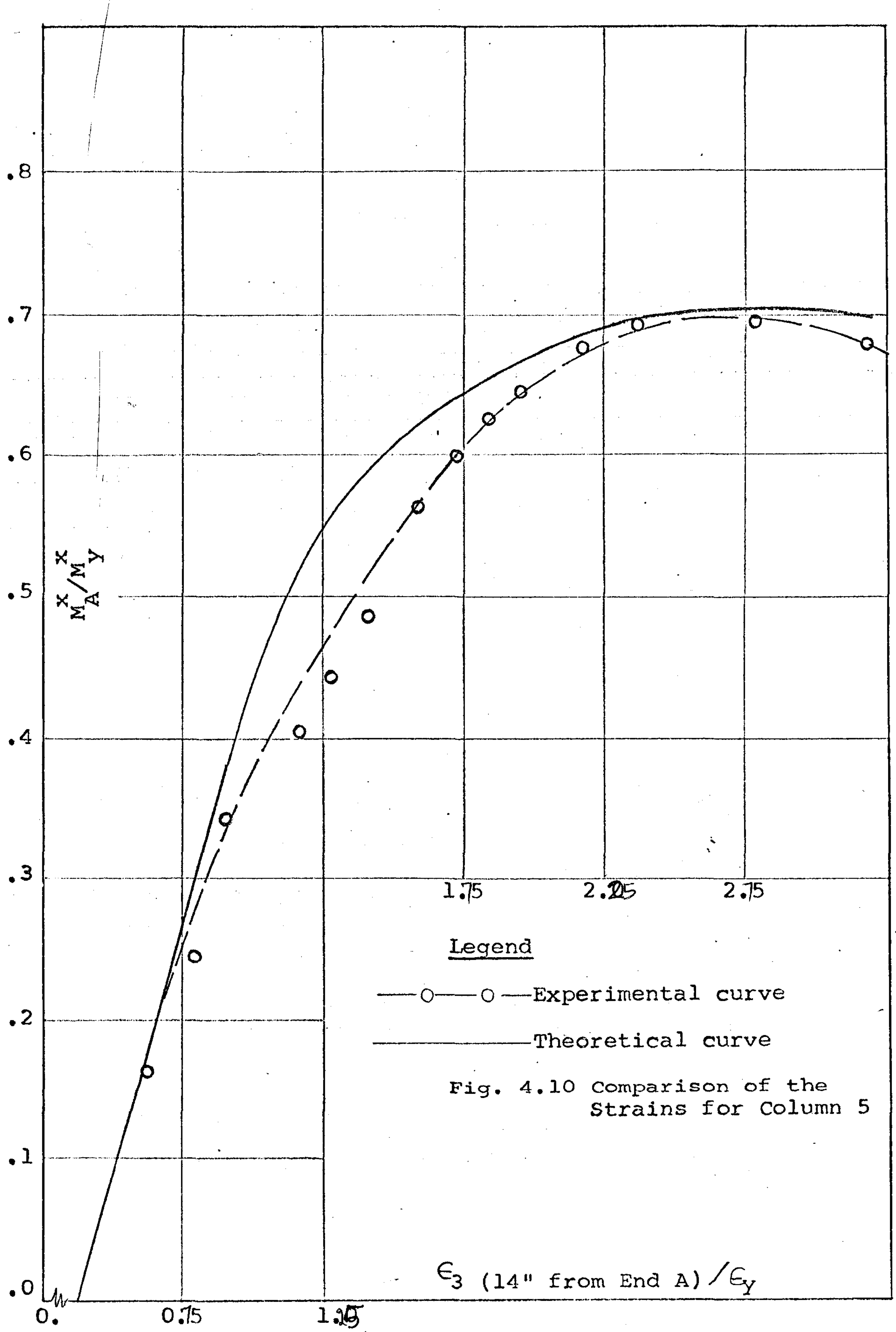

Fig. 4.10 Comparison of the Strains for Column 5

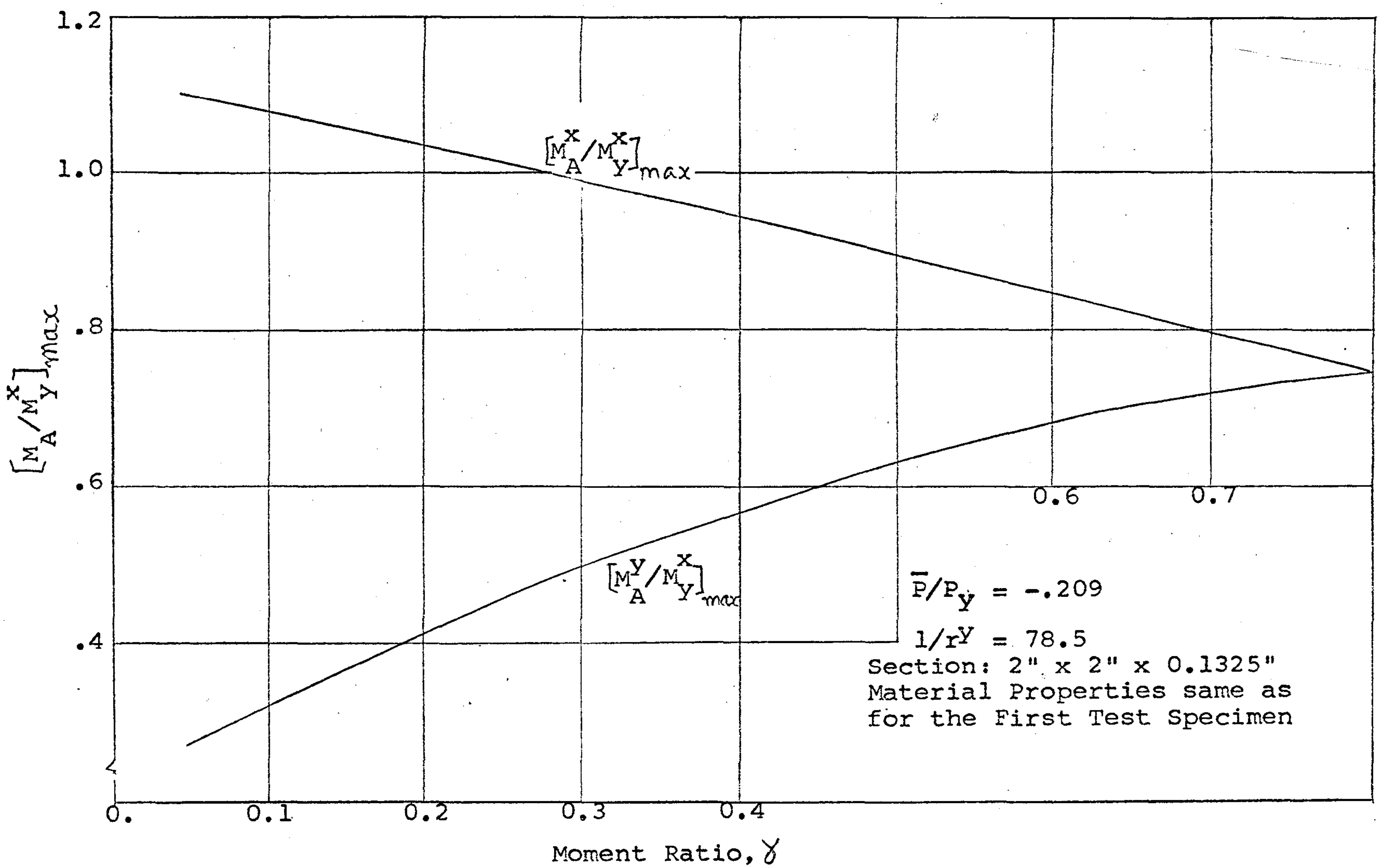

Fig. 4.11 Effect of Varying γ on the Peak Moments

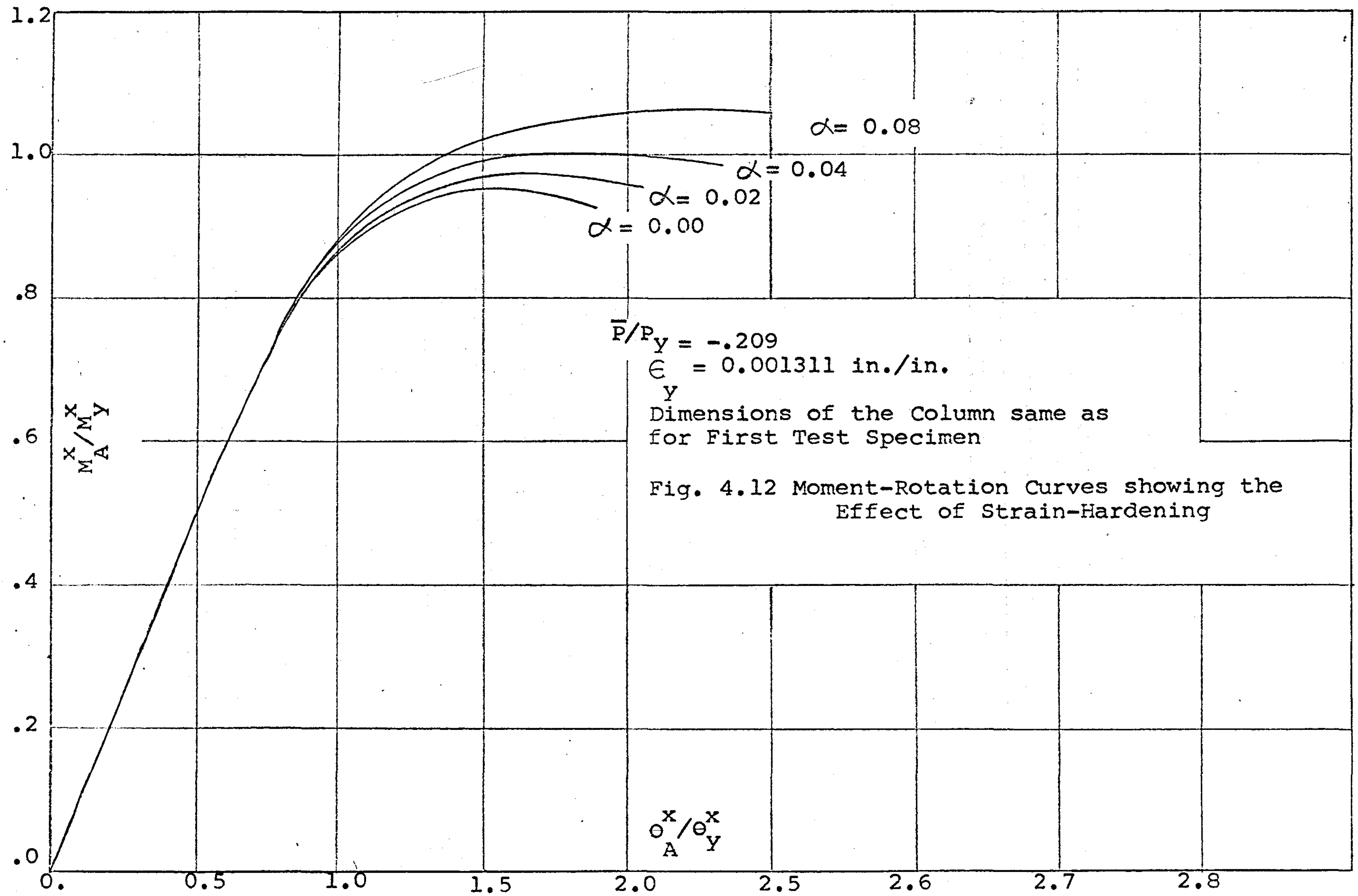

Fig. 4.12 Moment-Rotation Curves showing the Effect of Strain-Hardening

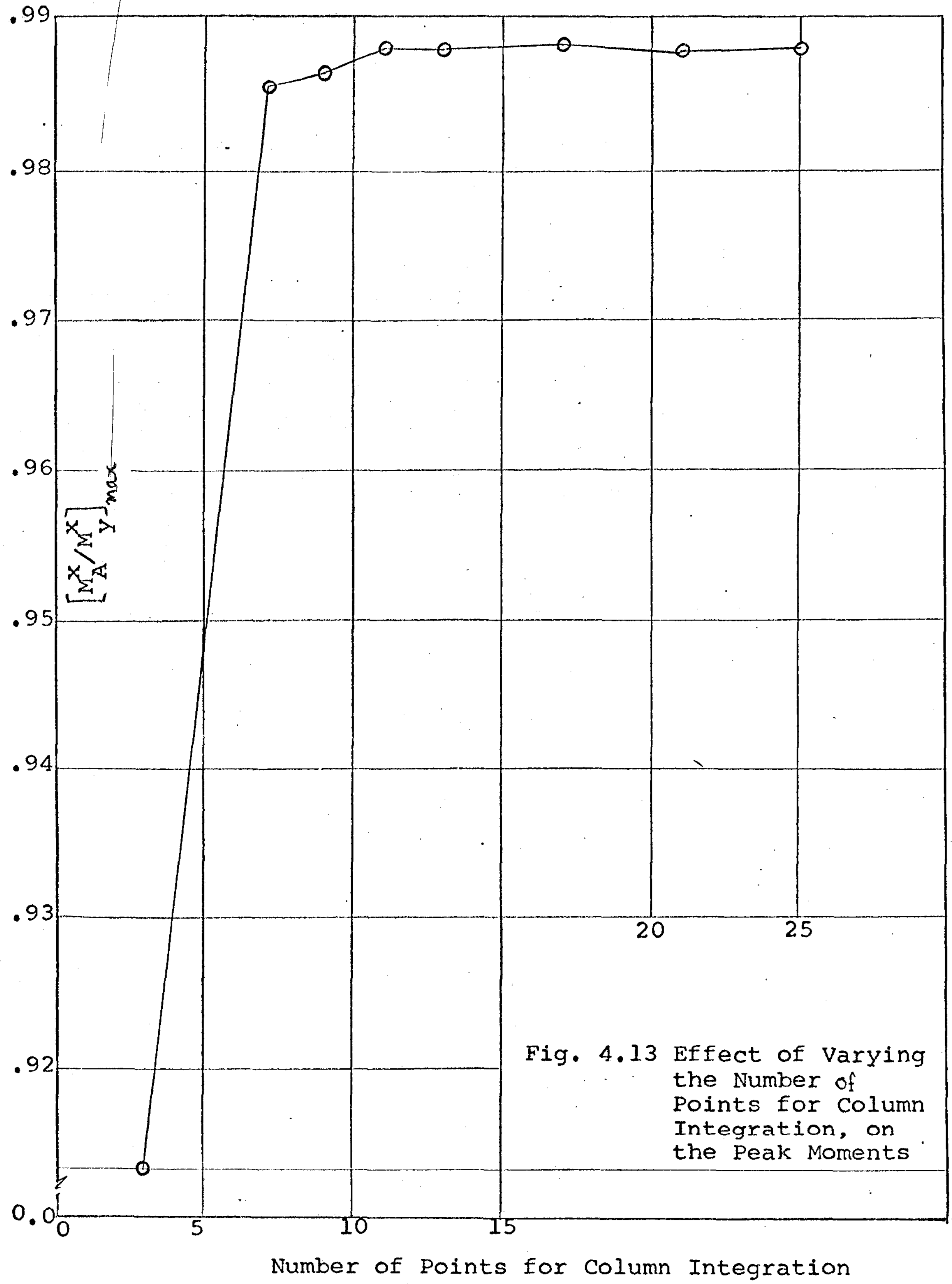

Fig. 4.13 Effect of Varying the Number of Points for Column Integration, on the Peak Moments

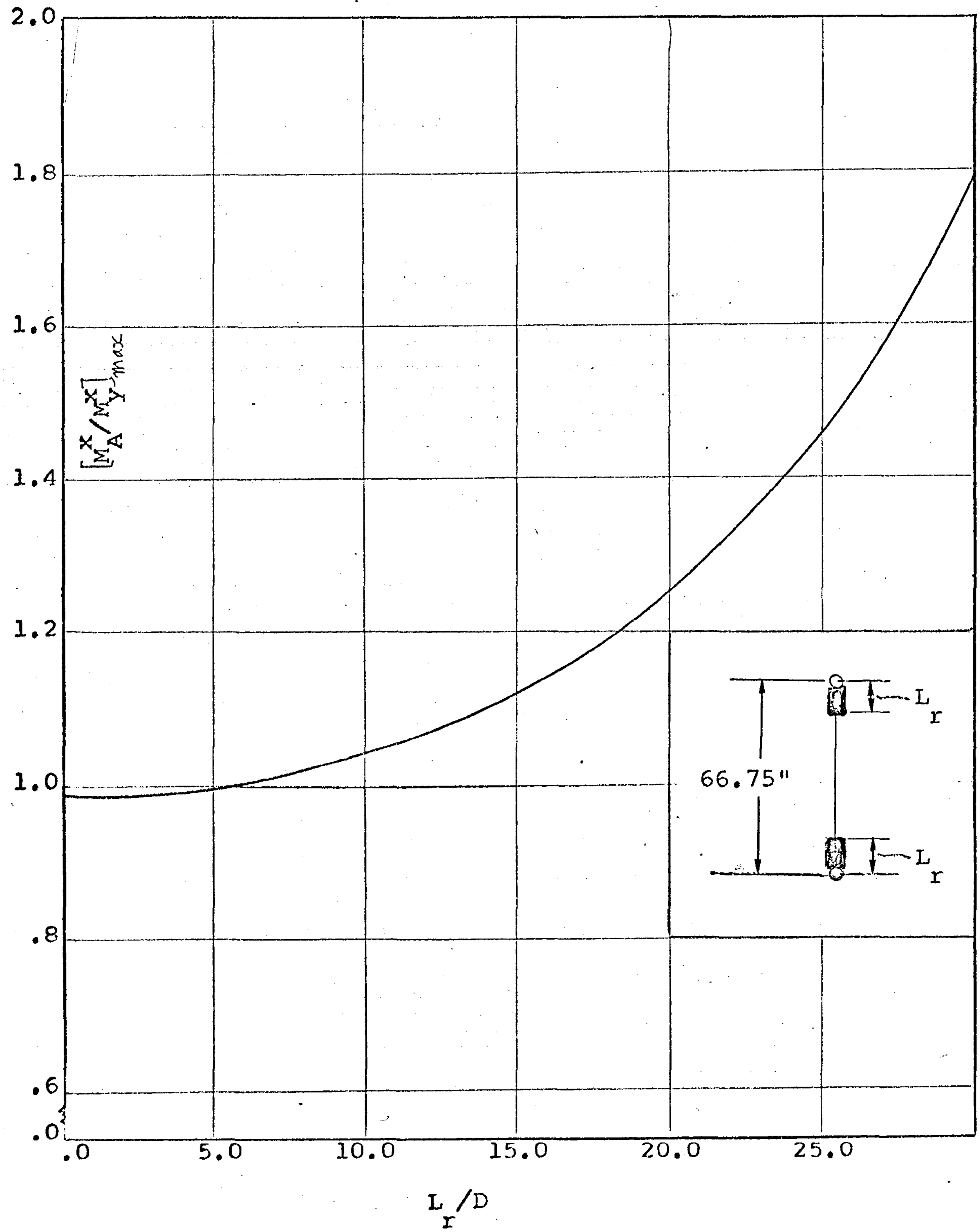

Fig. 4.14 Effect of Varying L_r on the Peak Moments

APPENDIX

THRUST-MOMENT-CURVATURE RELATIONS

This appendix describes how for a constant axial load $\overline{P}$ acting on top of a beam-column of known cross-section a set of moment-curvature curves such as those shown in Fig. 2.7 can be determined. The problem posed is to find what moments M^x and M^y should be applied, under a constant axial load $\overline{P}$, which would give a set of presumed curvatures ϕ^x and ϕ^y about the x and y axes of the column cross-section.

A.1 Cross-Section Properties

The terms used to describe the beam-column cross-section are defined in Fig. 2.2. K_1, K_2, and K_3 are non-dimensional factors describing the wall thickness, half the outside width, and half the inside width, respectively, in terms of half the depth of the section, D. The important properties of the section may, thus be written as

$$A_c = 4\,K_1(1 + K_3)\,D^2 \tag{A.1}$$

$$I_c^x = \frac{4}{3}\,K_1(1 + 3\,K_3 - 3\,K_1\,K_3 + K_1^2\,K_3)\,D^4 \tag{A.2}$$

$$I_c^y = \frac{4}{3}\,K_1(K_3^3 + 3\,K_3^2 + 3\,K_1\,K_3 + K_1^2)\,D^4 \tag{A.3}$$

These quantities in the non-dimensional form may be written using the following notation:

$$\overline{A}_c = A_c/D^2$$

$$\overline{I}_c^x = I_c^x/D^4$$

$$\overline{I}_c^y = I_c^y/D^4$$

The non-dimensionalizing factors for the thrust, moments, and curvatures are given, respectively, as follows:

$$P_y = E \epsilon_y A_c \tag{A.4}$$

$$M_y^x = E \epsilon_y I_c /D \tag{A.5}$$

$$\phi_y^x = \epsilon_y /D \tag{A.6}$$

A.2 Equilibrium Equations

Equations A.7, A.8, and A.9 are the non-dimensional equilibrium equations for the thrust and moments in terms of the strain on the cross-section. These equations follow directly from the Equations 2.10, 2.11, and 2.12, upon dividing by the appropriate non-dimensionalizing factors.

$$\frac{\bar{P}}{P_y} = \frac{D^2}{A_c} \int_A \frac{\epsilon}{\epsilon_y} \frac{dA}{D^2} - \frac{D^2}{A_c} (1 - \alpha) \int_A [\frac{\epsilon}{\epsilon_y} \pm 1] \frac{dA}{D^2} \tag{A.7}$$

$$\frac{M^x}{M_y^x} = \frac{D^4}{I_c^x} \int_A \frac{y}{D} \frac{\epsilon}{\epsilon_y} \frac{dA}{D^2} - \frac{D^4}{I_c^x} (1 - \alpha) \int_A \frac{y}{D} [\frac{\epsilon}{\epsilon_y} \pm 1] \frac{dA}{D^2} \tag{A.8}$$

$$\frac{M^y}{M_y^x} = \frac{D^4}{I_c^x} \int_A \frac{x}{D} \frac{\epsilon}{\epsilon_y} \frac{dA}{D^2} - \frac{D^4}{I_c^x} (1 - \alpha) \int_A \frac{x}{D} [\frac{\epsilon}{\epsilon_y} \pm 1] \frac{dA}{D^2} \tag{A.9}$$

The significance of the brackets [ ] of the second integral has been mentioned in Section 2.3. The strain at any point (x,y) of the cross-section is given by Equation 2.7. Dividing Equation 2.7 by ϵ_y and expressing x and y in terms of D gives the strain in terms of the yield strain, ϵ_y.

$$\frac{\epsilon}{\epsilon_y} = \frac{y}{D} \frac{\phi^x}{\phi_y^x} + \frac{x}{D} \frac{\phi^y}{\phi_y^x} + \frac{\epsilon_o}{\epsilon_y} \tag{A.10}$$

Equation A.10 is used in the evaluation of Equations A.7, A.8, and A.9.

Neglecting the variation in strain through the wall thickness, the strain distribution is specified by determining the strain at the center-line of the cross-section. Since plane sections are assumed to remain plane and residual strains are neglected, the strain distribution for any side of the cross-section is completely specified by the strains at the ends of the side. Therefore, only four strain values need to be evaluated. With reference to Fig. A.1 these are

$$\frac{\epsilon_1}{\epsilon_y} = - K_5 \frac{\phi^{y}}{\phi^{x}_{y}} + K_4 \frac{\phi^{x}}{\phi^{x}_{y}} + \frac{\epsilon_o}{\epsilon_y} \qquad \text{(A.11)}$$

$$\frac{\epsilon_2}{\epsilon_y} = K_5 \frac{\phi^{y}}{\phi^{x}_{y}} + K_4 \frac{\phi^{x}}{\phi^{x}_{y}} + \frac{\epsilon_o}{\epsilon_y} \qquad \text{(A.12)}$$

$$\frac{\epsilon_3}{\epsilon_y} = - K_5 \frac{\phi^{y}}{\phi^{x}_{y}} - K_4 \frac{\phi^{x}}{\phi^{x}_{y}} + \frac{\epsilon_o}{\epsilon_y} \qquad \text{(A.13)}$$

$$\frac{\epsilon_4}{\epsilon_y} = K_5 \frac{\phi^{y}}{\phi^{x}_{y}} - K_4 \frac{\phi^{x}}{\phi^{x}_{y}} + \frac{\epsilon_o}{\epsilon_y} \qquad \text{(A.14)}$$

The subscripts 1 through 4 in these equations refer to the four corners of the cross-section, and K_4 and K_5 are dimensionless factors describing dimensions of the center-line of the cross-section in terms of D. Equations A.11 through A.14 can be written as:

$$\epsilon_1/\epsilon_y = \bar{\epsilon}_1/\epsilon_y + \epsilon_o/\epsilon_y \tag{A.15}$$

$$\epsilon_2/\epsilon_y = \bar{\epsilon}_2/\epsilon_y + \epsilon_o/\epsilon_y \tag{A.16}$$

$$\epsilon_3/\epsilon_y = \bar{\epsilon}_3/\epsilon_y + \epsilon_o/\epsilon_y \tag{A.17}$$

$$\epsilon_4/\epsilon_y = \bar{\epsilon}_4/\epsilon_y + \epsilon_o/\epsilon_y \tag{A.18}$$

where $\bar{\epsilon}_1/\epsilon_y$, $\bar{\epsilon}_2/\epsilon_y$, $\bar{\epsilon}_3/\epsilon_y$, and $\bar{\epsilon}_4/\epsilon_y$ are the bending strains given by

$$\frac{\bar{\epsilon}_1}{\epsilon_y} = -K_5\frac{\phi^y}{\phi^x_y} + K_4\frac{\phi^x}{\phi^x_y} \tag{A.19}$$

$$\frac{\bar{\epsilon}_2}{\epsilon_y} = K_5\frac{\phi^y}{\phi^x_y} + K_4\frac{\phi^x}{\phi^x_y} \tag{A.20}$$

$$\frac{\bar{\epsilon}_3}{\epsilon_y} = \frac{\bar{\epsilon}_2}{\epsilon_y} \tag{A.21}$$

$$\frac{\bar{\epsilon}_4}{\epsilon_y} = \frac{\bar{\epsilon}_1}{\epsilon_y} \tag{A.22}$$

and depend on the values of ϕ^x/ϕ^x_y and ϕ^y/ϕ^x_y. The term ϵ_o/ϵ_y will depend on the magnitude of the axial thrust.

An examination of the possible yield patterns for the section (Fig. 2.8) shows that all may be made up of some combination of the five yield patterns shown in Fig. A.2. In this figure, the length of the side ij will depend on its position in the cross-section, thus K_k will take the values K_4 or K_5. The i end of the side represents the end with the algebraically largest strain. The length of tension and/or compression yield on a side, $a_{ij}K_kD$ and $a_{ji}K_kD$, respectively, can be found in terms of the strain at i and j. Consider the strain distribution for case V of Fig. A.2. By proportion

$$a_{ij} = \frac{2(\epsilon_i/\epsilon_y - 1)}{\epsilon_i/\epsilon_y - \epsilon_j/\epsilon_y} \qquad \text{(A.23)}$$

$$a_{ji} = \frac{2(\epsilon_j/\epsilon_y + 1)}{\epsilon_i/\epsilon_y - \epsilon_j/\epsilon_y} \qquad \text{(A.24)}$$

The strains at i and j are written in terms of the bending strains and the uniform strain as

$$\epsilon_i/\epsilon_y = \bar{\epsilon}_i/\epsilon_y + \epsilon_o/\epsilon_y \qquad \text{(A.25)}$$

$$\epsilon_j/\epsilon_y = \bar{\epsilon}_j/\epsilon_y + \epsilon_o/\epsilon_y \qquad \text{(A.26)}$$

Substituting A.25 and A.26 into A.23 and A.24 and introducing the notation

$$2\rho_k = \bar{\epsilon}_i/\epsilon_y - \bar{\epsilon}_j/\epsilon_y \qquad \text{(A.27)}$$

$$A_{ij} = (\bar{\epsilon}_i/\epsilon_y - 1)/\rho_k \qquad \text{(A.28)}$$

$$A_{ji} = -(\bar{\epsilon}_j/\epsilon_y + 1)/\rho_k \qquad \text{(A.29)}$$

these equations become

$$a_{ij} = A_{ij} + \frac{\epsilon_o/\epsilon_y}{\rho_k} \qquad \text{(A.30)}$$

$$a_{ji} = A_{ji} - \frac{\epsilon_o/\epsilon_y}{\rho_k} \qquad \text{(A.31)}$$

An examination of Equations A.19 through A.22 leads to the fact that

$$\rho_k = K_4 \frac{\phi^x}{\phi^x_y} \quad \text{when } k = 4 \tag{A.32}$$

$$\rho_k = K_5 \frac{\phi^y}{\phi^x_y} \quad \text{when } k = 5 \tag{A.33}$$

Equations A.15 through A.22 and A.28 through A.33 are used in the evaluation of Equation A.7.

The first term on the right side of Equation A.7 represents D^2/A_c times the volume of the ϵ/ϵ_y distribution on the cross-section if the section were to remain elastic. This quantity may be expressed in terms of ϵ_o as

$$\frac{D^2}{A_c} \int_A \frac{\epsilon}{\epsilon_y} \frac{dA}{D^2} = \frac{D^2}{A_c} \frac{\epsilon_o}{\epsilon_y} \frac{A_c}{D^2} \tag{A.34}$$

The second term on the right side of Equation A.7 accounts for the effect due to yielding. The integral in this term represents the volume of the $[\frac{\epsilon}{\epsilon_y} \pm 1]$ distribution on the cross-section. Table A.1 gives this volume for each of the five yield patterns of Fig. A.2. Table A.2 gives the values of A_{ij}, A_{ji}, a_{ij}, a_{ji} for different values of i and j. It may be noted that the initially eight A_{ij}, A_{ji} terms boil down to only four terms, namely, $Q_1 /(\phi^x/\phi^x_y)$, $Q_2 /(\phi^x/\phi^x_y)$, $Q_3 /(\phi^y/\phi^x_y)$, and $Q_4 /(\phi^y/\phi^x_y)$ as given in the table.

The total integral $\int_A [\epsilon/\epsilon_y \pm 1] \frac{dA}{D^2}$ for any particular yield pattern (Fig. A.2) is evaluated as the sum of the integrals for the four sides. Table A.3 gives the specific form of Equation 3.7 for each yield pattern.

As can be seen from Table A.3, Equation 3.7 in all cases reduces to an equation relating $\overline{P}/P_y$ to ϵ_o/ϵ_y of the form

$$\frac{\overline{P}}{P_y} = a\left(\frac{\epsilon_o}{\epsilon_y}\right)^2 + b\left(\frac{\epsilon_o}{\epsilon_y}\right) + c \tag{A.35}$$

where a, b, and c are coefficients depending upon the cross-sectional dimensions and the particular values of ϕ^x/ϕ^x_y and ϕ^y/ϕ^x_y selected. If $\overline{P}/P_y$ is specified, Equation A.35 reduces to a quadratic equation in ϵ_o/ϵ_y as given by

$$a\left(\frac{\epsilon_o}{\epsilon_y}\right)^2 + b\left(\frac{\epsilon_o}{\epsilon_y}\right) + \left(c - \frac{\overline{P}}{P_y}\right) = 0 \tag{A.36}$$

The solution of this equation is

$$\frac{\epsilon_o}{\epsilon_y} = \frac{-b \pm \sqrt{b^2 - 4a(c - \overline{P}/P_y)}}{2a} \tag{A.37}$$

except for a = 0, in which case the solution is

$$\frac{\epsilon_o}{\epsilon_y} = -(c - \overline{P}/P_y)/b$$

Since ϵ_o increases algebraically with $\overline{P}$, the sign with the radical in Equation A.37 must be positive so that

$$\frac{\epsilon_o}{\epsilon_y} = \frac{-b + \sqrt{b^2 - 4a(c - \overline{P}/P_y)}}{2a} \tag{A.38}$$

After ϵ_o has been evaluated, the moments are found using

Equations A.8 and A.9. The first term in each of these equations is the moment if the section were to remain elastic, and the second term accounts for the yielded material in the section. Accordingly, these equations may be rewritten as

$$\frac{M^x}{M^x_y} = \frac{\phi^x}{\phi^x_y} - \frac{D^4}{I^x_c}(1-\alpha)\int_A \frac{y}{D}\left[\frac{\epsilon}{\epsilon_y} \pm 1\right]\frac{dA}{D^2} \qquad (A.39)$$

$$\frac{M^y}{M^x_y} = \frac{I^y_c}{I^x_c}\,\frac{\phi^y_x}{\phi_y} - \frac{D^4_x}{I_c}(1-\alpha)\int_A \frac{x}{D}\left[\frac{\epsilon}{\epsilon_y} \pm 1\right]\frac{dA}{D^2} \qquad (A.40)$$

For any particular yield pattern the values of the integrals in Equations A.39 and A.40 are evaluated as the moments about the x and y axes of the volumes of the $[\frac{\epsilon}{\epsilon_y} \pm 1]$ distribution on the section. It should be noted that these equations are not applied until ϵ_o has been determined and consequently a particular yield pattern found. The form of Equations A.39 and A.40 for each yield pattern is given in Tables A.4 and A.5, respectively.

To verify the validity of the relationships given in this appendix, a numerical integration procedure was also used. This was accomplished by dividing the column cross-section into a number of small elements and then summing-up the contribution of forces acting on each element to give the axial load $\overline{P}/P_y$, and by taking moments of these forces about the centroidal axes of the cross-section to give the moments M^x/M^x_y and M^y/M^x_y, respectively.

Table A.1 - Volumes of Yielded Material

Case*	$\int_A [\epsilon/\epsilon_y \pm 1]\, dA/D^2$
I	$K_1K_k(\bar{\epsilon}_i/\epsilon_y+\bar{\epsilon}_j/\epsilon_y-2+2\epsilon_o/\epsilon_y)$
II	$K_1K_k(\bar{\epsilon}_i/\epsilon_y+\bar{\epsilon}_j/\epsilon_y+2+2\epsilon_o/\epsilon_y)$
III	$K_1K_k[(\epsilon_o/\epsilon_y)^2/\rho_k+(\bar{\epsilon}_i/\epsilon_y-1+\rho_kA_{ij})\epsilon_o/(\epsilon_y\rho_k)+A_{ij}(\bar{\epsilon}_j/\epsilon_y+1)]/2$
IV	$K_1K_k[-(\epsilon_o/\epsilon_y)^2/\rho_k+(\bar{\epsilon}_j/\epsilon_y+1-\rho_kA_{ji})\epsilon_o/(\epsilon_y\rho_k)+A_{ji}(\bar{\epsilon}_j/\epsilon_y+1)]/2$
V	$K_1K_k[(\bar{\epsilon}_i/\epsilon_y-\bar{\epsilon}_j/\epsilon_y+\rho_kA_{ij}+\rho_kA_{ji}-2)\epsilon_o/(\epsilon_y\rho_k)+A_{ij}(\bar{\epsilon}_i/\epsilon_y-1)+$ $A_{ji}(\bar{\epsilon}_j/\epsilon_y+1)]/2$

*Numbers refer to Fig. A.2.

Table A.2 - Various Forms of A_{ij}, A_{ji}, a_{ij}, and a_{ji}

Side*	Equations**
1-3	$A_{13}=A_{42}=(\epsilon_1-1)/K_4\phi^x=Q_1/\phi^x$
4-2	
3-1	$A_{31}=A_{24}=(\epsilon_2-1)/K_4\phi^x=Q_2/\phi^x$
2-4	
1-2	$A_{12}=A_{43}=-(\epsilon_1+1)/K_5\phi^y=Q_3/\phi^y$
4-3	
2-1	$A_{21}=A_{34}=(\epsilon_2-1)/K_5\phi^y=Q_4/\phi^y$
3-4	
1-2	$a_{12}=(Q_3-\epsilon_o/K_5)/\phi^y$
2-1	$a_{21}=(Q_4+\epsilon_o/K_5)/\phi^y$
1-3	$a_{13}=(Q_1+\epsilon_o/K_4)/\phi^x$
3-1	$a_{31}=(Q_2-\epsilon_o/K_4)/\phi^x$
2-4	$a_{24}=(Q_2+\epsilon_o/K_4)/\phi^x$
4-2	$a_{42}=(Q_1-\epsilon_o/K_4)/\phi^x$
3-4	$a_{34}=(Q_4-\epsilon_o/K_5)/\phi^y$
4-3	$a_{43}=(Q_3+\epsilon_o/K_5)/\phi^y$

*Numbers 1, 2, 3, and 4 refer to Fig. A.1.

**All strains are in terms of ϵ_y and all curvatures are in terms of ϕ_y^x.

Table A.3 - Equations for ϵ_o for Various Yield Patterns

Case*	Equation**
(a)	$-K_1[\,4K_5\phi^x+\bar{\epsilon}_1+\bar{\epsilon}_2-2+K_4(Q_1+Q_2)\ (1-\alpha)-\phi^x A_c/K_1]\epsilon_o=A_c\bar{P}\phi^x$
(b)	$-K_1[(1-\alpha)(\phi^x-\phi^y)]\epsilon_o^2/2-K_1[\ (\bar{\epsilon}_2-1)\phi^x+K_5\phi^x(Q_4+4\phi^y)+(2\bar{\epsilon}_2+\bar{\epsilon}_1-3)\phi^y+K_4\phi^y(Q_1+2Q_2)\ (1-\alpha)-2\phi^x\phi^y A_c/$ $K_1]\epsilon_o/2-K_1[K_5\phi^x\ Q_4(\bar{\epsilon}_2-1)/2-\phi^y(\bar{\epsilon}_1+\bar{\epsilon}_2-2)\ +K_4\phi^y Q_1(1-\bar{\epsilon}_1)/2](1-\alpha)=A_c P\phi^x\phi^y$
(c)	$-K_1[\ (\bar{\epsilon}_2-\bar{\epsilon}_1-2)\phi^x+(\bar{\epsilon}_2+\bar{\epsilon}_1-2)\phi^y+K_5\phi^x(Q_4+Q_3+4\phi^y)+K_4\phi^y(Q_2+Q_1+4\phi^x)\ (1-\alpha)-2\phi^x\phi^y A_c/K_1]\epsilon_o/2-K_1[$ $K_5\phi^x\ Q_4(\bar{\epsilon}_2-1)/2+Q_3(\bar{\epsilon}_1+1)/2-\phi^y(\bar{\epsilon}_1+\bar{\epsilon}_2-2)\ +K_4\phi^y\ Q_2(\bar{\epsilon}_2-1)/2+Q_1(1-\bar{\epsilon}_1)/2+\phi^x(\bar{\epsilon}_1-\bar{\epsilon}_2+2)\ ](1-\alpha)=$ $A_c\bar{P}\phi^x\phi^y$
(d)	$K_1[1-\alpha]\epsilon_o^2-K_1[\ (\bar{\epsilon}_2+\bar{\epsilon}_1-2)+K_4(Q_2+Q_1)+4K_5\phi^x\ (1-\alpha)-2\phi^x A_c/K_1]\epsilon_o/2-K_1[K_4\ Q_2(1-\bar{\epsilon}_2)+Q_1(1-\bar{\epsilon}_1)\ /2$ $+K_5\phi^x(\bar{\epsilon}_1+\bar{\epsilon}_2-2)](1-\alpha)=A_c\bar{P}\phi^x$
(e)	$K_1[(1-\alpha)(\phi^x+\phi^y)]\epsilon_o^2/2+K_1[\ (\bar{\epsilon}_1+1)\phi^x+(1-\bar{\epsilon}_1)\phi^y-K_5\phi^x(Q_3+4\phi^y)-K_4\phi^y(Q_1+4\phi^x)\ (1-\alpha)+2\phi^x\phi^y A_c/K_1]$ $\epsilon_o/2-K_1[K_5\phi^x\ Q_3(\bar{\epsilon}_1+1)/2-\phi^y(\bar{\epsilon}_1+\bar{\epsilon}_2-2)\ +K_4\phi^y\ Q_1(1-\bar{\epsilon}_1)/2+\phi^x(\bar{\epsilon}_1-\bar{\epsilon}_2+2)\ ](1-\alpha)=A_c\bar{P}\phi^x\phi^y$

OVER

*Letters refer to Fig. 2.8.

**All strains are in terms of ϵ_y and all Curvatures are in terms of ϕ_y^x.

Table A.3 - Contd'

Case*	Equation**
(f)	$-K_1[\ 4K_4\phi^y+\bar{\epsilon}_2-\bar{\epsilon}_1-2+K_5(Q_4+Q_3)\ (1-\alpha)-\phi^y A_c/K_1]\epsilon_o=A_c\bar{P}\phi^y$
(g)	$-K_1[(1-\alpha)(\phi^y-\phi^x)]\epsilon_o^2/2-K_1[\ (2\bar{\epsilon}_2-\bar{\epsilon}_1-3)\phi^x+(\bar{\epsilon}_2-1)\phi^y+K_5\phi^x(2Q_4+Q_3)+K_4\phi^y(Q_2+4\phi^x)\ (1-\alpha)-2\phi^x\phi^y A_c/K_1]$ $\epsilon_o/2-K_1[K_5Q_3\phi^x(\bar{\epsilon}_1+1)/2+K_4\phi^y\ Q_2(\bar{\epsilon}_2-1)/2+\phi^x(\bar{\epsilon}_1-\bar{\epsilon}_2+2)\ ](1-\alpha)=A_c\bar{P}\phi^x\phi^y$
(h)	$K_1[1-\alpha]\epsilon_o^2+K_1[\ \bar{\epsilon}_1-\bar{\epsilon}_2+2-K_5(Q_3+Q_4)-4K_4\phi^y\ (1-\alpha)+2\phi^y A_c/K_1]\epsilon_o/2-K_1[K_4\phi^y(\bar{\epsilon}_1-\bar{\epsilon}_2+2)+K_5\ Q_4(1-\bar{\epsilon}_2)+$ $Q_3(\bar{\epsilon}_1+1)\ /2](1-\alpha)=A_c\bar{P}\phi^y$
(i)	$-K_1[\ (\bar{\epsilon}_2-1)\phi^x+(\bar{\epsilon}_2-1)\phi^y+K_5\phi^x Q_4+K_4\phi^y Q_2\ (1-\alpha)-\phi^x\phi^y A_c/K_1]\epsilon_o=A_c\bar{P}\phi^x\phi^y$
(j)	$-K_1[(1-\alpha)(\phi^x+\phi^y)]\epsilon_o^2/2-K_1[\ (\bar{\epsilon}_2-1)\phi^y+(\bar{\epsilon}_2-1)\phi^x+K_4\phi^y Q_2+K_5\phi^x Q_4\ (1-\alpha)-2\phi^x\phi^y A_c/K_1]\epsilon_o/2-K_1[K_4Q_2\phi^y(1-$ $\bar{\epsilon}_2)+K_5Q_4\phi^x(1-\bar{\epsilon}_2)](1-\alpha)/2=A_c\bar{P}\phi^x\phi^y$

*Letters refer to Fig. 2.8.

**All strains are in terms of ϵ_y and all Curvatures are in terms of ϕ^x_y

Table A.4 - Equations for M^x/M_y^x for Various Yield Patterns

Case*	M^x/M_y^x **
(a)	$\phi^x+(1-\alpha)(K_1K_4/\bar{I}_c^x)[K_5(\epsilon_3+\epsilon_4-\epsilon_1-\epsilon_2+4)+K_4\ -a_{13}(1-a_{13}/3)(\epsilon_1-1)+a_{31}(1-a_{31}/3)(\epsilon_3+1)-a_{24}(1-a_{24}/3)(\epsilon_2-1)+a_{42}(1-a_{42}/3)(\epsilon_4+1)\ /2]$
(b)	$\phi^x+(1-\alpha)(K_1K_4/\bar{I}_c^x)[K_5\ (\epsilon_3+\epsilon_4+2-a_{21}(\epsilon_2-1)/2\ +K_4\ -a_{24}(1-a_{24}/3)(\epsilon_2-1)+a_{42}(1-a_{42}/3)(\epsilon_4+1)+a_{31}(1-a_{31}/3)(\epsilon_3+1)\ /2]$
(c)	$\phi^x+(1-\alpha)(K_1K_4/\bar{I}_c^x)[K_5\ -a_{21}(\epsilon_2-1)/2-a_{12}(\epsilon_1+1)/2+\epsilon_3+\epsilon_4+2\ +K_4\ (\epsilon_3-\epsilon_1)/3-a_{24}(1-a_{24}/3)(\epsilon_2-1)+a_{42}(1-a_{42}/3)(\epsilon_4+1)/2\ ]$
(d)	$\phi^x+(1-\alpha)(K_1K_4/\bar{I}_c^x)[K_4\ a_{42}(1-a_{42}/3)(\epsilon_4+1)+a_{31}(1-a_{31}/3)(\epsilon_3+1)\ /2+K_5(\epsilon_3+\epsilon_4+2)]$
(e)	$\phi^x+(1-\alpha)(K_1K_4/\bar{I}_c^x)[K_5\ -a_{12}(\epsilon_1+1)/2+\epsilon_3+\epsilon_4+2\ +K_4\ (\epsilon_3-\epsilon_1)/3+a_{42}(1-a_{42}/3)(\epsilon_4+1)/2\ ]$

OVER

*Letters refer to Fig. 2.8.

**All strains are in terms of ϵ_y and all Curvatures are in terms of ϕ_y^x.

Table A.4 - Contd'

Case*	M^x/M^x_y **
(f)	$\phi^x+(1-\alpha)(K_1K_4/\bar{I}^x_c)[K_4(\epsilon_4+\epsilon_3-\epsilon_1-\epsilon_2)/3+K_5\ a_{43}(\epsilon_4-1)-a_{34}(\epsilon_3+1)-a_{21}(\epsilon_2-1)-a_{12}(\epsilon_1+1)\ /2]$
(g)	$\phi^x+(1-\alpha)(K_1K_4/\bar{I}^x_c)[K_4\ -a_{24}(1-a_{24}/3)(\epsilon_2-1)/2+(\epsilon_3-\epsilon_1)/3\ +K_5\ a_{34}(\epsilon_3+1)-a_{21}(\epsilon_2-1)-a_{12}(\epsilon_1+1)\ /2]$
(h)	$\phi^x+(1-\alpha)(K_1K_4/\bar{I}^x_c)[K_5\ -a_{12}(\epsilon_1+1)+a_{34}(\epsilon_3+1)\ /2+K_4(\epsilon_3-\epsilon_1)/3]$
(i)	$\phi^x+(1-\alpha)(K_1K_4/\bar{I}^x_c)[K_5\ -a_{21}(\epsilon_2-1)+a_{34}(\epsilon_3+1)\ /2+K_4\ -a_{24}(1-a_{24}/3)(\epsilon_2-1)+a_{31}(1-a_{31}/3)(\epsilon_3+1)\ /2]$
(j)	$\phi^x+(1-\alpha)(K_1K_4/\bar{I}^x_c)[K_5a_{34}+K_4a_{31}(1-a_{31}/3)](\epsilon_3+1)/2$

*Letters refer to Fig. 2.8.

**All strains are in terms of ϵ_y and all Curvatures are in terms of ϕ^x_y.

Table A.5 - Equations for M^y/M^x_y for Various Yield Patterns

Case*	M^y/M^x_y **
(a)	$\phi^y\bar{I}^y_c/\bar{I}^x_c+(1-\alpha)(K_1K_5/\bar{I}^x_c)[K_5(\epsilon_1+\epsilon_3-\epsilon_2-\epsilon_4)/3+K_4\ a_{13}(\epsilon_1-1)+a_{31}(\epsilon_3+1)-a_{24}(\epsilon_2-1)-a_{42}(\epsilon_4+1)\ /2]$
(b)	$\phi^y\bar{I}^y_c/\bar{I}^x_c+(1-\alpha)(K_1K_5/\bar{I}^x_c)[K_5\ -a_{21}(1-a_{21}/3)(\epsilon_2-1)/2+(\epsilon_3-\epsilon_4)/3\ +K_4\ a_{31}(\epsilon_3+1)-a_{24}(\epsilon_2-1)-a_{42}(\epsilon_4+1)\ /2]$
(c)	$\phi^y\bar{I}^y_c/\bar{I}^x_c+(1-\alpha)(K_1K_5/\bar{I}^x_c)[K_5\ -a_{21}(1-a_{21}/3)(\epsilon_2-1)/2+a_{12}(1-a_{12}/3)(\epsilon_1+1)/2+(\epsilon_3-\epsilon_4)/3\ +K_4\ \epsilon_1+\epsilon_3+2-a_{24}(\epsilon_2-1)/2-a_{42}(\epsilon_4+1)/2\ ]$
(d)	$\phi^y\bar{I}^y_c/\bar{I}^x_c+(1-\alpha)(K_1K_5/\bar{I}^x_c)[K_4\ -a_{42}(\epsilon_4+1)+a_{31}(\epsilon_3+1)\ /2+K_5(\epsilon_3-\epsilon_4)/3]$
(e)	$\phi^y\bar{I}^y_c/\bar{I}^x_c+(1-\alpha)(K_1K_5/\bar{I}^x_c)[K_5\ a_{12}(1-a_{12}/3)(\epsilon_1+1)/2+(\epsilon_3-\epsilon_4)/3\ +K_4\ \epsilon_1+\epsilon_3+2-a_{42}(\epsilon_4+1)/2\ ]$

OVER

*Letters refer to Fig. 2.8.

**All strains are in terms of ϵ_y and all Curvatures are in terms of ϕ^x_y.

Table A.5 - Contd'

Case*	M^y/M^x_y **
(f)	$\phi^y\bar{I}^y_c/\bar{I}^x_c+(1-\alpha)(K_1K_5/\bar{I}^x_c)[K_4(\epsilon_1+\epsilon_3-\epsilon_4-\epsilon_2+4)+K_5 \;\; -a_{43}(1-a_{43}/3)(\epsilon_4-1)+a_{34}(1-a_{34}/3)(\epsilon_3+1)-a_{21}(1-a_{21}/3)(\epsilon_2-1)+a_{12}(1-a_{12}/3)(\epsilon_1+1) \;\; /2]$
(g)	$\phi^y\bar{I}^y_c/\bar{I}^x_c+(1-\alpha)(K_1K_5/\bar{I}^x_c)[K_4 \;\; \epsilon_3+\epsilon_1+2-a_{24}(\epsilon_2-1)/2 +K_5 \;\; -a_{21}(1-a_{21}/3)(\epsilon_2-1)+a_{12}(1-a_{12}/3)(\epsilon_1+1)+a_{34}(1-a_{34}/3)(\epsilon_3+1) \;\; /2]$
(h)	$\phi^y\bar{I}^y_c/\bar{I}^x_c+(1-\alpha)(K_1K_5/\bar{I}^x_c)[K_5 \;\; a_{12}(1-a_{12}/3)(\epsilon_1+1)+a_{34}(1-a_{34}/3)(\epsilon_3+1) \;\; /2+K_4(\epsilon_1+\epsilon_3+2)]$
(i)	$\phi^y\bar{I}^y_c/\bar{I}^x_c+(1-\alpha)(K_iK_5/\bar{I}^x_c)[K_5 \;\; -a_{21}(1-a_{21}/3)(\epsilon_2-1)+a_{34}(1-a_{34}/3)(\epsilon_3+1) \;\; /2+K_4 \;\; -a_{24}(\epsilon_2-1)+a_{31}(\epsilon_3+1) \;\; /2]$
(j)	$\phi^y\bar{I}^y_c/\bar{I}^x_c+(1-\alpha)(K_1K_5/\bar{I}^x_c)[K_4a_{31}+K_5a_{34}(1-a_{34}/3)](\epsilon_3+1)/2$

*Letters refer to Fig. 2.8.

**All strains are in terms of ϵ_y and all Curvatures are in terms of ϕ^x_y.

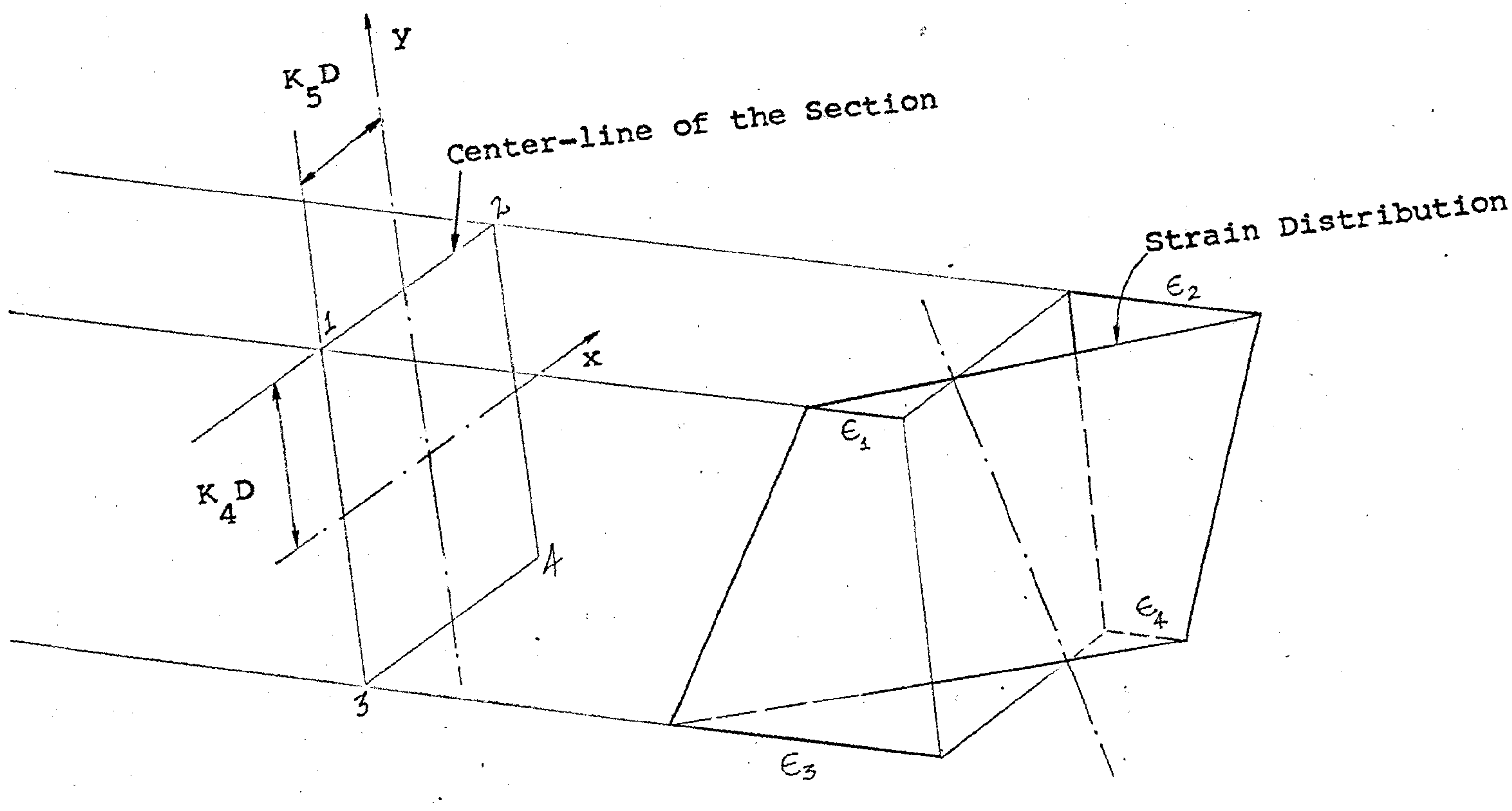

Fig. A.1 Typical Strain Distribution on a Section

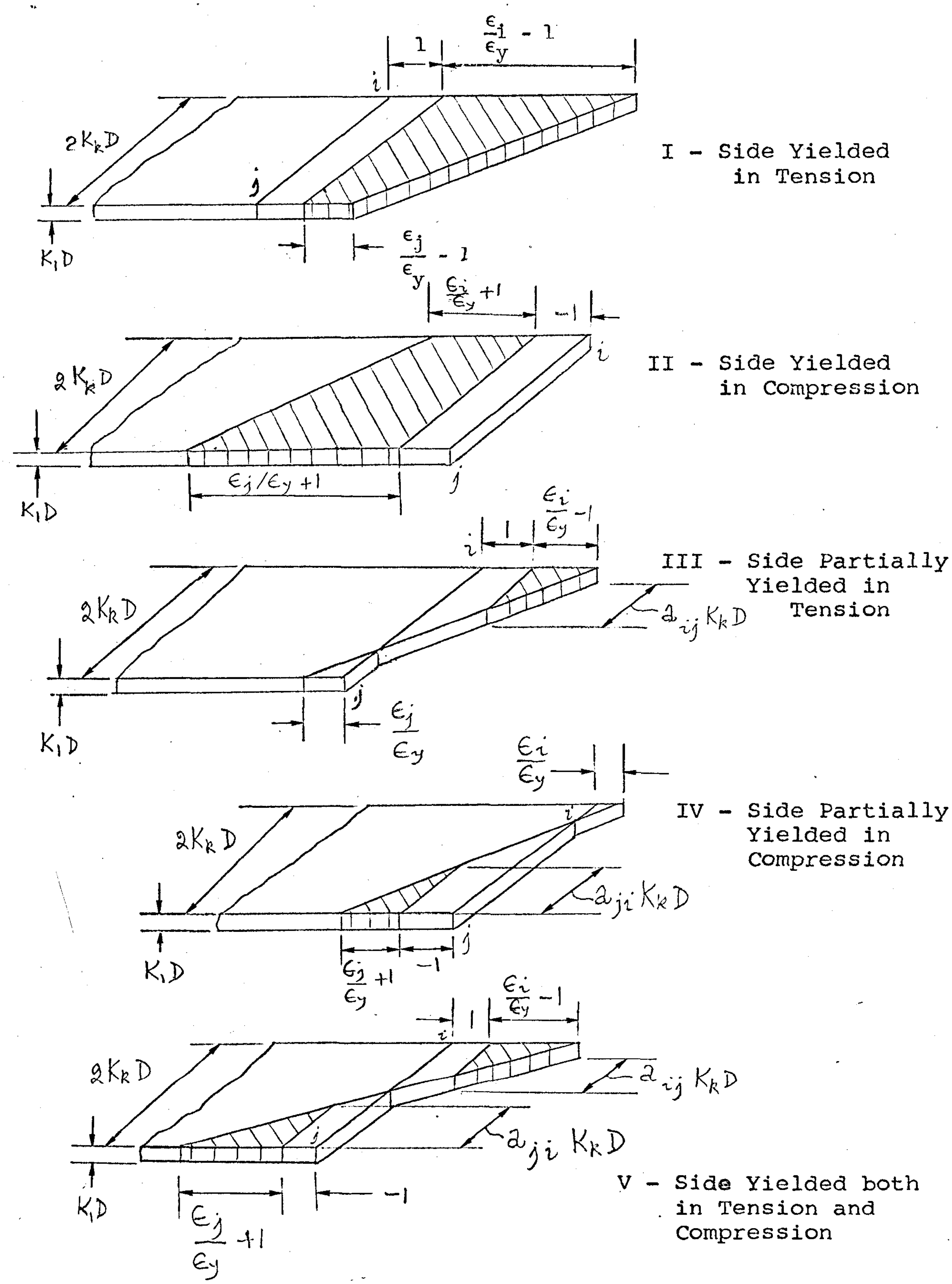

Fig. A.2 Correction Volumes for Various Side Yield Patterns

BIBLIOGRAPHY

1. Baker, A.L.L., M.R. Horne, and J. Heyman, The Steel Skeleton, Vol. 2, Plastic Behaviour and Design, Cambridge University Press, 1956.

2. Birnstiel, C., and J. Michalos, Ultimate Load of H-Columns Under Biaxial Bending, Proceedings, ASCE, Vol. 89, ST2, 1963.

3. Bleich, F., Buckling Strength of Metal Structures, McGraw-Hill Book Co., New York, 1952.

4. Culver, C.G., Exact Solution of the Biaxial Bending Equations, Proc. ASCE, Vol. 92, ST2, 1966.

5. Dabrowski, R., Dunnwandige Stabe Unter Zweiachsig Aussermittigem Druck, Der Stahlbau, Wilhelm Ernst and Sohn, Berlin-Wilmursdorf, Germany, December, 1961.

6. Ellis, J.S., Plastic Behaviour of Compression Members, Transactions of the Engineering Institute of Canada, Vol. 2, No. 2, 1958.

7. Ellis, J.S., E.J. Jury, and D.W. Kirk, Ultimate Capacity of Steel Columns Loaded Biaxially, Transactions of the Engineering Institute of Canada, Vol. 7, No. A-2, 1964.

8. Ellis, J.S., and P.J. Marshall, The Ultimate Capacity of Steel Columns Loaded Biaxially, Paper presented at the annual meeting of the Column Research Council, 1967.

9. Galambos, T.V. and R.L. Ketter, Columns Under Combined Bending and Thrust, Proceedings. ASCE, Vol. 85, EM2, 1959.

10. Goodier, J.N., Torsional and Flexural Buckling of Bars of Thin Walled Open Section Under Compressive and Bending Loads, Journal of Applied Mechanics, Transactions, ASME, Vol. 64, 1942.

11. Johnson, B.G., Guide to Design Criteria for Metal Compression Members, 2nd Ed., John Wiley & Sons, Inc., New York, 1966.

12. Jordan, W.D., The Inelastic Behavior of Eccentrically Loaded Columns, Ph.D. Thesis, University of Illinois, Urbana, Illinois, 1952.

13. Ketter, R.C., Stability of Beam-Columns Above the Elastic Limit, Proc. ASCE, Vol. 81, No. 692, October 1955.

14. Ketter, R.L., E.L. Kaminisky and L.S. Beedle, Plastic Deformation of Wide Flange Beam-Columns, Trans., ASCE, Vol. 120, 1950.

15. Mason, R.E., G.P. Fisher and G. Winter, Eccentrically Loaded Hinged Steel Columns, ASCE, Vol. 84, EM4, 1958.

16. McVinnie, W.W., Elastic and Inelastic Buckling of an Orthogonal Space Frame, Ph.D. Thesis, University of Illinois, Urbana, Illinois, 1966.

17. Newmark, N.M., Numerical Procedure for Computing Deflections, Moments, and Buckling Loads, Trans., ASCE, Vol. 108, 1943.

18. Osgood, W.R., Beam-Columns, Jour. of Aero. Sci., Vol. 14, No. 3, March 1947.

19. Prawel, S.P., and Lee, G.C., Biaxial Flexure of Columns by Analog Computers, Journal of the Engineering Mechanics Division, ASCE, Vol. 90, No. EM1, Proc. Paper 3805, Feb., 1964.

20. Salvadori, M.G., Numerical Computations of Buckling Loads by Finite Differences, Transactions, ASCE, Vol. 116, 1951.

21. Scott, T.L., Theoretical Analysis of Biaxially Loaded Beam-Columns, M.A.Sc. Thesis, University of Windsor, 1967.

22. Shanley, F.R., Strength Analysis of Eccentrically-Loaded Columns, Department of Engineering, University of California, Report 54-57, May 1954.

23. Sharma, S.S., Strength of Steel Columns with Biaxially Eccentric Loads, Ph.D. Thesis, University of Illinois, Urbana, Illinois, 1965.

24. Sherman, D.R., Residual Stress Measurement in Tubular Members, Unpublished Report by the author who is an Assistant Professor at the University of Wisconsin, Milwaukee, Wisconsin.

25. Smith, J.O., and O.M. Sidebottom, Inelastic Behavior of Load-Carrying Members, John Wiley & Sons, New York, 1965.

26. Timoshenko, S., Theory of Bending, Torsion and Buckling of Open Cross-Section, Journal, Franklin Inst., Philadelphia, Pa., March, April, May, 1945.

27. Timoshenko, S.P., and James M. Gere, Theory of Elastic Stability, McGraw-Hill Book Co., New York, 1961.

28. Vlasov, V.Z., <u>Thin Walled Elastic Beams</u>, 2nd Edition, Natl. Science Foundation, Washington, D.C., 1961.

NOMENCLATURE

a	length of a typical element of the column deflection curve
a_{ij}, a_{ji}	factors defining the length of tension or compression yield on an edge
e^x, e^y	eccentricities from the x and y axes respectively
$i, i+1$	points on the column deflection curve
i, j	corner of the edge under consideration
r^x, r^y	radius of gyration about the x and y axes respectively
u, v	lateral displacements of the shear center in the x and y directions respectively
z	cordinate along the member
A_c	area of the cross-section
D	half depth of the cross-section
E	Young's Modulus
E_t	Tangent Modulus
I^x, I^y	moment of inertia of the cross-section about the x and y axes respectively
K_1	factor defining the wall thickness of the cross-section in terms of D
K_2	factor defining half the outside width of the cross-section in terms of D
K_3	factor defining half the inside width of the cross-section in terms of D
K_4, K_5	factors describing dimensions of the center-line of the cross-section in terms of D
h	length of the column
M^x, M^y	bending moments about the x and y axes respectively
$\overline{P}$	axial load applied to the column
P_y	yield load

α	strain-hardening foactor of the material
γ	ratio of the y-moment to the x-moment at the same end of the column
ϵ	Strain
$\bar{\epsilon}$	bending strain
ϵ_o	uniform normal strain
ϵ_y	yield strain
θ^x, θ^y	rotations about the x and y axes respectively
θ^x_y	yield rotation
σ	stress
ϕ^x, ϕ^y	x and y axes curvatures
ϕ^x_y	yield curvature

VITA AUCTORIS

1945	Born in Peshawar, West Pakistan, on March 16.
1960	Matriculated from the Cantonment Public High School, Peshawar, West Pakistan.
1962	Completed Intermediate Science (Non-Medical) at Edwardes College, Peshawar, West Pakistan.
1966	Received the Bachelor of Engineering (Hons.) degree in Civil Engineering from the University of Peshawar, West Pakistan.
1966	Accepted into the Graduate School of the University of Windsor as a Candidate for the degree of Master of Applied Science in Civil Engineering.